

**LONG-TERM RATES OF DENUDATION AND SEDIMENT GENERATION
OVER DIFFERENT SPATIAL SCALES QUANTIFIED USING IN SITU
PRODUCED COSMOGENIC ^{10}BE AND ^{26}AL IN SEDIMENT AND ROCK**

A Dissertation Presented

by

Erik Matthew Clapp

to

The Faculty of the Graduate College

of

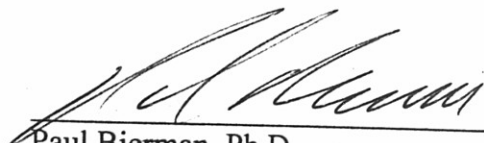
The University of Vermont

**In Partial Fulfillment of the Requirements
for the Degree of Doctor of Philosophy
Specializing in Geology**

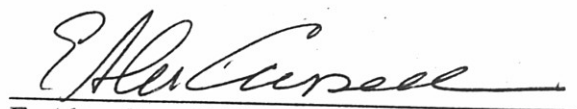
May, 2003

Accepted by the Faculty of the Graduate College, The University of Vermont, in partial fulfillment of the requirements for the degree of Doctor of Philosophy, specializing in Geology.

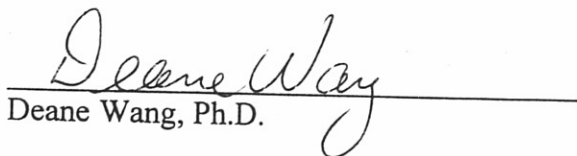
Dissertation Examination Committee:




Paul Bierman, Ph.D. Advisor




E. Alan Cassell, Ph.D.



Deane Wang, Ph.D.



Andrea Lini, Ph.D. Chairperson



David S. Dummit Special Assistant to the Provost
for Graduate Education

Date: March 26, 2003

Abstract

^{10}Be and ^{26}Al were measured in bedrock and sediment collected from three arid region drainage basins of different scales (0.62 to 187 km²) and geologic complexities, to determine long-term, time-integrated rates of sediment generation and bedrock-equivalent lowering (denudation), to identify sediment source areas and mechanisms of sediment delivery and, to evaluate the effects of basin scale on the interpretation of cosmogenic nuclide activities measured in sediment. The three drainage basins include: Arroyo Chavez (northern New Mexico), Nahal Yael (southern Israel), and Yuma Wash (southern Arizona). By measuring nuclide activities in individual geomorphic features throughout each drainage basin, the assumptions necessary for the interpretation of basin-wide erosion rates from stream channel sediments were tested. The results of the three studies suggest that for small basins (<20km²), storage of sediment is generally insignificant, the nuclide concentration of bedrock surfaces, hillslope colluvium, alluvial fans and terraces, and stream channel sediments are similar, and the drainage network appears to integrate sediment and associated cosmogenic nuclides from throughout each drainage basin. Thus, for small drainage basins, measuring nuclide activities in stream channel sediments leaving the basin via the trunk stream appears to provide reasonable estimates of basin-wide erosion rates calculated from the nuclide activities in the sediment. However, for the larger scale Yuma Wash basin (>100km²), sediment storage becomes significant, and the nuclide signature of the stream channel sediments in the trunk stream are most representative of the geomorphic features currently yielding the greatest amount of sediment.

Analyses of sediment samples divided into multiple grain sizes demonstrates that in arid regions, nuclide activities are independent of sediment grain size implying that both large and small particles are produced by similar processes, are transported at similar rates, and are produced over a similar range of altitudes. These findings are consistent with arid-region sediment transport theory, which suggests that turbulent flows from infrequent, intense storm events transport material of many different sizes at similar rates.

The results of the ^{10}Be and ^{26}Al analyses indicate that overall rates of sediment generation are similar for areas with similar lithologies and similar climates, but can differ dramatically when conditions differ. Poorly lithified sandstones of New Mexico's Arroyo Chavez basin, located on the Colorado Plateau (semi arid, seasonally cold climate), overall average bedrock erosion rates are on the order of 100 mMy⁻¹ (sediment generation rate of 275 t km⁻² y⁻¹). While arid regions (Yuma, Arizona and Nahal Yael, Israel) with more weathering resistant lithologies (granitoids), average bedrock erosion rates are on the order of 30 mMy⁻¹ (sediment generation rates of ~80 t km⁻² y⁻¹).

Finally, a program for correction of cosmogenic ages and erosion rates for geomagnetically-induced changes in in-situ-produced cosmogenic nuclide production rates is presented. Applying our corrections generally decreases calculated exposure ages, increases calculated rates of erosion, and suggests systematic age errors associated with time-averaged production rates be greater than 45% for older samples (> 100 ka) at high elevations (3 to 6 km asl), low latitudes (0 to 10°), and for younger samples may be on the order of 20% to 30% for samples > 40 ka at lower elevations (sea level to 1 km asl).

Citations

Material from this dissertation has been published in the following form:

Clapp, E. M., Bierman, P. R., Schick, A. P., Lekach, J., Enzel, Y., and Caffee, M., Sediment yield exceeds sediment production in arid region drainage basins. *Geology*, 28, 995-998, 2000.

Clapp, E.M., Bierman, P.R., Pavich, M., and Caffee, M., Rates of sediment supply to arroyos from uplands determined using in situ produced cosmogenic ^{10}Be and ^{26}Al in sediments, *Quaternary Research*, 55, 235-245, 2001.

Clapp, E.M., Bierman, P.R., and Caffee, M., Using ^{10}Be and ^{26}Al to determine sediment generation rates and identify sediment source areas in an arid region drainage basin, *Geomorphology*, 45, 67-87, 2002.

Material from this dissertation will be submitted for publication to *Radiocarbon* during Spring 2003, in the following form:

Clapp, E.M. and Bierman, P.R., Correcting cosmogenic exposure ages and erosion rates for secular variation in Earth's magnetic field intensity, *Radiocarbon*.

Acknowledgements

There are a tremendous number of people of heart who aided in this work and who have touched my life throughout the years spent on this journey. Above all, I would like to thank my wife Lynda and my son Henry without whom I could never have found the strength. This Dissertation is dedicated to all of the loved ones that have passed before us.

I would especially like to thank my advisors, Dr. Paul Sherman and Dr. Alan Cassell who have never wavered in their support of this work or in life's trials and tribulations. I'd like to express a special thanks to Dr. Robert Inge for chairing the thesis committee, Dr. Deane Wang for bringing perspectives and insights to this work, and the late Rolfe Stanley for making hard work both rewarding and a family life. I'd like to thank the School of Natural Resources and the Department of Zoology for providing a home over the years and a place to interact with other scientists and others who believe that the natural sciences will make the world a better, safer, and healthier place to live. I'd also like to thank all of those who helped in the field, laboratory, and analytical portions of this work including: Mike Abbott, Kyle Nichols, Sam Green, Kim Marsella, Susan Nies, Judith Lokach, Christine Muegge, Alan Gellis, Anna Moxham, John Spang, John Southon, Ben Copans, Val Morill, Allen Gillespie, and Doug Clark.

I'd like to take this opportunity to thank all of those who contributed to the financial support of this work, especially: Russell Harmon (US Army Research Office), Milan Pavich (USGS), Mike Caffee (Lawrence Livermore National Laboratory), John Sevee and Peter Malzer (Sevee and Malzer Engineers, Inc.), and Youssef Fouzi and the late Asher Schick (Hebrew University of Jerusalem). This work was supported by the following grants: U.S. Geological Survey grant # HQ96AC0189, NSF grant # EAR-9628559, Department of Energy contract # W-7405-ENG-48, EPA grants # DAAG559710180, #DAAG1049510P36, and US ARD STIC Grant DAAH04-95-1-0408.

Finally, this dissertation would not be complete without the support of my family and friends. I'd like to thank my parents, Joe and Faith Chapp and the rest of my family including Chris, Jon, CJ, Noah, Joe, Paula, Zach, Amanda, Gemma, Nancy, Steve, Greg, Big-Joe, and Brenda, for their support, generosity and friendship over the years. I'd also like to thank the Fitzpatrick Family, the Pratt Family, and the Cuthie Family for many wonderful days on Buzzard's Bay and many fantastic meals. And a final thanks to all of those friends that have made the past years so enjoyable.

Acknowledgements

There are a tremendous number of people who have contributed to this work and who have touched my life throughout the years spent on this research. Above all, I would like to thank my wife Lynda and my son Henry without whose love I could never have found the strength and determination to finish this rather large piece of my life's work.

I would especially like to thank my advisors Dr. Paul Bierman and Dr. Alan Cassell who have never wavered in their support of this work or in life's trials and tribulations. I'd like to express a special thanks to Dr. Andrea Lini for chairing the thesis committee, Dr. Deane Wang for bringing perspective and meaning to this work, and the late Rolfe Stanley for inspiring hard work both in academics and in family life. I'd like to thank the School of Natural Resources and the Department of Geology for providing a home over the years and a place to interact with other scientists and others who believe that the natural sciences can make the world a better, safer, and healthier place to live. I'd also like to thank all of those who helped in the field, laboratory, and analytical portions of this work including: Mike Abbott, Kyle Nichols, Sara Gran, Kim Marsella, Susan Nies, Judith Lekach, Christine Massey, Alan Gellis, Arim Matmon, John Stone, John Southon, Ben Copans, Val Morrill, Allen Gillespie, and Doug Clark.

I'd like to take this opportunity to thank all of those who contributed to the financial support of this work, especially: Russell Harmon (US Army Research Office), Milan Pavich (USGS), Marc Caffee (Lawrence Livermore National Laboratory), John Sevee and Peter Maher (Sevee and Maher Engineers, Inc.), and Yehuda Enzel and the late Asher Schick (Hebrew University of Jerusalem). This work was supported by the following grants: U.S. Geological Survey grant # HQ96AG01589; NSF grant # EAR-9628559; Department of Energy contract # W-7405-ENG-48; US ARO grants #DAAG559710180, #DAAH049610036, and US ARO STIR Grant DAAH04-95-1-0408.

Finally, this dissertation would not be complete without the support of my family and friends. I'd like to thank my parents, Joe and Faith Clapp and the rest of my family including Chris, Jen, CJ, Noah, Joe, Paula, Zack, Amanda, Gramma, Nancy, Steve, Greg, Big-Joe, and Brenda, for their support, generosity and friendship over the years. I'd also like to thank the Fitzpatrick Family, the Pratt Family, and the Gillis Family for many wonderful days on Buzzard's Bay and many fantastic meals. And a final thanks to all of those friends that have made the past years so enjoyable.

2.0 Array of Contents

2.1 Abstract

2.2 Introduction

2.3 Geomorphic Setting

2.4 In-Situ Proximal Transport

2.5 Methods

Acknowledgements

There are a tremendous number of people who have contributed to this work and who have touched my life throughout the years spent on this research. Above all, I would like to thank my wife Lynda and my son Henry without whose love I could never have found the strength and determination to finish this rather large piece of my life's work.

I would especially like to thank my advisors Dr. Paul Bierman and Dr. Alan Cassell who have never wavered in their support of this work or in life's trials and tribulations. I'd like to express a special thanks to Dr. Andrea Lini for chairing the thesis committee, Dr. Deane Wang for bringing perspective and meaning to this work, and the late Rolfe Stanley for inspiring hard work both in academics and in family life. I'd like to thank the School of Natural Resources and the Department of Geology for providing a home over the years and a place to interact with other scientists and others who believe that the natural sciences can make the world a better, safer, and healthier place to live. I'd also like to thank all of those who helped in the field, laboratory, and analytical portions of this work including: Mike Abbott, Kyle Nichols, Sara Gran, Kim Marsella, Susan Nies, Judith Lekach, Christine Massey, Alan Gellis, Arim Matmon, John Stone, John Southon, Ben Copans, Val Morrill, Allen Gillespie, and Doug Clark.

I'd like to take this opportunity to thank all of those who contributed to the financial support of this work, especially: Russell Harmon (US Army Research Office), Milan Pavich (USGS), Marc Caffee (Lawrence Livermore National Laboratory), John Sevee and Peter Maher (Sevee and Maher Engineers, Inc.), and Yehuda Enzel and the late Asher Schick (Hebrew University of Jerusalem). This work was supported by the following grants: U.S. Geological Survey grant # HQ96AG01589; NSF grant # EAR-9628559; Department of Energy contract # W-7405-ENG-48; US ARO grants #DAAG559710180, #DAAH049610036, and US ARO STIR Grant DAAH04-95-1-0408.

Finally, this dissertation would not be complete without the support of my family and friends. I'd like to thank my parents, Joe and Faith Clapp and the rest of my family including Chris, Jen, CJ, Noah, Joe, Paula, Zack, Amanda, Gramma, Nancy, Steve, Greg, Big-Joe, and Brenda, for their support, generosity and friendship over the years. I'd also like to thank the Fitzpatrick Family, the Pratt Family, and the Gillis Family for many wonderful days on Buzzard's Bay and many fantastic meals. And a final thanks to all of those friends that have made the past years so enjoyable.

2.0	Abstract	13
2.1	Introduction	14
2.2	Geomorphic Setting	16
2.3	In-Situ-Produced Cosmogenic Isotopes in Sediments	17
2.4	Methods	18

Table of Contents

	<u>Page</u>
Citations	ii
Dedication	iii
List of Tables	ix
List of Figures	x
 <u>Chapter</u>	
1.0 Introduction.....	1
1.1 In Situ Produced Cosmogenic Nuclides	3
1.2 Research Questions	6
1.3 Field-Based Studies	7
Arroyo Chavez.....	7
Nahal Yael	9
Yuma Wash.....	9
1.4 Correction of Cosmogenic Exposure Ages and Erosion Rates.....	11
2.0 Arroyo Chavez Manuscript.....	13
2.1 Abstract	14
2.2 Introduction.....	15
2.3 Geomorphic Setting	16
2.4 In-Situ-Produced Cosmogenic Isotopes in Sediments.....	17
2.5 Methods.....	18

<u>Chapter</u>	<u>Page</u>
4.0 Sample Collection.....	18
Sample Preparation.....	19
4.1 Abstract.....	19
Data Interpretation.....	19
4.2 Introduction.....	19
2.6 Results and Discussion.....	20
4.3 Geomorphic Setting.....	20
Model Evaluation.....	20
4.4 Methods.....	20
Lack of Grain Size Dependence.....	26
Erosion Rates, Sediment Generation, and Arroyo Cycling.....	26
2.7 Conclusions.....	29
2.8 Acknowledgements.....	29
4.5 Results and Discussion.....	29
2.9 References Cited.....	30
3.0 Nahal Yael Manuscript.....	45
3.1 Abstract.....	46
3.2 Introduction.....	46
3.3 Background.....	47
3.4 Sampling Locations and Methods.....	48
3.5 Results and Discussion.....	50
5.0 Bedrock Erosion and Sediment Generation.....	50
Dynamics of Sediment Production and Transport.....	51
5.1 Abstract.....	51
Sediment Production Versus Sediment Yield.....	53
5.2 Introduction.....	53
3.6 Acknowledgments.....	55
5.3 Nucleide Systematics.....	55
3.7 References Cited.....	55
5.4 Correction for Geomagnetic Field Strength.....	103

<u>Chapter</u>	<u>Page</u>
4.0 Yuma Wash Manuscript	63
4.1 Abstract	64
4.2 Introduction.....	65
4.3 Geomorphic Setting	67
4.4 Methods.....	69
Sample Collection.....	69
Sample Preparation	70
Data Interpretation	71
4.5 Results and Discussion	72
Grainsize	72
Southwest Sub-basin.....	73
Main Drainage Basin	77
Rates of Sediment Generation and Denudation.....	79
4.6 Implications.....	80
4.7 Acknowledgements.....	82
4.8 References Cited	82
5.0 Cosmo-Calibrate Manuscript.....	99
5.1 Abstract	100
5.2 Introduction.....	100
5.3 Nuclide Systematics.....	101
5.4 Correction for Geomagnetic Field Strength.....	103

<u>Chapter</u>	<u>List of Tables</u>	<u>Page</u>
	Model Structure	104
	Paleointensity Data	105
	Interpretation of Instantaneous Production Rates from Paleointensity Data	106
	Determination of Initial Production Rates (P_0)	108
	Uncertainty Analysis	108
5.5	Results and Discussion	110
	Comparison to Other Corrections	111
	Case Studies	113
	Contemporary Production Rates (P_0)	115
5.6	Conclusions	116
5.7	Acknowledgments	116
5.8	References Cited	116
6.0	Conclusions	128
	Comprehensive Bibliography	133
	Appendix A Sediment Grainsize Data	144
	Appendix B Nahal Yael Supporting Information	148
	Appendix C Cosmocalibrate Documentation	153

List of Tables

<u>Table</u>	<u>Page</u>
2-1. Locations and descriptions of samples from Arroyo Chavez Basin.....	33
2-2. Concentrations of ^{10}Be and ^{26}Al Measured in Samples from Arroyo Chavez Basin.	34
2-3. Sediment-generation rates and bedrock-equivalent lowering rates for Arroyo Chavez area.....	35
3-1. Sediment generations and equivalent rock erosion rates for Nahal Yael and other sites.	58
4-1A. Locations and descriptions of samples from Yuma Wash, for samples with multiple grain-sizes.....	86
4-1B. Locations and descriptions of samples from Yuma Wash, for samples with single grainsize.	87
4-2. Concentrations of ^{10}Be and test of statistical differences between concentrations in geomorphic features of southwest sub-basin, Yuma Wash.	88
4-3. Sediment generation and denudation rates for Yuma Wash Drainage.....	89
4-4. Mixing model results for area upstream from YPG-19 at Yuma Wash.	90
5-1. Estimated contemporary production rates at time = 0 (Po)	121

4-6. Sediment grainsize versus ^{10}Be concentration for YPG-2 and YPG-19 96

FigurePage

4-7. ^{10}Be concentrations plotted against depth for profiles measured in two basin fill

1-1. World map showing general study locations.....	12
2-2. Topography of the Arroyo Chavez sub-basin.....	37
2-3. Schematic cross-section of the Arroyo Chavez sub-basin.....	38
2-4. Balance of cosmogenic ^{10}Be in the Arroyo Chavez basin.....	39
2-5. Average ^{10}Be concentrations for individual sediment reservoirs in the Arroyo Chavez sub-basin	40
2-6. ^{10}Be concentrations measured in basin alluvium and alluvial fan profiles.....	41
2-7. Steady state and rapid-deposition models for basin alluvium.	42
2-8. Calculated isotopic depth profiles.	43
2-9. ^{10}Be concentrations for different sediment grain size fractions of four samples.....	44
3-1. Upstream view of Nahal Yael drainage basin	59
3-2. Map of Nahal Yael and site location	60
3-3. Average ^{10}Be concentrations measured in samples from geomorphic features of Nahal Yael	61
3-4. ^{10}Be concentrations measured at three transects in Nahal Yael	62
4-1. Map of Yuma Wash drainage basin.	91
4-2. Photograph of main stem of Yuma Wash.....	92
4-3. Photograph of southwest sub-basin.	93
4-4. ^{10}Be and ^{26}Al concentrations for all Yuma Wash samples.....	94
4-5. Sediment grainsize versus ^{10}Be concentration for all sediment samples analyzed. .	95

<u>Figure</u>	<u>Page</u>
4-6. Sediment grainsize versus ^{10}Be concentration for YPG-2 and YPG-19.	96
4-7. ^{10}Be concentrations plotted against depth for profiles measured in two basin fill deposits.	97
4-8. Trend of sample distance downstream versus ^{10}Be concentrations along with results of mixing model for the main stem of Yuma Wash.....	98
5-1. Relative magnetic field strength curve used to control model calculations.	122
5-2. Model graphical output.....	123
5-3. Age errors calculated for ^{10}Be exposure ages as a function of time, elevation, and geographic latitudes	124
5-4. Relative, long-term, time-integrated production rates.....	125
5-5. Average corrected and uncorrected ^{10}Be exposure ages for boulders of five debris flow fans along the Fish Springs Fault.	126
5-6. Average corrected and uncorrected bedrock outcrops across west-central Namibia.	127

1.0 Introduction

The rate at which a landscape changes is directly related to the physical and biological processes occurring on that landscape (Summerfield, 1991; Bull, 1991). Changes in environmental conditions, either natural or human-induced, can lead to periods of increased stream channel incision, which result in the dissection of a landscape, decreases in hillslope vegetation, increased sediment loads to streams, disruption of water supplies, disturbance of culturally significant historical sites, and disturbance of delicate ecosystems (Leopold et al., 1966; Bull, 1991; Cooke and Revees, 1976; Bull and Schick, 1979; Schick and Lekach, 1993; Nichols and Bierman, 2001).

Sediment can be considered one of the greatest environmental pollutants (Keller, 1992). Understanding the rate at which sediment is generated can tell us how long it may take to fill harbors, reservoirs, ponds or lakes. Increased sediment loads can make rivers uninhabitable for many organisms and during high water periods can bury vegetation or fertile soils in river flood plains (Keller, 1992). Sediment is also a key element in transporting many pollutants in a fluvial environment (Rosensteel and Strom, 1991; Pilleboue and Dorioz, 1986; Drake and Heaney, 1987; Thoman and Mueller, 1987; Clapp, 1995).

Establishing long-term ($>10^3$ yrs), baseline rates of sediment production and erosion may be invaluable to the management of public and private lands. Reclamation and restoration of public lands disturbed by military activities, harvesting or mining of natural resources, overgrazing, or natural disasters, can be greatly improved if long-term conditions are understood for the establishment of restoration criteria. Quantifying

historical rates of sediment production, storage, and yield from a basin can help determine the long-term effects of climate change or land-use on a landscape (Bull and Schick, 1979; Bull, 1991). How do current rates of denudation, and sediment yield from a basin compare to the long-term rates (Meade, 1969; Trimble, 1977, 1999; Walling, 1983; Bull, 1991)? How do seemingly accelerated rates of landscape change compare to long-term rates of landscape change? (Leopold et al., 1966; Bull, 1991; Gellis et al., 2000; Clapp et al., 2000). Answering these questions relies on our ability to quantify rates of geomorphic processes both in the present, and in the past.

Long-term rates of sediment production (rock erosion) are typically extrapolated from estimates of sediment yield measured either as a flux of sediment past a gauging station or determined by measuring the accumulation of sediment in a reservoir (Ahnert, 1970; Schumm, 1963; Judson, 1968; Judson and Ritter, 1964; Meade, 1969; Trimble, 1977; Saunders and Young, 1983; Pinet and Souriau, 1988; Schick and Lekach, 1993). Equating sediment yield and sediment production implies steady-state behavior and assumes no change in the volume of sediment stored within a basin, an assumption repeatedly questioned (Meade, 1969; Trimble, 1977, 1999; Walling, 1983; Bull, 1991). When extrapolations are used to infer sediment generation rates over thousands of years, significant errors in estimates of long-term rates are inevitable (Meade, 1988, 1969; Trimble, 1977).

1.1 In Situ Produced Cosmogenic Nuclides

^{10}Be and ^{26}Al provide a potential tool for more accurately determining long-term ($>10^3$ years) rates of sediment production (Cerling and Craig, 1994; Bierman, 1994; Zreda and Phillips, 1998; Gosse and Phillips, 2001; Bierman et al., 2001). ^{10}Be and ^{26}Al , are long-lived radionuclides that are produced in rock and sediment, at or near Earth's surface (within the top several meters), by the interaction of cosmic radiation with a variety of target atoms in the rock and sediment; a process referred to as in-situ production (Lal, 1988). The in situ production of ^{10}Be and ^{26}Al occurs primarily through the splitting (spallation) of O and Si atoms by collisions with high speed neutrons (Lal, 1988). ^{10}Be and ^{26}Al are also produced, to a lesser extent, through interactions with slow muons ($\sim 3\%$ according to Stone, 2000) and in very low concentrations by the radio-disintegration of U and Th (Sharma and Middleton, 1989). Production of nuclides decreases exponentially with depth below Earth's surface due to shielding of incoming cosmic rays (Lal, 1988). In situ produced ^{10}Be and ^{26}Al in rock and sediment record the number of interactions between the atoms within the rock or sediment and the incoming cosmic radiation.

Because the interactions leading to nuclide production have been shown to occur at a known rate over time (Lal, 1988; Lal and Peters, 1967; Nishiizumi et al., 1989), the accumulation of ^{10}Be and ^{26}Al atoms in-situ can be used to approximate the near-surface residence time of rock or sediment, the duration of surface exposure, and rates of surface lowering (denudation) and sediment production (Lal, 1988, 1991; Nishiizumi et al., 1989).

For over a decade, researchers have used in situ produced cosmogenic nuclides to date specific geologic and geomorphic features or events and to quantify rates of specific geomorphic processes (Gosse and Phillips, 2001). Cosmogenic nuclides in rock have been used to date glacial events (Brown et al., 1991; Brook et al., 1993, 1995a,b, 1996; Gosse et al., 1995a,b; Ivy-Ochs et al., 1995; Davis et al., 1999; Bierman et al., 1999; Marsella et al., 2000; Phillips et al., 2000), volcanic eruptions (Shepard et al., 1995), landslides (Nichols et al., 2000) and alluvial fan deposits (Bierman et al., 1995b; Brown et al., 1998; Zehfuss et al., 2001). These nuclides have been used to determine recurrence intervals for earthquakes and to date and quantify tectonic offset (Bierman et al., 1995b; Ritz et al., 1995; Brown et al., 1998; Zehfuss et al., 2001). Additionally, cosmogenic nuclides have been used to date river and marine terraces (Anderson et al., 1996; Phillips et al., 1997; Repka et al., 1997; Hancock et al., 1999; Perg et al., 2001) and to determine rates of river incision (Burbank et al., 1996; Leland et al., 1998; Hancock et al., 1998; Granger et al., 1997, 2001a; Weissel and Seidl, 1998). More recently, cosmogenic nuclides in sediment have been used, to a limited extent, to determine basin-wide rates of sediment generation and basin denudation (Brown et al., 1995a; Granger et al., 1996; Small et al., 1999; Bierman et al., 2001; Clapp et al., 2000, 2001, 2002).

Bierman and Steig (1996), based on past works by Lal (1991), hypothesized that in situ produced nuclides in stream channel sediments could be used to determine basin-wide rates of denudation and sediment production. Because sediment transported and stored in stream channels is derived from erosion of upstream drainage basins, and these sediments are a mixture of sediments from upstream tributaries draining many smaller basins, the sediments leaving a drainage basin via a trunk stream should be representative

of eroding lithologies throughout a drainage. Furthermore, the sediments should carry ^{10}Be and ^{26}Al signatures that represent denudation rates of lithologies from throughout the drainage basin. Therefore, because for any sediment sample collected from a stream channel, there are many individual sediment particles most likely derived from many different locations throughout the basin, the measured isotopic abundance from a stream sediment sample has the potential to give a spatially integrated, average erosion rate for the entire basin.

The hypothesis presented by Bierman and Steig (1996) for the use of ^{10}Be and ^{26}Al in stream channel sediments as a tool to determine basin-wide rates of denudation and sediment generation included many assumptions necessary for successful application. The assumptions and limitations of such measurements and their interpretations are discussed in detail by Lal (1991), Bierman and Steig (1996), Brown et al. (1995), Granger et al., (1996), Clapp et al. (1997 and 1998), and Small et al. (1999).

Prior to the research conducted as part of this dissertation, several research groups (Small et al., 1999; Granger et al., 1996; Brown et al., 1995a;) had measured ^{10}Be and ^{26}Al in only a few, small drainages constrained by the strict set of assumptions and with little geologic variation. None of these previous studies tested the assumptions of the theory or the validity of the theory in basins of different scales, with heterogeneous lithologies and complex geology.

This dissertation specifically sets out to test the following hypotheses:

1.2 Research Questions

- Cosmogenic nuclide activities measured in sediments throughout a drainage basin can be used to infer baseline, long-term, denudation rates over landscapes of different scales.
- Cosmogenic nuclide activities can be used as a tracer to identify current, specific areas of landscape degradation within a larger landscape.
- Cosmogenic nuclide activities can be used to infer specific geomorphic processes that contribute sediment to drainage systems.
- Cosmogenic nuclide activities can be used to determine if a basin is in a long-term condition of steady state with respect to sediment generation and sediment yield.
- The grain size distribution of a sediment sample may significantly affect the results of a cosmogenic nuclide study in sediments, (i.e., different sediment grain sizes have different cosmogenic nuclide activities).
- The accuracy of cosmogenic exposure ages and erosion rates can be improved by correcting for the effects of changes in the strength of Earth's magnetic field.

1.3 Field-Based Studies

To test the hypotheses presented above, three field-based studies were carried out in arid regions, on drainage basins of different scales. Each of the study areas was of environmental, geological, or scientific interest to the parties responsible for managing the natural resources of the areas. The three study areas included: Arroyo Chavez Drainage basin (17.3 km²), located in central New Mexico; Yuma Wash Drainage Basin (187 km²), located in southern Arizona; and Nahal Yael Drainage Basin (0.62 km²), located in southern Israel (Figure 1-1).

In each of the study areas, we collected samples from throughout the drainage basin and from different geomorphic features (stream channels, stream banks, alluvial fans, hillslopes, and bedrock uplands) to test the hypothesis that the drainage network of a basin is a good integrator of sediments from throughout the basin. This spatial distribution of samples also allows us to show that cosmogenic nuclides can be used as tracers to identify specific sediment source areas within larger drainages and to show the relationship between lithology and sediment generation in different portions of a basin. Finally, our sampling method allows us to determine if a basin is generally in a long-term steady-state with respect to sediment production and sediment yield.

Arroyo Chavez

Arroyo Chavez is a tributary to the Rio Puerco and ultimately the Rio Grande. Rapid incision of arroyos in this region has led to destruction of roadways, lowering of groundwater tables below stream baseflows and below the pump intake levels of water supply wells, and to rapid sedimentation in larger rivers (Gellis et al., 2000; Gellis and

Elliott, 1998; Elliott et al., 1999). Throughout the semi-arid, southern Colorado Plateau, changes in climate and land use have significantly influenced landscape evolution and the onset of arroyo incision (Leopold et al., 1966; Bull, 1991; Gellis et al., 2000). Arroyo incision and subsequent backfilling form a cycle that has repeated itself several times in the past three millennia (Love and Young, 1983; Love, 1986; Gellis et al., 2000). Cycles of arroyo cutting and filling require a sediment source sufficient to re-fill the arroyo following periods of incision (Cooke and Reeves, 1976). There are two primary sources for this sediment; erosion of the uplands and aeolian input. Recent sediment-trap data (Gellis et al., 2000) indicate that the aeolian transport is responsible for less than 1% of the total sediment moving in our study area. Therefore, in the Arroyo Chavez study, we focus on rates of sediment generation from bedrock erosion in the uplands.

In order to quantify long-term sediment generation rates within Arroyo Chavez, we measured in-situ-produced cosmogenic ^{10}Be and ^{26}Al in the quartz fraction of 16 sediment and 3 bedrock samples. We use the drainage network of the basin as an integrator of sediment from throughout the basin and interpret ^{10}Be and ^{26}Al concentrations in stream channel sediments as representative of basin-wide average concentrations (Bierman and Steig, 1996). Our results demonstrate the value of cosmogenic nuclides in providing rapid estimates of long-term sediment generation rates and illustrate one of the many different spatial scales at which the method may be applied. The results of the work conducted at Arroyo Chavez are published in the journal *Quaternary Research*, in a manuscript entitled "Rates of Sediment Supply to Arroyos from Upland Erosion Determined Using In Situ Produced Cosmogenic ^{10}Be and ^{26}Al ". This manuscript is included as Chapter 2 of this document.

Nahal Yael

Nahal Yael is a small drainage basin (0.62 km²) in the Negev Desert of southern Israel. The Nahal Yael Drainage provides data from a hyper-arid climatic region and is in an area of concern to the countries of Israel and Jordan where sedimentation in the Gulf of Acaba presents great difficulties in shipping industries and in transport of water for agricultural uses. Erosion and sediment transport has been intensely studied in this basin over the past 33 years (Schick and Lekach, 1993). An earthen dam at the outlet of this drainage captures nearly 100% of the sediment leaving the drainage, thus providing an ideal location for comparison of long-term sediment generation and short-term sediment yield. Using 33 paired ¹⁰Be and ²⁶Al analyses collected in bedrock, hillslope colluvium, alluvial deposits, and stream channel sediments and a 33 yr sediment budget (Schick and Lekach, 1993), we determined long-term sediment generation rates, identified significant sediment sources, and tested for landscape steady state (Trimble, 1977; Brown et al., 1995; Clapp et al., 1997) in Nahal Yael. Additionally, the Nahal Yael basin is comprised of three distinct lithologies (Bull and Schick, 1979; Schick and Lekach, 1993), allowing us to test our methods in a geologically heterogeneous basin. The results of the work conducted at Nahal Yael are published in the journal *Geology*, in a manuscript entitled "Sediment Yield Exceeds Sediment Production in Arid Region Drainage Basins". This manuscript is included as Chapter 3 of this document.

Yuma Wash

Yuma Wash, an ephemeral tributary to the Colorado River, is located in the Sonoran Desert in southwestern Arizona. The Yuma Wash Drainage basin is of great

concern to the environmental managers of Yuma Proving Grounds who must balance the military's use and disturbance of the land with sedimentation issues in the Colorado River, disturbance of historically significant cultural sites, and disturbance of delicate arid-region ecosystems. Yuma Wash provides a test of our methods and assumptions on two scales. A small ($\sim 8 \text{ km}^2$) sub-basin gives a controlled study area to conduct our tests and apply the techniques developed for determining basin-wide sediment generation rates in small basins (Small et al., 1999; Bierman and Steig, 1996; Granger et al., 1996; Brown et al., 1995a). The larger, Yuma Wash drainage basin (187 km^2) provides a test of methods on a large scale and in an area with diverse lithologies. Evaluating the basin on two different spatial scales allows us to evaluate the effects of basin scale on the interpretation of cosmogenic nuclide concentrations measured in sediment

We measured ^{10}Be and ^{26}Al in 64 sediment and bedrock samples collected throughout the Yuma Wash drainage basin. From the measurements, we determine long-term, time-integrated rates of upland sediment generation and bedrock equivalent lowering. Nuclide concentrations, measured in channel sediment from tributaries of Yuma Wash and in samples collected along the length of the Wash were used to construct mixing models and determine sediment sources to the main-stem channel. Nuclide concentrations measured in individual geomorphic features within the sub-basin help to identify processes supplying sediment to the stream channels. The data are also evaluated to determine if there is a relationship between sediment grain size and nuclide concentration. The results of the work conducted at Yuma Wash are published in the journal *Geomorphology*, in a manuscript entitled "Using ^{10}Be and ^{26}Al to Determine

Sediment Generation Rates and Identify Sediment Source Areas in an Arid Region Drainage Basin". This manuscript is included as Chapter 4 of this document.

1.4 Correction of Cosmogenic Exposure Ages and Erosion Rates

The fifth chapter of this dissertation presents a computer model designed to quantify and correct cosmogenic exposure ages and erosion rates for the effects of varying nuclide production rates over time. Systematic uncertainties, inherent to the interpretation of cosmogenic nuclide measurements, make correlations with other dating systems uncertain (Clark et al., 1995; Dunai, 2001; Masarik et al., 2001; Shanahan and Zreda, 2000). The greatest uncertainties in determining cosmogenic exposure ages or erosion rates of samples for which exposure history is well constrained, are nuclide production rates as a function of time, altitude, and latitude. Recent work has begun to address altitude and latitude scaling for spallation (Dunai, 2000, Desilets and Zreda, 2001) and for muons (Stone, 2000). The model we present builds on the earlier works of Clark et al. (1995), Clapp and Bierman (1996), Nishiizumi et al. (1996), and Shanahan and Zreda (2000), which consider the effect of changing dipole field strength on nuclide production rates. The results of our corrections are compared to those of several other groups who have recently made similar corrections using different methodologies. The results of the geomagnetic correction model will be submitted for publication in the journal *Radiocarbon*, in a manuscript entitled "Correcting Cosmogenic Exposure Ages and Erosion Rates for Secular Variation in Earth's Magnetic Field Intensity". This manuscript is included as Chapter 5 of this document.

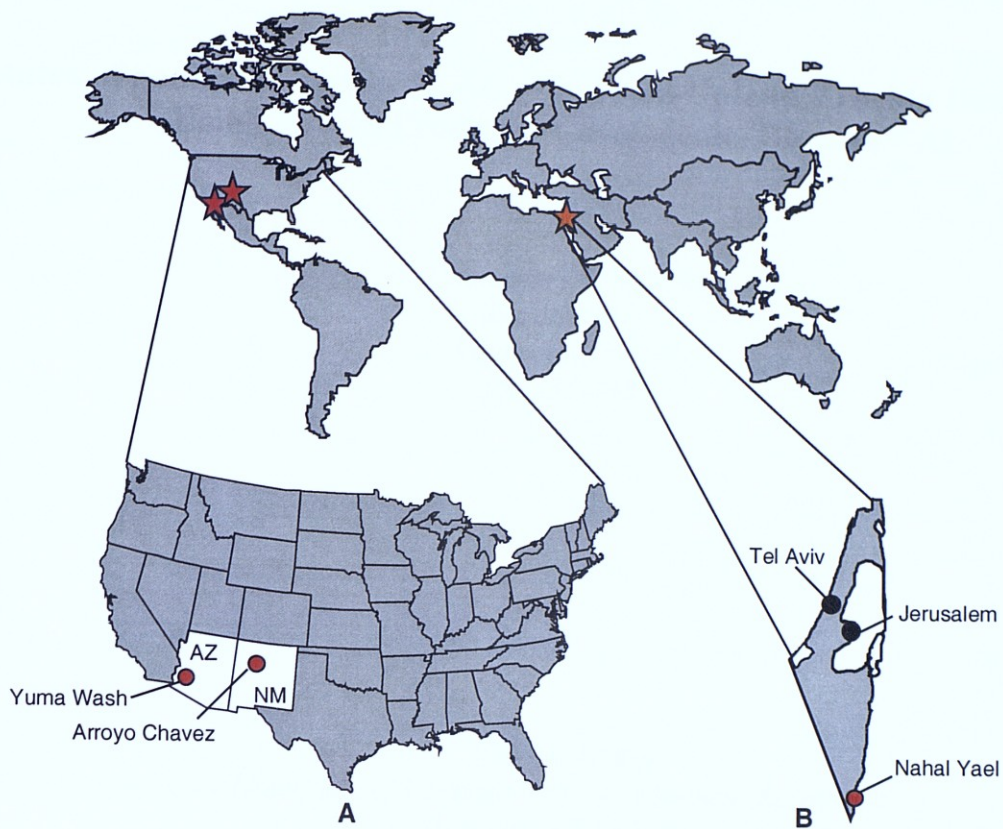


Figure 1-1. World map showing general study locations (red stars). Inset A is map of United States showing Yuma Wash and Arroyo Chavez study areas (red circles). Inset B is map of Israel showing Nahal Yael study area (red circle).

2.0 Arroyo Chavez Manuscript

Rates of Sediment Supply to Arroyos From Upland Erosion Determined Using In Situ Produced Cosmogenic ^{10}Be and ^{26}Al

Quaternary Research
March 2001,
Volume 55, No. 2
pp. 235-245

*Erik M. Clapp
University of Vermont, School of Natural Resources
Burlington VT 05401

Paul R. Bierman and Kyle K. Nichols
University of Vermont, School of Natural Resources and Department of Geology
Burlington VT 05401

Milan Pavich
United States Geological Survey, Reston VA, 22092

Marc Caffee
Center for Accelerator Mass Spectrometry
Lawrence Livermore National Laboratory, Livermore CA 94550

2.1 Abstract

Using ^{10}Be and ^{26}Al measured in sediment and bedrock, we quantify rates of upland erosion and sediment supply to a small basin in northwestern New Mexico. This and many other similar basins in the southwestern United States have been affected by cycles of arroyo incision and backfilling several times in the past few millennia. The sediment generation ($275 \pm 65 \text{ g m}^{-2} \text{ yr}^{-1}$) and bedrock equivalent lowering rates ($102 \pm 24 \text{ m myr}^{-1}$) we determine are sufficient to support at least three arroyo cycles in the past 3,000 years, consistent with rates calculated from a physical sediment budget within the basin and regional rates determined using other techniques. Nuclide concentrations measured in different sediment sources and reservoirs suggest that the arroyo is a good spatial and temporal integrator of sediment and associated nuclide concentrations from throughout the basin, that the basin is in steady state, and that nuclide concentration is independent of sediment grain size. Differences between nuclide concentrations measured in sediment sources and reservoirs reflect sediment residence times and indicate that sub-colluvial bedrock weathering on hillslopes supplies more sediment to the basin than erosion of exposed bedrock.

In order to quantify long-term sediment generation rates within Arroyo Chavez (Figures 1 and 2), a tributary of the Rio Puerco, we measured in-situ produced cosmogenic ^{10}Be and ^{26}Al in the quartz fraction of 16 sediment and 3 bedrock samples. We use the drainage network of the basin as an integrator of sediment from throughout

2.2 Introduction

Determining rates of sediment generation is important for understanding landscape evolution and landscape response to changes in climate and land use. On the semi-arid, southern Colorado Plateau, changes in climate and land use have significantly influenced landscape evolution (Leopold et al., 1966; Bull, 1991; Gellis et al., 2000). For example, during the Holocene, the Rio Puerco underwent multiple cycles of aggradation and gullying (Bryan, 1925; Love, 1986; Love and Young, 1983). The arroyo network of this 1600-km² basin last began incising during the late 1800's (Bryan, 1925; Aby, 1997; Gellis and Elliott, 1998); however, since ~ 1940, these arroyos, with the exception of some low order channels that continue to migrate headwards (Figure 1), have been aggrading (Gellis et al., 2000; Gellis and Elliott, 1998; Elliott et al., 1999)

Arroyo incision and subsequent backfilling form a cycle that has repeated itself several times in the past three millennia (Love and Young, 1983; Love, 1986; Gellis *et al.*, 2000). Cycles of arroyo cutting and filling require a sediment source sufficient to re-fill the arroyo following periods of incision (Cooke and Reeves, 1976). There are two primary sources for this sediment; erosion of the uplands and aeolian input. Recent sediment-trap data (Gellis et al., 2000) indicate that the aeolian transport is responsible for less than 1% of the total sediment moving in our study area. Therefore, in this paper we focus on rates of sediment generation from bedrock erosion in the uplands.

In order to quantify long-term sediment generation rates within Arroyo Chavez (Figures 1 and 2), a tributary of the Rio Puerco, we measured in-situ-produced cosmogenic ¹⁰Be and ²⁶Al in the quartz fraction of 16 sediment and 3 bedrock samples. We use the drainage network of the basin as an integrator of sediment from throughout

the basin and interpret ^{10}Be and ^{26}Al concentrations in stream channel sediments as representative of basin-wide average concentrations (Bierman and Steig, 1996). Our methods are better suited to determining long-term sediment generation rates than traditional sediment monitoring because the accumulation of nuclides integrates rates over thousands of years, a time span over which short-term (decadal) fluctuations in climate and sediment generation will not be significant. Our results demonstrate the value of cosmogenic isotopes in providing rapid estimates of long-term sediment generation rates and illustrate one of the many different spatial scales at which the method may be applied.

2.3 Geomorphic Setting

Arroyo Chavez occupies a small basin (17.3 km^2) on the Colorado Plateau $\sim 2 \text{ km}$ above sea level (Figure 2). The climate is semi-arid (mean annual precipitation, 377 mm , Gellis et al., 2000). Our study focuses on the headwaters, a 1.1-km^2 sub-basin underlain primarily by homogeneous, arkosic sandstone. The basin is characterized by more resistant, flat-lying sandstones that form mesa tops, overlying less resistant, hillslope-forming sandstones and shales (Figure 3).

Regolith is present on most hillslope and mesa surfaces. The mesa tops have a thin, 0- to 20-cm veneer of fine-grained, quartz-rich sand and silt ($69\% < 2000 \mu\text{m}$). The hillslopes have similar colluvial deposits generally less than 30 cm deep ($\mu = 15.3 \pm 14.3 \text{ cm}$, $n=50$); bedrock hollows contain deposits as deep as 90 cm. At the base of some hillslopes, gently sloping alluvial fans have formed ($<5 \text{ m}$ thick). The fan deposits are

weakly stratified, are the same color and texture as the hillslope colluvium, and do not contain distinct paleosols, thus suggesting rapid or steady aggradation.

Material shed from the basin hillslopes is deposited on alluvial fans and on the valley bottom. The valley fill is < 5 m thick based on bedrock outcrops observed at the bottom of the arroyo. The channel is 1 to >4 m wide. The basin alluvium comprises alternating layers of fine sand, medium to coarse sand, and coarse sand with occasional pebbles. It is weakly cemented by calcium carbonate, crudely stratified, and there are no distinct soil horizons.

2.4 In-Situ-Produced Cosmogenic Isotopes in Sediments

^{10}Be and ^{26}Al are produced in quartz from the interaction of secondary cosmic rays (primarily high-energy neutrons) with Si and O (Lal, 1988). These cosmogenic radionuclides accumulate most rapidly in sediment and bedrock residing at or near Earth's surface (< 3 m depth); accumulation or "production" rates decrease exponentially with depth (Lal, 1988). An inverse relationship exists between the rate at which sediment is being generated and transported from a drainage basin (erosion) and the concentration of in-situ-produced cosmogenic nuclides in that sediment (Lal, 1991; Brown et al., 1995a; Bierman and Steig, 1996; Granger et al., 1996). The relationship between nuclide concentration and sediment generation rate has been quantified using interpretive models (Lal, 1991; Bierman and Steig, 1996); nuclide measurements have been used to estimate time-integrated rates of sediment generation, bedrock lowering, and sediment yield (e.g., Bierman and Turner, 1995; Brown et al., 1995a; Granger et al., 1996; Small et al., 1999).

The Arroyo Chavez basin can be thought of as a series of reservoirs (hillslope colluvium, alluvial fan sediment, basin alluvium, and channel sediment) through which sediment flows en-route from bedrock source areas to the basin outlet (Figure 3). During transport and storage, nuclides accumulate and record the relative time of sediment residence. We measured ^{10}Be and ^{26}Al concentrations in individual reservoirs to test assumptions used to interpret cosmogenic nuclide concentrations in sediment.

Differences between nuclide concentrations in different reservoirs can be used to track sediment contributions.

The interpretive model used to determine sediment generation rates from cosmogenic nuclides measured in sediments (Brown et al., 1995a; Bierman and Steig, 1996; Granger et al., 1996) is based on a balance between nuclides produced in or entering a drainage basin and those leaving the basin (Figure 4). To calculate meaningful sediment generation rates from nuclide abundances, two assumptions must be valid: the total reservoir of cosmogenic nuclides (C) within the basin must remain constant over time (steady state) and the sediment leaving the basin must be well mixed.

2.5 Methods

Sample Collection

Sediment and bedrock samples were collected from the reservoirs described in the previous sections (Table 1, Figures 2 and 3). We collected three bedrock samples from ridges surrounding the sub-basin. Three evenly spaced sediment samples were collected along a hillslope transect 320 m long; each was an integration of the 10- to 20-cm depth of hillslope colluvium; we assumed complete mixing of sediment would occur for such

shallow cover. Four homogenized sediment samples were collected from different sites along the bottom of the active stream channel (Figure 2). Additionally, four alluvial fan sediment samples were collected from a 4-m-deep vertical profile (Figure 2). Fan samples were collected at approximately 100-cm depth increments, each sample was integrated over a 10-cm depth range. A similar 3.8-m-deep profile was sampled where the basin alluvium was exposed by the main stem of Arroyo Chavez (Figure 2).

Sample Preparation

All sediment samples were pre-washed in HCl to remove carbonate. Four samples (ECAC-11, -14, -19A, and -19D) were sieved to test the relationship between grain size and nuclide concentration. The remaining twelve sediment samples were sieved to yield only the 250- to 1000- μm size fraction (sediment grain size data is included in Appendix A). All particles smaller than 125 μm were discarded to minimize aeolian contribution (Reheis and Kihl, 1995). Samples were heated and ultrasonically etched to isolate 20 to 30 g of pure quartz (Kohl and Nishiizumi, 1992), which was dissolved in HF containing 250 μg of Be carrier. Be and Al were then isolated using ion chromatography and isotopic ratios were determined by accelerator mass spectrometry at Lawrence Livermore National Laboratory. Al was measured in duplicate aliquots by Inductively Coupled Argon Plasma Spectrometry – Optical Emission.

Data Interpretation

The ^{10}Be and ^{26}Al measured in 26 samples from 19 locations (Tables 1, 2, and Figure 5) are well correlated. The time scale over which our samples could have been

buried is too short to affect the $^{26}\text{Al}/^{10}\text{Be}$ ratio, thus the ^{26}Al measurements can be considered replicates of the ^{10}Be measurements. Both the ^{10}Be and ^{26}Al measurements are used in the calculation of average erosion and sediment generation rates. To streamline data presentation, our discussion focuses on the ^{10}Be data.

Production rates of 6.03 and 36.8 (atoms $\text{g}^{-1} \text{yr}^{-1}$) for ^{10}Be and ^{26}Al , respectively (Nishiizumi et al., 1989), were used in calculation of erosion rates. The production rates were scaled for latitude and elevation according to Lal (1991), assuming no muon production (Brown et al., 1995b) and 20% uncertainty (Clark et al., 1995). No corrections have been made for quartz enrichment (Small et al., 1999) as our quartz-yield data indicate ~25% quartz content for bedrock samples and ~22% for sediment samples. All statistical comparisons were made using a confidence interval of 90% and independent, t-tests assuming unequal variance (Ott, 1993).

2.6 Results and Discussion

Isotopic data indicate that Arroyo Chavez sediment is well mixed and that the basin is in steady state. Based on this evidence, we use the data to determine basin-wide sediment generation rates.

Model Evaluation

Fluvial Integration of Basin Sediments. Sediments generated from the upland hillslopes and bedrock outcrops are mixed together by bioturbation, rain splash, and freeze-thaw. In the Arroyo Chavez Basin, there are few direct pathways for upland sediment to enter the main stem of the arroyo without first mixing with hillslope colluvium. Mixing and

integration of sediment and associated nuclides continues as material is transported and deposited in alluvial fans and valley alluvium. As the channel meanders across the basin, the arroyo incises through the basin alluvium, and arroyo walls collapse into the channel (at the time of sampling, more than five recent wall failures and hundreds of subsurface pipes were observed along the channel above the sampling sites). Subsurface piping removes sediment from the valley fill and delivers it to the arroyo channel. These processes mix sediment from much of the width and depth of the basin as well as the length of the channel. Therefore, the channel-sediment nuclide concentration and the resultant erosion and sediment generation rates we calculate are integrated both spatially (as described above) and temporally by cutting through the depth profile that represents a long-term record of nuclide concentrations.

The ^{10}Be data we have collected are consistent with the above description. The average ^{10}Be concentration measured in the stream-channel sediment ($1.57 \pm 0.18 \times 10^5$ atoms g^{-1}) is statistically indistinguishable from the average concentration of the basin alluvium profile samples, weighted by percent of profile depth ($1.36 \pm 0.09 \times 10^5$ atoms g^{-1}). Additionally, there are no significant differences between the nuclide concentration of the channel sediment and other sediment reservoirs throughout the basin (Table 2) with the exception of the alluvial fan, which occupies only a small portion (<3%) of the basin. Channel-sediment nuclide concentrations are thus representative of basin-wide sediment nuclide concentrations.

Steady State Erosion and Nuclide Inventory. Calculation of basin-wide erosion rates, from sediment nuclide concentrations in well-mixed alluvium, requires that a basin have

a steady state nuclide inventory for which the flux of nuclides into the basin equals the flux out (Bierman and Steig, 1996). A basin with a steady state nuclide inventory (constant C) must be losing sediment mass (m) and associated nuclides at a constant rate (steady state erosion). Although we cannot directly determine if a basin has a steady state nuclide inventory, we can use steady state erosion as a proxy. Several lines of evidence suggest that the Arroyo Chavez basin is eroding steadily: down-basin isotopic homogeneity, depth-profile isotopic homogeneity, and steady state deposition of basin alluvium.

Down-Basin Isotopic Homogeneity. Isotopic concentrations in sediment reservoirs throughout the Arroyo Chavez basin are similar (Table 2 and Figure 5) suggesting steady state erosion without long periods of storage. Particles systematically approach the landscape surface and accumulate nuclides at similar rates throughout the basin. Differences in isotopic concentrations between sample locations can be attributed to slight, local variations (at the 100-m² scale) in erosion rates related to differences in lithology, catchment size, and slope. Slightly higher nuclide concentrations in basin alluvium ($1.36 \pm 0.09 \times 10^5$ atoms g⁻¹) and channel sediment ($1.57 \pm 0.18 \times 10^5$ atoms g⁻¹) compared to hillslope colluvium ($1.10 \pm 0.18 \times 10^5$ atoms g⁻¹) are likely the effect of nuclide accumulation integrated over several thousands of years following deposition.

By contrast, a basin that was undisturbed by erosion for thousands of years (i.e., a long period of nuclide accumulation), and was only recently stripped of its upland sediment cover, should have deposits of high-concentration sediment in alluvial-fan and basin alluvium, leaving newly exposed (previously shielded from cosmic rays), low-concentration bedrock and sediment in the uplands. However, exposed bedrock surfaces

in the Arroyo Chavez basin have higher average nuclide concentrations ($1.89 \pm 0.37 \times 10^5$ atoms g^{-1}) than other reservoirs. Fan deposits have lower average nuclide concentrations ($0.87 \pm 0.07 \times 10^5$ atoms g^{-1}), uncharacteristic of material that has been exposed for long periods of time and then stripped from the landscape prior to deposition.

Depth Profile Isotopic Homogeneity. Nuclide concentrations in depth profiles of the alluvial deposits will record substantial changes in nuclide concentrations if erosion rates change over time. The basin alluvium profile (Figure 6A) displays a regular increase in nuclide concentration with depth, consistent with post-depositional nuclide accumulation rather than substantial, erratic changes in concentration indicative of changes in basin-wide erosion rates over time.

Steady State Deposition. A basin eroding at a constant rate will accumulate sediment at a constant rate, if the rate of sediment generation is faster than the rate of sediment export. Isotopic data collected from the basin alluvium profile are consistent with steady state deposition. We use the constant-deposition model (equation 1) of Lal and Arnold (1985) to approximate isotopic concentrations in sediments deposited in the basin over time.

$$N = C_i + \frac{P_0 \Lambda}{s \rho} (1 - e^{-(hp / \Lambda)}) \quad (\text{eq.1})$$

In this relationship, nuclide concentration (N atoms g^{-1}) at a given depth (h cm) is a function of the initial nuclide concentration (C_i atoms g^{-1}), the production rate at the

surface (P_o atoms $\text{g}^{-1} \text{yr}^{-1}$), the characteristic attenuation coefficient for fast neutrons (Λ g cm^{-2}), the density of the overlying material (ρ g cm^{-3}) and the rate of sediment accumulation (s cm yr^{-1}).

Following deposition, grains of sediment continue to accumulate nuclides until buried deeply enough (200 to 300 cm) to shield them from cosmic rays. Steady state deposition produces a nuclide depth profile which is constant at depths greater than ~ 200 cm; nuclide abundance decreases with decreasing depth of burial (Figure 7A). The basin alluvium depth profile we measured (Figure 6A) is consistent with steady state deposition and therefore steady rates of sediment generation.

Assuming the nuclide abundance at the time of deposition was greater than or equal to the lowest concentration measured throughout the basin ($\sim 0.66 \times 10^5$ atoms g^{-1} , ECAC 14-1), we produced a series of curves representing model depth profiles at different sediment accumulation rates (Figure 8). By visually fitting the measured data to the curves, we find the data correlate best with the curve representing a minimum limiting deposition rate of 280 m myr^{-1} ($\rho=1.6$ g cm^{-3}), equivalent to 165 m myr^{-1} of upland bedrock erosion ($\rho=2.7$ g cm^{-3}). This bedrock equivalent erosion rate is within one standard deviation of other estimates (Dethier et al., 1988; Gellis et al., 2000) and the calculations we describe later in this discussion (Table 3). The deposition rate we estimate indicates that sediment accumulation in the basin began $\sim 13,000$ yr B.P., consistent with Late Pleistocene/Early Holocene changes in climate and associated hydrologic controls on sediment generation and transport (Bull, 1991).

Although our model suggests steady state erosion over the depositional history of the basin, our solution is not a unique explanation of the data. A systematic increase in

rates of sediment deposition related to increased basin-wide erosion rates could account for the lower nuclide concentrations near the profile top. Alternatively, a recent stripping event depositing up to 100 cm of sediment in the basin could result in greater nuclide concentrations low in the profile (post depositional nuclide accumulation) while recently deposited sediments near the top of the profile would have lower nuclide concentrations similar to the hillslope colluvium. However, stripping of the uplands would leave behind low-concentration (previously shielded) sediment and bedrock. The upland bedrock surfaces have the highest nuclide concentrations in the basin suggesting long-term upland stability.

On a smaller scale, the isotopic profile data collected from the alluvial fan show little variation with depth (Figure 6) suggesting rapid, recent deposition. Several radiocarbon dates taken in the alluvial fan profile (M. Pavich, USGS, previously unpublished data) demonstrate that the uppermost 300 cm were deposited in the last 1760 ± 60 ^{14}C yr B.P. (Figure 6). Although the average ^{10}Be concentration of the fan sediment is lower than the average of the hillslope colluvium, hillslope samples collected directly above the fan (ECAC14-1, -2, and -3), in an area of active incision, have average nuclide concentrations ($0.74 \pm 0.05 \times 10^5$ atoms g^{-1}) indistinguishable from the average fan nuclide concentrations ($0.87 \pm 0.07 \times 10^5$ atoms g^{-1}). These data illustrate the localized variations in erosion rates at the 100-m^2 scale that are integrated by arroyo cycling. Although our data do not unequivocally prove steady state erosion or a steady state nuclide inventory, the three lines of evidence presented above indicate that the steady state assumption is reasonable over the $\sim 13,000$ -yr depositional history of the basin alluvium.

Lack of Grain Size Dependence

Arroyo Chavez data indicate that nuclide concentrations are independent of sediment grain size (Figure 9). These data are consistent with measurements from other locations (Granger et al., 1996; Clapp et al., 2000); however, Brown et al. (1995a) found that the ^{10}Be concentration in river sediment from the Luquillo Experimental Forest, Puerto Rico, was inversely proportional to grain size due to different erosional mechanisms responsible for generating and transporting material of different sizes. Together, these studies suggest that the geomorphic processes such as mass wasting or deep-seated land slides likely result in nuclide dependence on grain size. In a semi-arid drainage, where sediments of many different sizes move by the slow processes of soil creep and surface wash, differential transport is less likely to occur and thus nuclide abundances are largely independent of grain size.

Erosion Rates, Sediment Generation, and Arroyo Cycling

Using cosmogenic ^{10}Be and ^{26}Al data, we have calculated basin-wide, time-integrated rates of sediment generation for the Arroyo Chavez basin (Table 3). We present erosion rates as bedrock-equivalent lowering rates for comparison with other studies. The basin-wide average erosion rate of $102 \pm 24 \text{ m myr}^{-1}$ (determined from arroyo channel sediments) is less than the rate determined by Gellis and Aby (1998) from sediment traps on the Arroyo Chavez Basin hillslopes ($146 \pm 25 \text{ m myr}^{-1}$) but similar to that determined by Dethier et al. (1988), who calculated retreat rates on hypsometric profiles of weakly lithofied sandstones in the nearby Western Espanola Basin ($\sim 100 \text{ m}$

myr⁻¹). The difference between the nuclide-based erosion rate and the sediment-budget erosion rate (Gellis et al., 2000) probably illustrates the importance of integration time (10¹ vs. 10³ yr) and scale (m² vs. 100m²). Interestingly, the nuclide-based erosion rate determined only from hillslope colluvium samples (149 ± 51 m myr⁻¹) is very similar to that of Gellis and Aby (146 ± 25 m myr⁻¹).

The erosion rate we have determined for Arroyo Chavez (102 ± 24 m myr⁻¹) is substantially greater than bedrock rates measured in more arid regions, with more erosion resistant bedrock, and less soil development such as south-central Australia ~ 0.6 to 6 m myr⁻¹ (Bierman and Turner, 1995) and Antarctica ~ 0.1 to 1.0 m myr⁻¹ (Nishiizumi et al., 1991). Our higher erosion rates are consistent with an easily eroded lithology in a slightly wetter climate (semi-arid) and in a location where mechanical weathering is more prevalent. Our estimates are also consistent with more general, large-scale rates determined for the Colorado Plateau of 165 m myr⁻¹ and 83 m myr⁻¹ by Judson and Ritter (1964) and Holeman (1968), respectively.

Both our cosmogenic data and the physical data collected by Gellis and Aby (1998), indicate that hillslopes are eroding faster than more resistant bedrock uplands. The average nuclide activity in bedrock outcrops (1.89 ± 0.37 x 10⁵ atoms g⁻¹) is greater (90% confidence) than that of hillslope samples (1.10 ± 0.18 x 10⁵ atoms g⁻¹), as would be expected when comparing the most resistant materials in the basin (mesa-forming sandstones) to less resistant materials (slope-forming interbedded sandstones and shales). Based on the isotopic evidence for higher hillslope erosion rates and the greater basin slope area than outcrop area (< 5% of the basin contributing area is exposed bedrock), our measurements indicate that bedrock-to-soil conversion on the hillslopes generates

substantially more sediment within the basin than does erosion of bedrock outcrops. Our findings of greater rates of regolith production beneath a cover of colluvium are consistent with previous works (Gilbert, 1877; Bull, 1991; and Small et al., 1999) suggesting that, in more arid environments, colluvium retains moisture from infrequent precipitation events that, when held in contact with bedrock, facilitates chemical and mechanical weathering. In more humid regions, such as those described by Heimsath et al. (1997 and 1999), colluvium appears to hinder the production of regolith.

We have calculated a basin-wide, average sediment generation rate ($275 \pm 65 \text{ g m}^{-2} \text{ yr}^{-1}$) based on nuclide concentrations in channel sediment. Using the present-day sediment-contributing area of the basin (0.51 km^2) and an estimated maximum sediment volume of the present-day arroyo cut ($\sim 20,000 \text{ m}^3$, length of the arroyo and tributaries multiplied by average width and depth of the channel), the total volume of sediment generated ($88 \text{ m}^3 \text{ yr}^{-1}$ based on a sediment density of 1.6 g cm^{-3}) is sufficient to fill the present-day arroyo approximately once every 230 years. This calculation assumes that no sediment is exported from the basin during filling (e.g., a 100% trapping efficiency) and that the net aeolian contribution is negligible (estimated at $< 1\%$ by Gellis and Aby (1998)). However, estimates of even 50% to 75% sediment export would allow arroyo backfilling roughly every 1000 years. Our data therefore show that in this small, high-elevation, semi-arid basin, sufficient sediment is generated from the hillslopes to fill the current arroyo and perpetuate the arroyo cycles that have recurred several times during the past 3000 years (Elliott et al., 1999).

2.7 Conclusions

Measurements of ^{10}Be and ^{26}Al in the sediment and bedrock of the Arroyo Chavez basin indicate that the basin is in long-term erosional steady state, that fluvial sediment is isotopically representative of the basin as a whole, that grain size does not control nuclide abundance, and that sufficient sediment is produced ($275 \pm 65 \text{ g m}^{-2} \text{ yr}^{-1}$) to support rapid arroyo cycling. The long-term bedrock-equivalent basin-scale lowering rate ($102 \pm 24 \text{ m myr}^{-1}$) we calculate is in good agreement with other regional denudation estimates and local short-term measurements of sediment generation. Differences in nuclide concentrations measured in bedrock and hillslope colluvium indicate that weathering of sub-colluvial bedrock generates more sediment than weathering of exposed bedrock.

2.8 Acknowledgements

U.S. Geological Survey grant # HQ96AG01589, NSF grant # EAR-9628559, and Department of Energy contract # W-7405-ENG-48 supported this work. We thank M. Abbott, A. Gellis, and S. Aby for field assistance, S. Nies and K. Marsella for lab assistance, E.A. Cassell, R. Stanley, D. Wang, S. Gran, A. Noren, K. Jennings, and D. Santos for reviews, and J. Sevee and P. Maher for support.

2.9 References Cited

- Aby, S. B., 1997, Date of channel trenching (arroyo cutting) in the arid Southwest revisited: Geological Society of America Abstracts with Programs, v. 29, p. 373.
- Bierman, P., and Steig, E., 1996, Estimating rates of denudation and sediment transport using cosmogenic isotope abundances in sediment: Earth Surface Processes and Landforms, v. 21, p. 125-139.
- Bierman, P. R., and Turner, J., 1995, ^{10}Be and ^{26}Al evidence for exceptionally low rates of Australian bedrock erosion and the likely existence of pre-Pleistocene landscapes: Quaternary Research, v. 44, p. 378-382.
- Brown, T. B., Stallard, R. F., Larsen, M. C., Raisbeck, G. M., and Francoise, Y., 1995a, Denudation rates determined from accumulation of in situ-produced ^{10}Be in the Luquillo Experimental Forest, Puerto Rico: Earth and Planetary Science Letters, v. 129, p. 193-202.
- Brown, E. J., Bourles, D. L., Colin, F., Raisbeck, G. M., Yiou, F., and Desgarceaux, S., 1995b, Evidence for muon-induced production of ^{10}Be in near surface rocks from the Congo: Geophysical Research Letters, v. 22, p. 703-706.
- Bryan, K., 1925, Date of channel trenching in the arid Southwest: Science, v. 62, p. 338-344.
- Bull, W. B., 1991, "Geomorphic Responses to Climate Change." Oxford University Press, New York, 326 p.
- Clapp, E. M., Bierman, P. R., Schick, A. P., Lekach, J., Enzel, Y., and Caffee, M., 2000, Sediment yield exceeds sediment production in arid region drainage basins: Geology, v. 28, p. 995-998.
- Clark, D. H., Bierman, P. R., and Larsen, P., 1995, Improving in situ cosmogenic chronometers: Quaternary Research, v. 44, p. 366-376.
- Cooke, R. U., and Reeves, R. W., 1976, "Arroyos and Environmental Change in the American Southwest." Clarendon Press, Oxford, 295 p.
- Dethier, D. P., Harrington, C.D., and Aldrich, M.J., 1988, Late Cenozoic rates of erosion in the western Espanola basin, New Mexico - Evidence from geologic dating of erosion surfaces: Geological Society of America Bulletin, v. 100, p. 928-937.
- Elliott, J. G., Gellis, A. C., and Aby, S. B., 1999, Evolution of arroyos: Incised channels of the southwestern United States: In "Incised River Channels." (S. E. Dorby, and A. Simon, Eds.), John Wiley and Sons, Chinchester, pp. p. 153-185.
- Gellis, A.C. Pavich, M.J., Bierman, P.R., Ellwein, A., Aby, S., Clapp, E.M., 2000, Measuring erosion rates using modern geomorphic and isotopic measurements in

- the Rio Puerco, New Mexico: Geological Society of America Abstracts with Programs, v. 32, p. 207.
- Gellis, A. C., and Elliott, J. G. ,1998, Arroyo changes in selected watersheds of New Mexico, United States. In "Applying Geomorphology to Environmental Management, a special publication honoring Stanley A. Schumm." (M. Harvey, and D. Anthony, Eds.), Water Resources Publications, LLC, Highlands Ranch, Colorado pp. p. 271-284.
- Gilbert, G. K. ,1877, Geology of the Henry Mountains (Utah): US Geographical and Geological Survey of the Rocky Mountains Region, 160 pp.
- Granger, D. E., Kirchner, J. W., and Finkel, R. ,1996, Spatially averaged long-term erosion rates measured from in-situ produced cosmogenic nuclides in alluvial sediment: *Journal of Geology*, v. 104, p. 249-257.
- Heimsath, A. M., Dietrich, W. E., Nishiizumi, K., and Finkel, R. C. ,1999, Cosmogenic nuclides, topography, and the spatial variation of soil depth: *Geomorphology*, v. 27, p. 151-172.
- Heimsath, A. M., Dietrich, W. E., Nishiizumi, K., and Finkel, R. C. ,1997, The soil production function and landscape equilibrium: *Nature*, v. 388, p. 358-361.
- Holeman, J. N. ,1968, The sediment yield of major rivers of the world: *Water Resources Research*, v. 4, p. 737-747.
- Judson, S., and Ritter, D. F. ,1964, Rates of regional denudation in the United States: *Journal of Geophysical Research*, v. 69, p. 3395-3401.
- Kohl, C. P., and Nishiizumi, K. ,1992, Chemical isolation of quartz for measurement of in-situ-produced cosmogenic nuclides: *Geochemica et Cosmochemica Acta*, v. 56, p. 3583-3587.
- Lal, D. ,1988, In situ-produced cosmogenic isotopes in terrestrial rocks: *Annual Reviews of Earth and Planetary Science*, v. 16, p. 355-388.
- Lal, D. ,1991, Cosmic ray labeling of erosion surfaces: In situ production rates and erosion models: *Earth and Planetary Science Letters*, v. 104, p. 424-439.
- Lal, D., and Arnold, J. R. ,1985, Tracing quartz through the environment: *Proceedings of the Indian Academy of Science (Earth and Planetary Science)*, v. 94, 1-5.
- Leopold, L. B., Emmett, W.W., and Myrick, R.M. ,1966, Channel and hillslope processes in a semiarid area, New Mexico: U.S. Geological Survey Professional Paper, 352-G, p. 193-253.

- Love, D. W. ,1986, A geological perspective of sediment storage and delivery along the Rio Puerco: In "Drainage Basin Sediment Delivery." (R. F. Hadley, Ed.), IAHS Publication 159, Wallingford, UK, p. 305-322.
- Love, D. W., and Young, J. D. ,1983, Progress report on the late Cenozoic geologic evolution of the lower Rio Puerco: In "New Mexico Geological Society Guidebook 33, Socorro Region II." (S.G. Wells, J.A. Grambling, and J.F. Calender, Eds.), p. 277-284.
- Nishiizumi, K., Kohl, C. P., Arnold, J. R., Klein, J., Fink, D., and Middleton, R. ,1991, Cosmic ray produced ^{10}Be and ^{26}Al in Antarctic rocks: exposure and erosion history: Earth and Planetary Science Letters, v. 104, p. 440-454.
- Nishiizumi, K., Winterer, E. L., Kohl, C. P., Klein, J., Middleton, R., Lal, D., and Arnold, J. R. ,1989, Cosmic ray production rates of ^{10}Be and ^{26}Al in quartz from glacially polished rocks: Journal of Geophysical Research, v. 94, p. 17907-17915.
- Ott, R. L. ,1993, "An Introduction to Statistical Methods and Data Analysis." Wadsworth Publishing Co., Belmont, California, 1049 p.
- Reheis, M. C., and Kihl, R. ,1995, Dust deposition in southern Nevada and California, 1984-1989: relations to climate, source area and source lithology: Journal of Geophysical Research, v. 100, p. 8893-8918.
- Sharma, P., and Middleton, R. ,1989, Radiogenic production of ^{10}Be and ^{26}Al in uranium and thorium ores: Implications for studying terrestrial samples containing low levels of ^{10}Be and ^{26}Al : Geochimica et Cosmochimica Acta, v. 53, p. 709-716.
- Small, E. E., Anderson, R. S., and Hancock, G. S. ,1999, Estimates of the rate of regolith production using ^{10}Be and ^{26}Al from an alpine slope: Geomorphology, v. 27, p. 131-150.
- U.S. Geological Survey ,1961, San Luis, New Mexico Quadrangle: USGS, Reston, Virginia.
- York, D., ,1969, Least squares fitting of a straight line with correlated errors: Earth and Planetary Science Letters, v. 5, p. 320-324.

Table 2-1. Locations and descriptions of samples from Arroyo Chavez Basin New Mexico.

sample	*latitude	*longitude	⁺ elevation (km)	sample type	grain size (microns)
ECAC 1	N35°42.301'	W107°06.063'	2.030	bedrock	not applicable
ECAC 4	N35°42.106'	W107°06.487'	2.042	bedrock	not applicable
ECAC 6	N35°42.359'	W107°06.619'	2.042	bedrock	not applicable
ECAC 8-2	N35°40.163'	W107°05.415'	1.951	channel sediment	500-1000
ECAC 9	N35°41.565'	W107°06.018'	1.963	channel sediment	>250
ECAC 10	N35°41.941'	W107°06.068'	1.972	channel sediment	>250
ECAC 11-1	N35°42.246'	W107°06.415'	1.978	channel sediment	125-500
ECAC 11-2	N35°42.246'	W107°06.415'	1.978	channel sediment	500-1000
ECAC 11-3	N35°42.246'	W107°06.415'	1.978	channel sediment	>1000
ECAC 12	N35°42.179'	W107°06.652'	2.006	hillslope colluvium	>250
ECAC 14-1	N35°42.188'	W107°06.610'	2.003	hillslope colluvium	125-500
ECAC 14-2	N35°42.188'	W107°06.610'	2.003	hillslope colluvium	500-1000
ECAC 14-3	N35°42.188'	W107°06.610'	2.003	hillslope colluvium	>1000
ECAC 16	N35°42.211'	W107°06.557'	1.998	hillslope colluvium	>250
ECAC 19A-1	N35°42.271'	W107°06.423'	1.984	basin alluvium	125-500
ECAC 19A-2	N35°42.271'	W107°06.423'	1.984	basin alluvium	500-1000
ECAC 19C	N35°42.271'	W107°06.423'	1.985	basin alluvium	>250
ECAC 19D-1	N35°42.271'	W107°06.423'	1.986	basin alluvium	125-500
ECAC 19D-2	N35°42.271'	W107°06.423'	1.986	basin alluvium	500-1000
ECAC 19E	N35°42.271'	W107°06.423'	1.986	basin alluvium	>250
ECAC 19G	N35°42.271'	W107°06.423'	1.987	basin alluvium	>250
ECAC 19G-3	N35°42.271'	W107°06.423'	1.987	basin alluvium	>1000
ECAC 20A	N35°42.271'	W107°06.423'	1.991	alluvial fan sediment	>250
ECAC 20B	N35°42.271'	W107°06.423'	1.992	alluvial fan sediment	>250
ECAC 20C	N35°42.271'	W107°06.423'	1.992	alluvial fan sediment	>250
ECAC 20E	N35°42.271'	W107°06.423'	1.995	alluvial fan sediment	>250

* measured using Garmin 75 handheld GPS

⁺ measured using handheld altimeter calibrated to local benchmark

Table 2-2. Concentrations of ^{10}Be and ^{26}Al measured in samples from Arroyo Chavez Basin, New Mexico.

Sample	^{10}Be (10^5 atoms g^{-1})	^{26}Al (10^5 atoms g^{-1})
BEDROCK OUTCROPS		
ECAC1	1.19 ± 0.07	7.43 ± 0.53
ECAC4	2.48 ± 0.12	15.70 ± 1.15
ECAC6	1.98 ± 0.09	12.82 ± 0.75
Average	1.89 ± 0.37	11.98 ± 2.42
[#] bedrock nuclide abundance > hillslope ($P=0.08$) and fan ($P=0.06$)		
HILLSLOPE COLLUVIUM		
ECAC12	1.31 ± 0.08	8.07 ± 0.57
ECAC14-1	0.66 ± 0.15	4.99 ± 0.47
ECAC14-2	0.82 ± 0.11	3.80 ± 0.39
ECAC14-3	0.75 ± 0.14	4.11 ± 0.44
ECAC16	1.24 ± 0.12	7.02 ± 0.47
* Average	1.10 ± 0.18	6.46 ± 1.12
[#] hillslope nuclide abundance < bedrock ($P=0.08$) and channel ($P=0.06$)		
ALLUVIAL FAN PROFILE		
ECAC20A	0.76 ± 0.06	4.69 ± 0.36
ECAC20B	1.09 ± 0.06	6.42 ± 0.43
ECAC20C	0.80 ± 0.06	4.90 ± 0.38
ECAC20E	0.89 ± 0.06	5.24 ± 0.40
+ Average	0.87 ± 0.07	5.23 ± 0.38
[#] fan nuclide abundance < bedrock ($P=0.06$), basin ($P=0.001$), and channel ($P=0.01$)		
BASIN ALLUVIUM PROFILE		
ECAC19A-1	1.76 ± 0.17	9.78 ± 0.75
ECAC19A-2	1.36 ± 0.21	10.53 ± 1.05
ECAC19C	1.55 ± 0.10	9.46 ± 0.60
ECAC19D-1	1.46 ± 0.13	9.65 ± 0.73
ECAC19D-2	1.62 ± 0.08	9.38 ± 0.66
ECAC19E	1.37 ± 0.09	8.73 ± 0.77
ECAC19G	1.16 ± 0.07	6.13 ± 0.45
ECAC19G-3	0.97 ± 0.17	6.99 ± 0.71
** Average	1.36 ± 0.09	8.51 ± 0.62
[#] basin nuclide abundance > fan ($P=0.06$)		
ARROYO CHANNEL SEDIMENTS		
ECAC8-2	1.74 ± 0.09	10.07 ± 1.05
ECAC9	1.35 ± 0.06	8.44 ± 0.58
ECAC10	1.98 ± 0.09	12.19 ± 1.04
ECAC11-1	1.30 ± 0.10	7.05 ± 0.53
ECAC11-2	1.20 ± 0.08	7.06 ± 0.61
ECAC11-3	1.08 ± 0.21	5.98 ± 0.52
* Average	1.57 ± 0.18	9.35 ± 1.17
[#] channel nuclide abundance > hillslope ($P=0.06$) and fan ($P=0.01$)		

Samples ending with -1, -2, and -3 are grain-size fractions
(125-500 μm , 500-1000 μm , and >1000 μm , respectively)

Measurements are average $\pm 1\sigma$ analytical error (Lawrence Livermore-National Laboratory)

Averages reported with ± 1 standard error of the mean

* Size fractions were averaged together before calculating total averages.

+ Averages for profiles are weighted by sampled depth interval

[#] Statistical comparisons between sediment reservoirs made using independent t -test assuming unequal variance at 90% confidence interval ($\alpha=0.1$)

Table 2-3. Sediment-generation rates and bedrock-equivalent lowering rates for Arroyo Chavez area, New Mexico

	¹⁰ Be & ²⁶ Al in channel sediment	¹⁰ Be & ²⁶ Al in hillslope colluvium	¹⁰ Be & ²⁶ Al deposition model	⁺ sediment budget	[#] hypometric calculation
Sediment Generation Rate (g m ⁻² yr ⁻¹)	275 ± 65	402 ± 138	446 ± 140	394 ± 68	~270 ± na
Bedrock-Equivalent Lowering Rate (m My ⁻¹)	102 ± 24	149 ± 51	165 ± 52	146 ± 25	~100 ± na
*Effective Time Scale (yrs)	~10 to 20 x 10 ³	~10 to 20 x 10 ³	~10 to 20 x 10 ³	2	1.1 x 10 ⁶

* amount of time over which calculations are integrated

⁺ Gellis et al., 2000

[#] Dethier et al., 1988

Figure 2-1. Arroyo Chavez sub-basin, southeastern edge of the Colorado Plateau. Looking north into the sub-basin. Northern boundary of the watershed is far center of the photograph where road joins. Front of photograph is 2.5 km across.



Figure 2-1. Arroyo Chavez sub-basin, southeastern edge of the Colorado Plateau. Looking north into the sub-basin. Northern boundary of the watershed is far center of the photograph where roads join. Front of photograph is 2.5 km across.

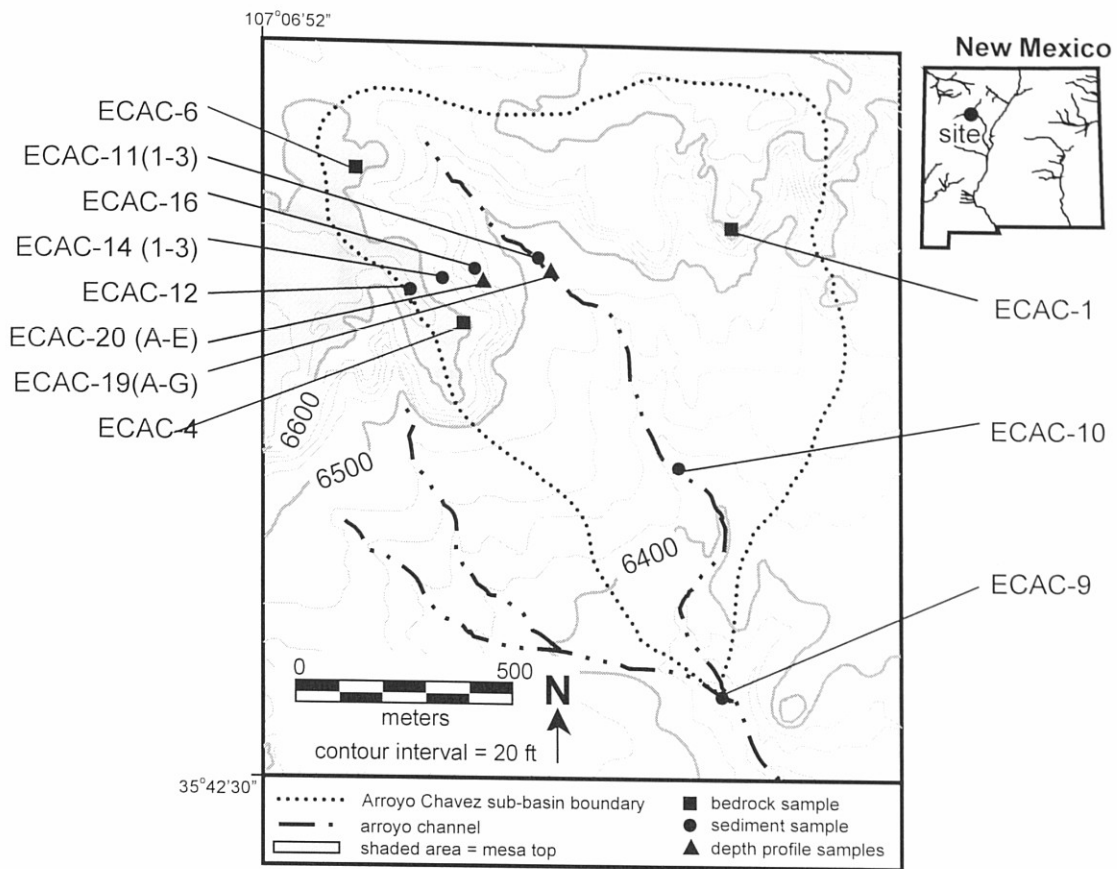


Figure 2-2. Topography of the Arroyo Chavez sub-basin. Samples designated with squares (bedrock), circles (sediment and colluvium), and triangles (depth profiles). Shaded areas represent mesa tops. Sample ECAC 8-2 is located in the main channel, approximately 1200 m south of the southern edge of the map. Map adapted from 7.5-minute San Luis Quadrangle Map (U.S. Geological Survey, 1961).

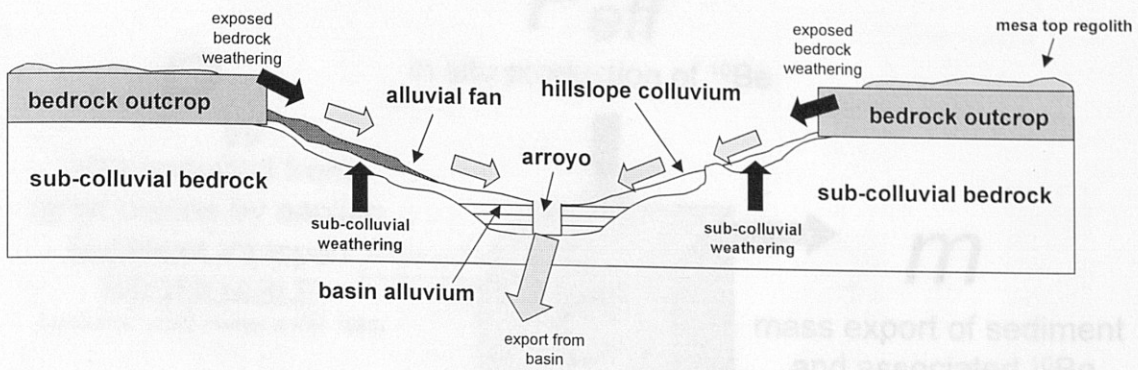


Figure 2-3. Schematic cross-section of the Arroyo Chavez sub-basin depicting the general flow of sediment from sources (weathering of exposed bedrock outcrops and sub-colluvial bedrock), to the reservoirs (hillslope colluvium, alluvial fan, and basin alluvium), and the transport of sediment out of the basin. Black arrows represent bedrock weathering. Gray arrows represent sediment transport.

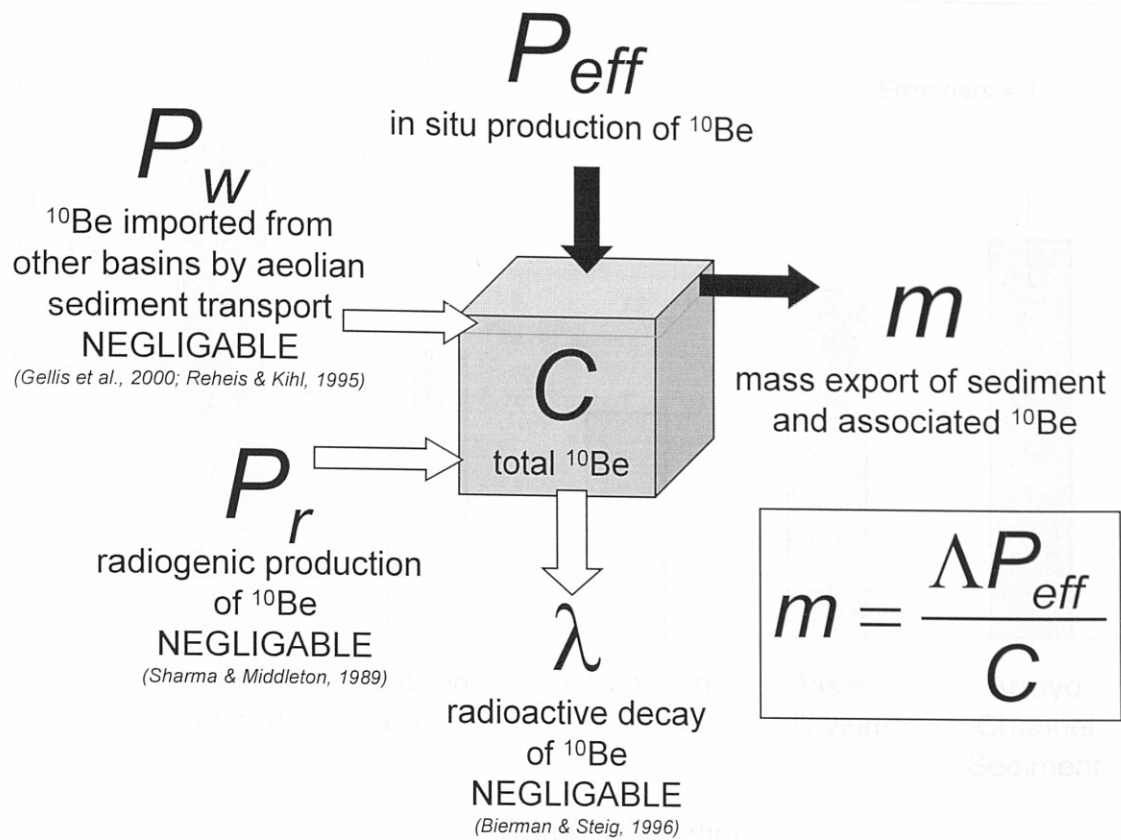


Figure 2-4. Balance of cosmogenic ^{10}Be in the Arroyo Chavez basin (adapted from Bierman and Steig, 1996). Unshaded arrows represent nuclide inputs or outputs which are negligible. Black arrows represent nuclide inputs or outputs which control the total nuclide inventory (C) of the basin. Basin-wide nuclide inventory is controlled by in-situ production (P_{eff}) and the rate that nuclides are carried away with sediment through mass export (m). The characteristic attenuation length for fast neutrons (Λ) is constant (165 g cm^{-2}).

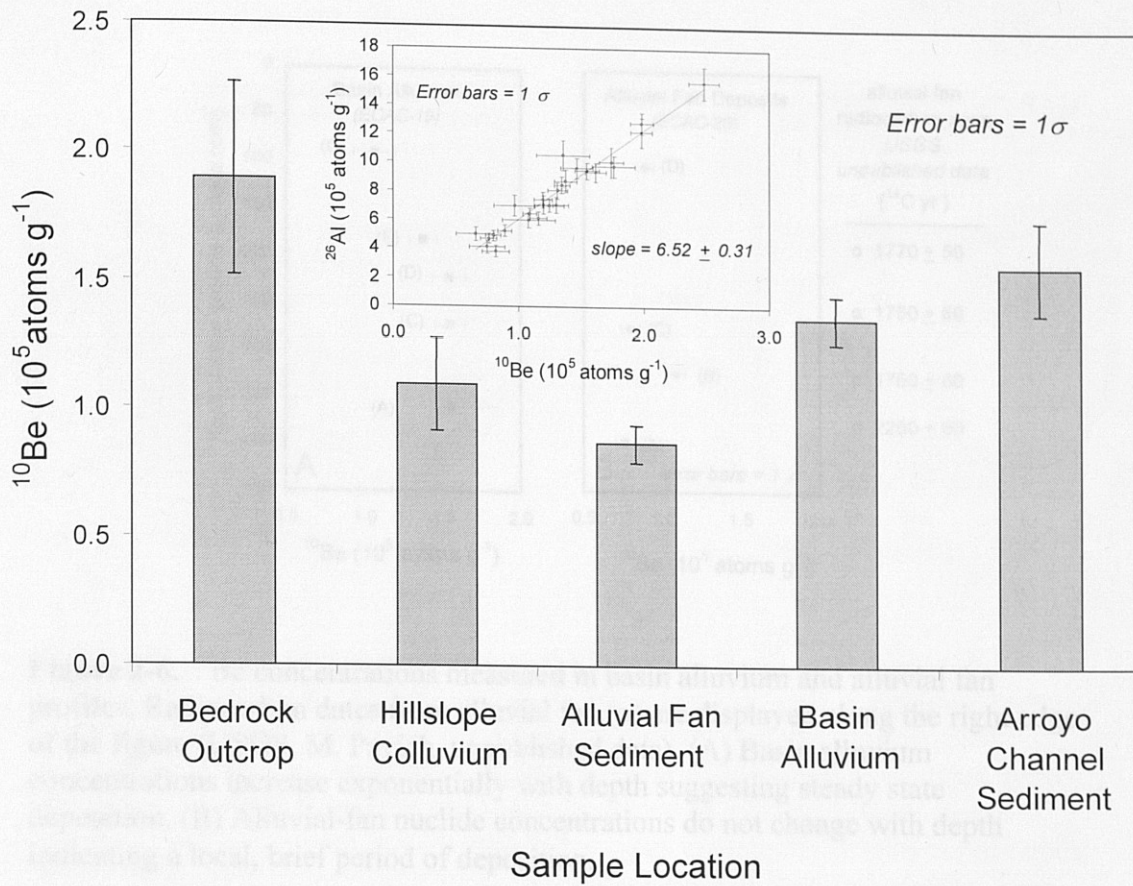


Figure 2-5. Average ^{10}Be concentrations for individual sediment reservoirs in the Arroyo Chavez sub-basin. Inset, ^{10}Be vs. ^{26}Al concentrations for all Arroyo Chavez samples. Best-fit line has a slope of 6.52 ± 0.31 (based on methods of York, 1969) consistent with the currently accepted $^{26}\text{Al}:$ ^{10}Be production ratio of $\sim 6:1$ (Nishiizumi et al., 1989).

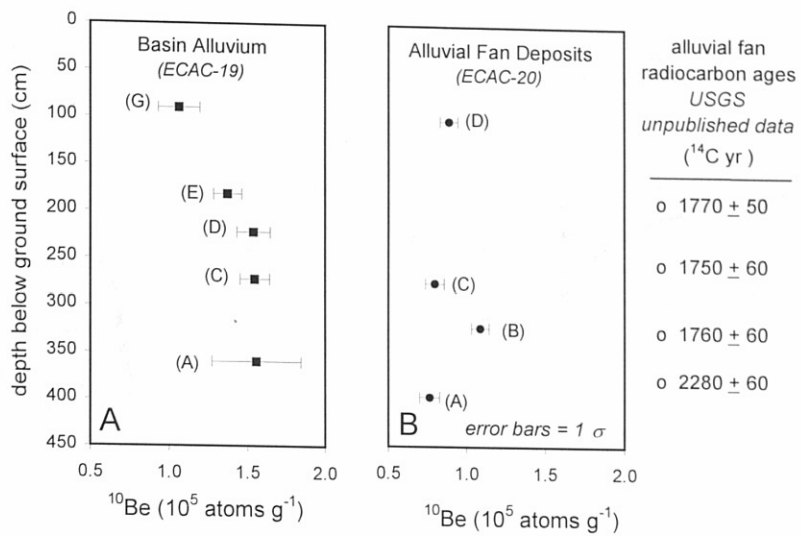


Figure 2-6. ^{10}Be concentrations measured in basin alluvium and alluvial fan profiles. Radiocarbon dates from alluvial fan (o) are displayed along the right edge of the figure (USGS, M. Pavich, unpublished data). (A) Basin alluvium concentrations increase exponentially with depth suggesting steady state deposition. (B) Alluvial-fan nuclide concentrations do not change with depth indicating a local, brief period of deposition.

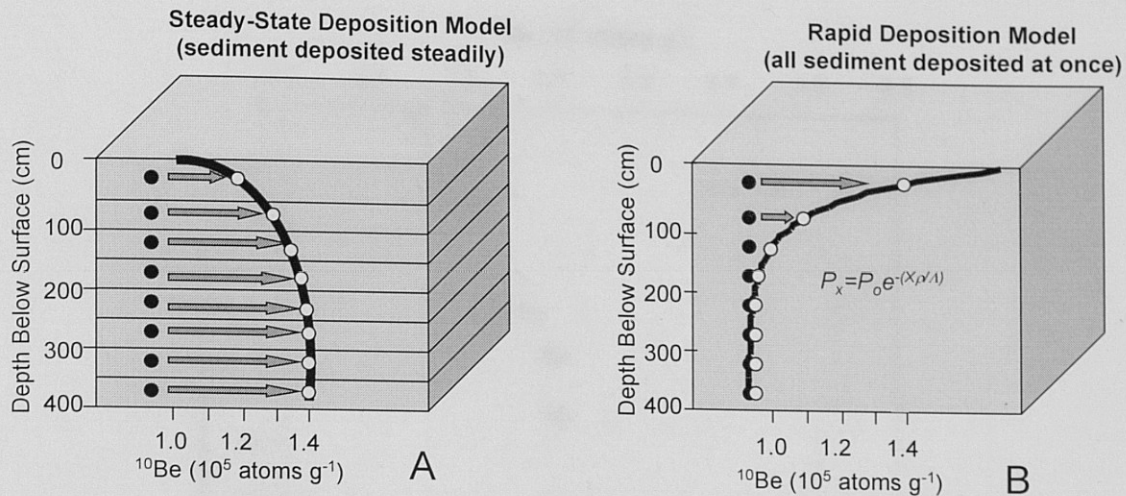


Figure 2-7. Steady state and rapid-deposition models for basin alluvium. A) Sediment, deposited at a steady rate has an initial concentration determined by the erosion rate of upland source areas. If basin is eroding steadily, all deposited sediment will have the same initial isotope concentration shown by the dark circles. As the sediment sits in storage and is slowly buried, it will accumulate atoms (arrows pointing to right) at a rate which decreases exponentially with burial depth. When sediment is buried 2 to 3 m, production approaches zero and accumulation stops (open circles). Particles higher in the profile will accumulate isotopes for a shorter period of time (deposited later) and thus will not yet have reached steady state. B) Sediment deposited rapidly will have initial concentrations that are homogenous with depth (black circles). Nuclides then accumulate based on the depth-production relationship (Lal, 1991) resulting in an exponentially decreasing depth profile (open circles).

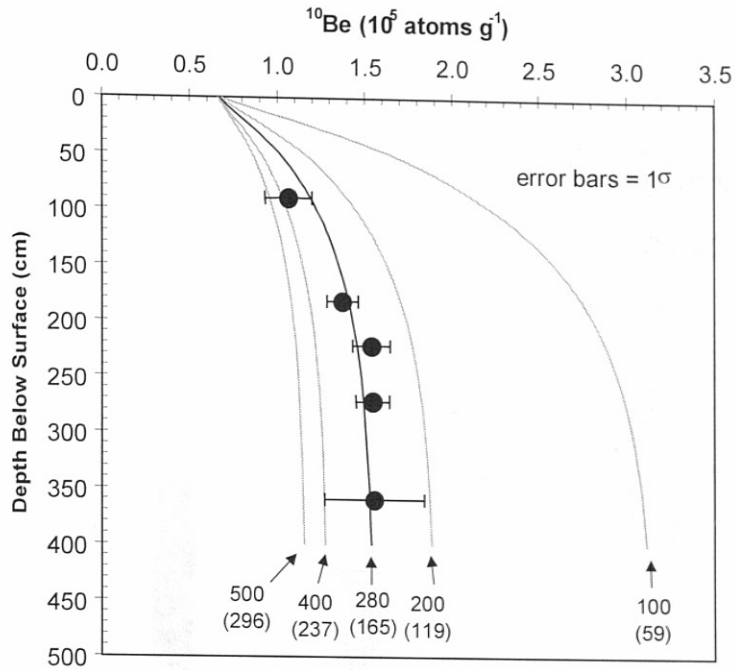


Figure 2-8. Calculated isotopic depth profiles based on eq. 1, the steady state deposition model of Lal and Arnold (1985). Each curve represents a rate of deposition (m myr^{-1}) indicated beneath the curve. Numbers in parentheses are the associated bedrock-equivalent erosion rates (m myr^{-1}). Deposition rates converted to erosion rates based on bedrock density of 2.7 g cm^{-3} and sediment density of 1.6 g cm^{-3} . An initial ^{10}Be concentration of $0.66 \times 10^5 \text{ atoms g}^{-1}$ was (the lowest nuclide measurement in the basin, ECAC 14-1). Error bars represent 1σ analytical error.

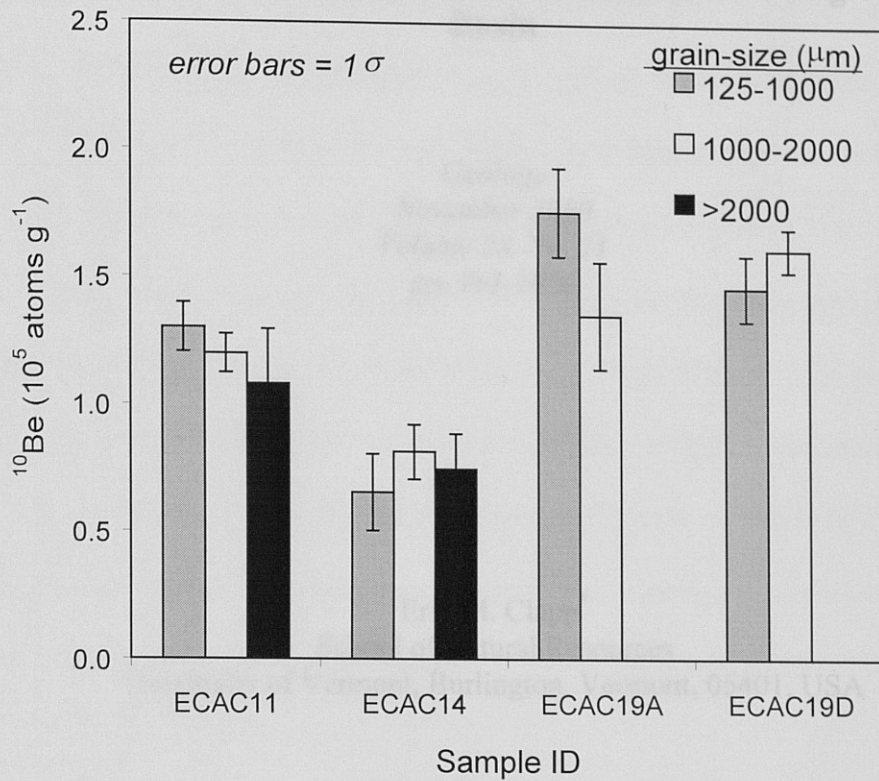


Figure 2-9. ^{10}Be concentrations for different sediment grain size fractions of four samples. Nuclide concentration is independent of grain size.

3.0 Nahal Yael Manuscript

Sediment Yield Exceeds Sediment Production in Arid Region Drainage Basin

Geology
November 2000
Volume 28, No. 11
pp. 961-1056

Erik M. Clapp*
School of Natural Resources
University of Vermont, Burlington, Vermont, 05401, USA

Paul R. Bierman
School of Natural Resources & Department of Geology,
University of Vermont, Burlington, Vermont, 05401, USA

Asher P. Schick
Judith Lekach
Yehouda Enzel
Department of Geography,
Hebrew University of Jerusalem, Israel

Marc Caffee
Center for Accelerator Mass Spectrometry
Lawrence Livermore National Laboratory, Livermore California, 94551, USA

3.1 Abstract

We use ^{10}Be and ^{26}Al to determine long-term sediment generation rates, identify significant sediment sources, and test for landscape steady state in Nahal Yael, an extensively studied, hyper arid drainage basin in southern Israel. Comparing a 33 yr sediment budget with 33 paired ^{10}Be and ^{26}Al analyses indicates that short-term sediment yield ($113 - 138 \text{ t km}^{-2} \text{ yr}^{-1}$) exceeds long-term sediment production ($74 \pm 16 \text{ t km}^{-2} \text{ yr}^{-1}$) by 53% - 86%. The difference suggests that the basin is not in steady state, but is currently evacuating sediment accumulated during periods of more rapid sediment generation and lower sediment yield. Nuclide data indicate that (1) sediment leaving the basin is derived primarily from hillslope colluvium, (2) bedrock weathers more rapidly beneath a cover of colluvium than when exposed, and (3) long-term erosion rates of granite, schist, and amphibolite are similar.

3.2 Introduction

Quantifying the rate at which rock erodes and sediment is produced is fundamental to understanding Earth as a system. Rates of sediment production (rock erosion) are typically inferred from estimates of sediment yield measured either as a flux of sediment past a gauging station or determined by measuring the accumulation of sediment in a reservoir (Schumm, 1963; Judson and Ritter, 1964; Meade, 1969; Trimble, 1977; Saunders and Young, 1983; Schick and Lekach, 1993). Equating sediment yield and sediment production implies steady-state behavior and assumes no change in the

volume of sediment stored within a basin, an assumption repeatedly questioned (Meade, 1969; Trimble, 1977, 1999; Walling, 1983; Bull, 1991).

We compare 33 yrs of sediment yield data from Nahal Yael to long-term, time-integrated rates of sediment generation determined by measuring in situ produced cosmogenic ^{10}Be and ^{26}Al . Significant differences between rates of sediment generation and sediment yield indicate that Nahal Yael, an intensively instrumented, hyper-arid basin in southern Israel (Schick and Lekach, 1993), is currently exporting more sediment than is being generated by the weathering of bedrock. These data and others (Trimble, 1977; Brown et al., 1995; Clapp et al., 1997) suggest that over human time-scales, balanced sediment production and yield may be the exception rather than the rule.

3.3 Background

Nahal Yael occupies a small (0.6 km^2), mountainous drainage basin in the Negev Desert, Israel (Figs. 1 and 2). The basin is underlain by Precambrian rock (Shimron, 1974; Schick and Lekach, 1993), gneissic granite in the north, schist in the middle, and amphibolite to the south (Fig. 2). In the northern (granite) and middle (schist) sections, exposed bedrock dominates the uplands; significant colluvial cover is limited to bedrock hollows and the lowermost portions of hillslopes (Fig. 1). Sediment storage within these sections is confined to isolated colluvial deposits and alluvial terraces (generally $<3 \text{ m}$ thick) along the narrow valley bottom (Figure A, Appendix XX) In contrast, hillslopes in the southern section (amphibolite) have bedrock exposed on the top 10 – 20 m and substantial colluvial cover over the lower hillslopes.

In 1967, Hebrew University researchers (Bull and Schick, 1979; Schick and Lekach, 1993) began constructing a sediment budget for Nahal Yael using automatically collected hydrologic and suspended sediment data, estimates of bedload yield from scour chains and pebble tracing, and surveying of sediment deposition behind an earthen dam constructed in 1977 to trap and monitor sediment yields with nearly 100% efficiency (Schick and Lekach, 1993). Over the 33 yr monitoring history, 14 yrs had no flow and 8 yrs had events during which flow did not exit the basin (Schick and Lekach, 1993). In October 1997, a storm with an estimated recurrence interval >50 yrs delivered >460 t of sediment to the mouth of the basin. The 33 yr record, including the large storm of 1997 and the 14 yrs without flow, results in an integrated sediment yield of $138 \pm 19 \text{ t km}^{-2} \text{ yr}^{-1}$. The average sediment yield excluding the large storm of 1997 is $113 \pm 16 \text{ t km}^{-2} \text{ yr}^{-1}$. We measured ^{10}Be and ^{26}Al in quartz to determine the maximum limiting, long-term rate at which sediment is generated and to identify areas where sediment is generated and stored. The assumptions and limitations of such measurements and their interpretations are discussed by Lal (1991), Bierman and Steig (1996), Bierman and Turner (1995), Brown et al. (1995), Granger et al., (1996), Clapp et al. (1997 and 1998), and Small et al. (1999).

3.4 Sampling Locations and Methods

We measured nuclide concentrations in bedrock outcrops, hillslope colluvium, alluvial terraces, and channel alluvium (Figs. 2 and 3, Table A, Appendix B). Laboratory methods are detailed in Appendix B. Individual nuclide measurements discussed in the text include an analytical error of 1σ .

We sampled channel alluvium at four locations along Nahal Yael (Fig. 2) using the channel as an integrator of different sediment sources and associated ^{10}Be and ^{26}Al from throughout the drainage basin. As flow within the channel travels down basin, sediment from terraces and tributaries along the channel's length is entrained and mixed. As the channel cuts through alluvial deposits, it temporally integrates sediment deposited by many different depositional events.

Bedrock outcrops were sampled in three lithologically distinct transects (Fig. 2). Within the granitic terrain, where quartz is uniformly distributed throughout the bedrock, three samples were collected from a single hillslope at evenly spaced, 20 m elevation intervals. Within the schist terrain, where quartz is concentrated in crosscutting veins that are no more or less resistant to weathering than the surrounding rock, we collected three samples from the quartz veins keeping as close to 20 m elevation spacing as possible. In the amphibolite terrain, quartz is also concentrated in veins; however, shorter hillslopes and fewer quartz veins limited us to only two samples ~20 m apart in elevation.

Three composite samples of hillslope colluvium, each composed of samples taken at ~1 m intervals across the base of the slope but above any channel-derived sediment, were collected from hillslopes below the three bedrock transects (Fig. 2). Two composite samples of alluvial terrace sediment were collected by mixing subsamples collected at evenly spaced depth increments (~10 cm) in the alluvium exposed by channel incision. Each sediment sample was divided into three grain size fractions (sediment grain size data is included in Appendix A); we find no relationship between nuclide concentration and sediment grain size (Fig. B, Appendix B).

Measured $^{26}\text{Al}/^{10}\text{Be}$ ratios ($\mu = 5.9 \pm 0.48$) of (Fig. 3, inset) are consistent with the currently accepted production ratio of $\sim 6:1$ (Nishiizumi et al., 1989), indicating that the sediment and bedrock we sampled do not have long-term (>100 ky), complex histories of burial and exhumation. Because the two isotopes are well correlated ($r^2 = 0.95$), we present primarily the ^{10}Be measurements; however, the ^{26}Al measurements are used in all calculations (Table 1).

3.5 Results and Discussion

Bedrock Erosion and Sediment Generation

We use nuclide concentrations in geomorphic features to identify significant sources of sediment to the channel and compare relative rates of processes shaping desert environments. Average ^{10}Be concentrations in bedrock outcrops ($2.18 \pm 0.31 \times 10^5$ atoms g^{-1} , $n = 8$) are higher than those in hillslope colluvium ($1.54 \pm 0.30 \times 10^5$ atoms g^{-1} , $n = 3$) suggesting that exposed bedrock weathers more slowly (more nuclide accumulation) than bedrock beneath a colluvial cover (Fig. 3). These observations are consistent with previous cosmogenic measurements (Bierman, 1994; Clapp et al., 1997, 1998; Small et al., 1999).

Lower average nuclide concentrations in colluvium could result from cosmic-ray shielding (less exposure) by material now eroded. However, the 6.3×10^4 atoms g^{-1} difference between exposed bedrock and colluvium would require shielding by colluvium deeper than 50 cm, far thicker than we observed on the steep slopes of Nahal Yael. Most likely, the nuclide abundance difference can be attributed to shielding beneath shallow

(cm to dm) colluvium coupled with associated increases in both physical and chemical weathering, the result of increased water retention and moisture – bedrock contact time beneath a cover of coluvium (Bull, 1991; Small et al., 1999).

Nuclide concentrations, and thus erosion rates, are not statistically discernible between the three lithologies (Fig. 4). Nuclide concentrations measured in the granitic transect, where quartz is uniformly distributed, imply a positive relationship between elevation above the stream channel and nuclide concentration (Fig. 4 inset), perhaps reflecting a period of time when the lower granitic hillslopes held a cover of colluvium consistent with suggestions of a late Pleistocene - early Holocene stripping of hillslope colluvium (Bull and Schick, 1979; Bull, 1991) . Schist and amphibolite transects show no significant relationship between nuclide abundance and elevation.

Dynamics of Sediment Production and Transport

Nuclide data allow us to fingerprint sediment sources and suggest that most sediment in Nahal Yael is supplied by the middle and lower parts of the basin; the upper portion of the Nahal Yael basin has more stable colluvial cover and contributes less sediment to the channel. The most important sediment source is colluvium stored in hollows and at the bottom of the slopes. Other sediment sources (exposed bedrock and terraces) contribute significantly less sediment.

Upper Basin In the upper amphibolitic basin, nuclide concentrations in widespread hillslope colluvium ($2.16 \pm 0.06 \times 10^5$ atoms g^{-1} , NY15) are higher than those measured in colluvium of the lower (granite and schist) portions of the basin (1.21 ± 0.02 to $1.28 \pm 0.02 \times 10^5$ atoms g^{-1} , NY12 and NY8, respectively, Fig. 4). Average nuclide

concentrations from the upper basin bedrock ($2.33 \pm 0.50 \times 10^5$ atoms g^{-1} , NY13 and NY14) are only slightly greater than in the upper basin colluvium ($2.16 \pm 0.06 \times 10^5$ atoms g^{-1} , NY15), indicating that exposed bedrock may be a significant source of sediment to the upper basin hillslopes. The nuclide concentration ($1.42 \pm 0.09 \times 10^5$ atoms g^{-1}), measured in channel alluvium exiting the upper portion of the basin (NY18), is greater than concentrations measured lower in the basin (1.22 ± 0.04 to $1.32 \pm 0.02 \times 10^5$ atoms g^{-1} , NY20 and NY4, respectively), consistent with longer colluvial residence time in the upper basin.

Middle Basin In the middle basin, sediment is currently stored along the valley bottom and to a lesser degree on the lower hillslopes in discontinuous alluvial terraces shown to be Pleistocene in age by optically stimulated luminescence (OSL) dating (Lekach et al., 1999). Consistent with these observations, nuclide data (Fig. 4) suggest some storage of sediment in alluvial terraces, as nuclide concentrations in these terraces (1.45 ± 0.11 and $1.66 \pm 0.06 \times 10^5$ atoms g^{-1} , NY16 and NY17, respectively) are slightly greater than in samples from the sediment-supplying hillslopes above ($1.21 \pm 0.02 \times 10^5$ atoms g^{-1} , NY12). The difference between NY17 (terrace) and NY12 (colluvium) is significant at the 2σ level, while the difference between NY16 (terrace) and NY12 (colluvium) is significant at 1σ but not 2σ . The nuclide concentration of the channel alluvium ($1.24 \pm 0.04 \times 10^5$ atoms g^{-1} , NY19) is similar to the hillslope samples, but less than terrace samples, suggesting that hillslopes supply more sediment to the channel than alluvial terraces.

The difference in concentrations between the colluvium and the terrace sediment ($\sim 3.0 \times 10^4$ atoms g^{-1}) may reflect cosmic-ray dosing of terrace alluvium either prior to or

following deposition. If we assume that the terraces were deposited rapidly at some point in the past, and integrate nuclide production ($5.77 \text{ atoms of } ^{10}\text{Be g}^{-1} \text{ yr}^{-1}$) over the average terrace depth ($\sim 2 \text{ m}$), assuming sediment density of 1.6 g cm^{-3} , we calculate rapid deposition of alluvial terraces ca. 11 ka consistent with the hypothesized late Pleistocene - early Holocene stripping of hillslopes in response to climate change (Bull and Schick, 1979; Bull, 1991). Alternatively, the alluvial terraces could have been deposited steadily, during which time nuclide accumulation continually occurred (Clapp et al., 1997). Steady-state deposition at $\sim 125 \text{ m m.y.}^{-1}$ over $\sim 16 \text{ ky}$ would account for the additional $\sim 3.0 \times 10^4 \text{ atoms g}^{-1}$ measured in the $\sim 2 \text{ m}$ of alluvium.

Lower Basin In the lower basin, colluvium resides only in hollows and isolated, thin deposits at the base of the slopes, suggesting minimal storage and short residence time. Consistent with short, near-surface residence, the average nuclide concentration of the hillslope colluvium in the lower basin (Fig. 4) is low ($1.28 \pm 0.02 \times 10^5 \text{ atoms g}^{-1}$, NY8). Channel alluvium ($1.25 \pm 0.03 \times 10^5 \text{ atoms g}^{-1}$, average of NY4 and NY20) and hillslope colluvium (NY8) nuclide concentrations are similar, suggesting that in the lower basin hillslopes supply most sediment to the channel of Nahal Yael.

Sediment Production Versus Sediment Yield

From nuclide concentrations measured in the channel sediment at the outlet of Nahal Yael (NY4 and NY20), we estimate (using Bierman and Steig, 1996 and nuclide production rate estimates of Nishiizumi et al., 1989) a maximum, limiting, basin-wide sediment generation rate of $74 \pm 16 \text{ t km}^{-2} \text{ yr}^{-1}$, consistent with rates determined for other

regions using similar methods (Table 1). This is likely an overestimate as recent work suggests long-term production rates of ^{10}Be and ^{26}Al are 10% - 15% lower (Clark et al., 1995).

Sediment yield from Nahal Yael ($113 - 138 \text{ t km}^{-2} \text{ yr}^{-1}$), calculated from the sediment budget, is at least 53% - 86% greater than the long-term rate of sediment generation estimated using ^{10}Be and ^{26}Al (Table 1). The difference between sediment yield and generation rates, along with the isotopic data, suggest that sediment is being mined from colluvium stored during a period when sediment generation outpaced sediment yield. Two of three similar studies elsewhere (Table 1) also suggest that current sediment yields exceed long-term rates of sediment generation (Brown et al., 1995; Granger et al., 1996; Clapp et al., 1997). Together, these data show that the assumption of short-term landscape steady state is likely invalid. Episodic periods of sediment aggradation are followed by downcutting and sediment evacuation, possibly resulting from changes in climate or land use (Bull and Schick, 1979; Bull, 1991).

The measured differences between rates of sediment generation and sediment yield illustrate the danger of using short-term sediment yields to estimate long-term, basin-wide rates of bedrock erosion. Cosmogenic nuclides can provide direct estimates of long-term, basin-scale sediment generation rates and fingerprint significant sediment storage and source areas within drainage basins. These nuclides are invaluable in quantitatively addressing fundamental questions in arid region geomorphology and may be used to identify temporal changes in sediment generation.

3.6 Acknowledgments

Supported by the US Army Research Office DAAG559710180 and DAAH04961003; additional support provided by A. Schick and Y. Enzel, Hebrew University of Jerusalem, Lawrence Livermore National Laboratory, J. Sevee, and P. Maher. We thank A. Matmon, S. Gran, and C. Massey for field assistance, S. Nies, J. Southon, and B. Copans for laboratory assistance, and K. Nichols and L. Clapp for editing.

3.7 References Cited

- Bierman, P.R., 1994, Using in situ cosmogenic isotopes to estimate rates of landscape evolution: A review from the geomorphic perspective: *Journal of Geophysical Research*, v. 99, p. 13885-13896.
- Bierman, P., and Steig, E., 1996, Estimating rates of denudation and sediment transport using cosmogenic isotope abundances in sediment: *Earth Surface Processes and Landforms*, v. 21, p. 125-139.
- Bierman, P.R., and Turner, J., 1995, ^{10}Be and ^{26}Al evidence for exceptionally low rates of Australian bedrock erosion and the likely existence of pre-Pleistocene landscapes: *Quaternary Research*, v. 44, p. 378-382.
- Brown, T.B., Stallard, R.F., Larsen, M.C., Raisbeck, G.M., and Francoise, Y., 1995, Denudation rates determined from accumulation of in situ-produced ^{10}Be in the Luquillo Experimental Forest, Puerto Rico: *Earth and Planetary Science Letters*, v. 129, p. 193-202.
- Bull, W.B., 1991, *Geomorphic Responses to Climate Change*: New York, Oxford University Press, 326 p.
- Bull, W.B., and Schick, A.P., 1979, Impact of climate change on an arid region watershed: Nahal Yael, southern Israel: *Quaternary Research*, v. 11, p. 153-171.
- Clapp, E.M., Bierman, P.B., Pavich, M., and Caffee, M., 1997, Rates of erosion determined using in situ-produced cosmogenic isotopes in a small arroyo basin, northwestern New Mexico: *Geological Society of America Abstracts with Programs*, v. 29, p.281.

- Clapp, E.M., Bierman, P.B., and Caffee, M.W., 1998, Estimating long-term erosion rates in a hyper-arid region using in situ-produced cosmogenic ^{10}Be and ^{26}Al in sediment and Bedrock: Geological Society of America Abstracts with Programs, v. 30, p. 361.
- Clark, D., Bierman, P.R., and Larsen, P., 1995, Improving in situ cosmogenic chronometers: Quaternary Research, v. 44, p. 367-377.
- Granger, D.E., Kirchner, J.W., and Finkel, R., 1996, Spatially averaged long-term erosion rates measured from in-situ produced cosmogenic nuclides in alluvial sediment: Journal of Geology, v. 104, p. 249-257.
- Judson, S., and Ritter, D.F., 1964, Rates of regional denudation in the United States: Journal of Geophysical Research, v. 69, p. 3395-3401.
- Lal, D., 1991, Cosmic ray labeling of erosion surfaces: In situ production rates and erosion models: Earth and Planetary Science Letters, v. 104, p. 424-439.
- Lekach, J., Amit, R., Ayalon, A., Porat, N., and Schick, A., 1999, Fluvio-pedogenic processes in an active desert stream, in Lekach, J., and Hassan, M.A., eds., Drainage basin dynamics and morphology, Negev Desert, conference excursion: Jerusalem, Hebrew University of Jerusalem, p. 114-122.
- Meade, R.H., 1969, Errors in using modern stream-load data to estimate natural rates of denudation: Geological Society of America Bulletin, v. 80, p. 1265-1274.
- Nishiizumi, K., Winterer, E.L., Kohl, C.P., Klein, J., Middleton, R., Lal, D., and Arnold, J.R., 1989, Cosmic ray production rates of ^{10}Be and ^{26}Al in quartz from glacially polished rocks: Journal of Geophysical Research, v. 94, p. 17907-17915.
- Saunders, I., and Young, A., 1983, Rates of surface processes on slopes, slope retreat, and denudation: Earth Surface Processes and Landforms, v. 8, p. 473-501.
- Schick, A.P., and Lekach, J., 1993, An evaluation of two ten-year sediment budgets, Nahal Yael, Israel: Physical Geography, v. 14, p. 225-238.
- Schumm, S.A., 1963, Disparity between present rates of denudation and orogeny, U.S. Geological Survey Professional Paper 454-H, 13 p.
- Shimron, A., 1974, Geology of the Nahal Yael watershed, in Schick, A.P., and Sharon, D., eds., Geomorphology and climatology of arid watersheds: Project Report DAJA-72C-3874, U.S. Army European Research Office, Department of Geography, Hebrew University of Jerusalem, p. 12-23.

Small, E.E., Anderson, R.S., and Hancock, G.S., 1999, Estimates of the rate of regolith production using ^{10}Be and ^{26}Al from an alpine slope: *Geomorphology*, v. 27, p. 131-150.

Trimble, S.W., 1977, The fallacy of stream equilibrium in contemporary denudation studies: *American Journal of Science*, v. 277, p. 876-887.

Trimble, S.W., 1999, Decreased rates of alluvial sediment in the Coon Creek Basin: *Science*, v. 285, p. 1244-1246.

Walling, D.E., 1983, The sediment delivery problem: *Journal of Hydrology*, v. 65, p. 209-237.

Table 3-1. Sediment generations and equivalent rock erosion rates for Nahal Yael and other sites.

Location	Reference	Sediment generation rate		Sediment yield Sediment budget (t km ² yr ⁻¹)	Rock erosion rate			Site average elevation (m)	Annual precipitation (mm yr ⁻¹)	Lithology
		¹⁰ Be (t km ² yr ⁻¹)	²⁶ Al (t km ² yr ⁻¹)		¹⁰ Be (m m.y. ⁻¹)	²⁶ Al (m m.y. ⁻¹)	Sediment budget (m m.y. ⁻¹)			
Nahal Yael [†] , Israel	(this paper)	78 ± 16	70 ± 16	113 to 138	29 ± 6	26 ± 6	42 to 51	240	30	granite, schist, amphibolite
Yuma Wash, Arizona	(Clapp et al., 1996)	81 ± 5	81 ± 8	N.D.	30 ± 2	30 ± 3	N.D.	220	91	rhyolite, granite
Arroyo Chavez, New Mexico	(Clapp et al., 1997)	273 ± 62	281 ± 73	394 ± 68	101 ± 23	104 ± 27	146 ± 25	2000	377	sandstone
Fort Sage Mts., California	(Granger et al., 1996)	162 ± 38		157 ± 38	60 ± 14		58 ± 14	1300	>370	granodiorite
Wind River Range, Wyoming	(Small et al., 1999)	39 ± 11	35 ± 11	N.D.	14 ± 4	13 ± 4	N.D.	3600	>285	gneiss
Luquillo Forest, Puerto Rico	(Brown et al., 1995)	116 ± 41	N.D.	202	43 ± 15	N.D.	75	700	4000	quartz-diorite

Note: N.D. = No data.

[†]Published rate is average of ¹⁰Be and ²⁶Al rates.

[†]Sediment generation and rock erosion rates calculated from sample NY20 (located closest to basin outlet) using formulation of Bierman and Steig (1996) and production rates of Nishizumi et al. (1989) scaled for latitude and elevation according to Lal (1991) and assuming no muon production. Conversion between erosion and sediment generation rates based on densities of 2.7 (g cm⁻³) for bedrock and 1.6 (g cm⁻³) for sediment.

Figure 3-1. Upstream view of Nahal Yael drainage basin from near sample site NY7 (see Fig. 2). Field of view is 600 m.



Figure 3-1. Upstream view of Nahal Yael drainage basin from near sample site NY7 (see Fig. 2). Field of view is 600 m.

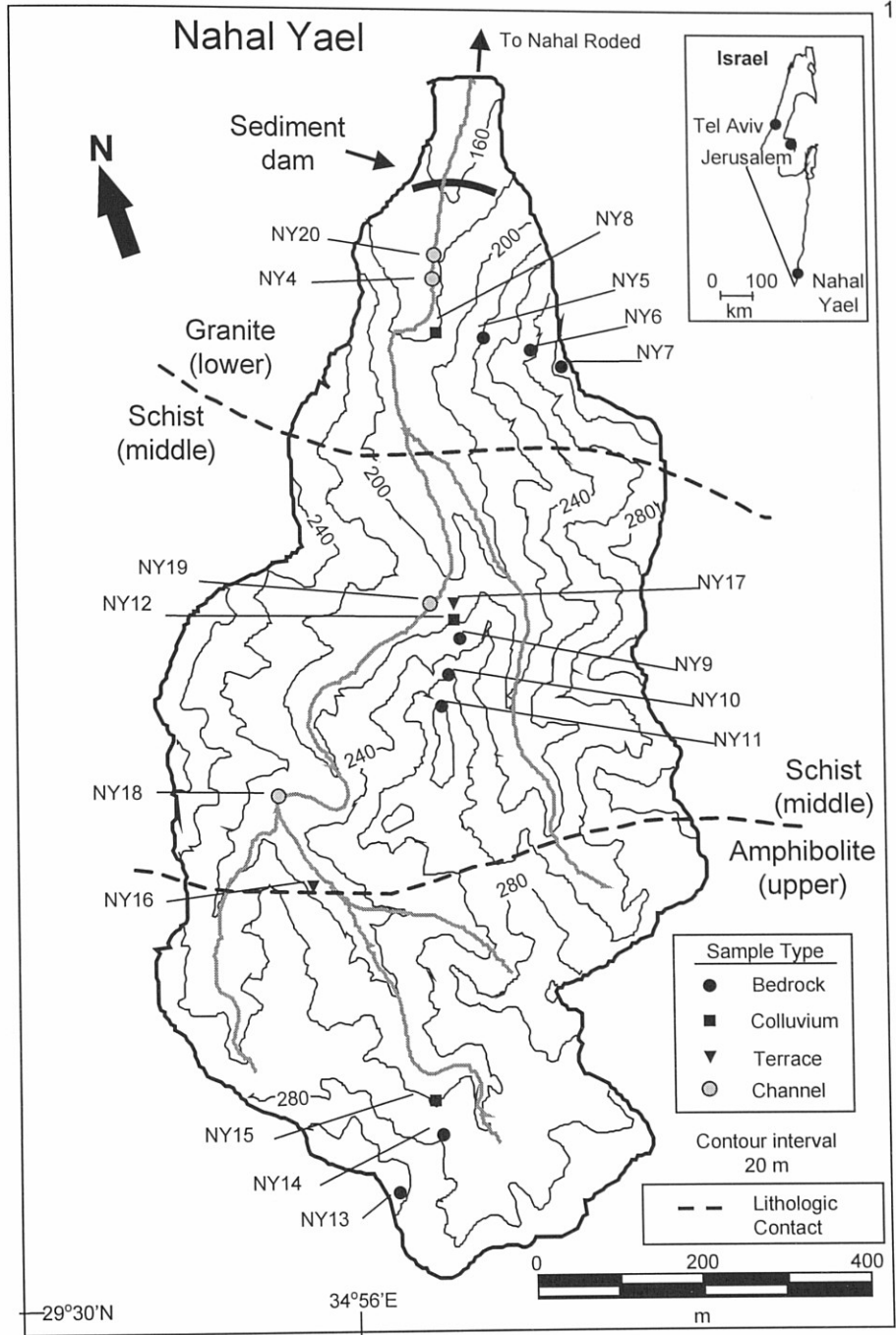


Figure 3-2. Map of Nahal Yael and site location (inset). Sample locations shown for bedrock (black circles), hillslope colluvium (squares), alluvial terraces (triangles), and channel sediment (shaded circles). Channels are shaded gray lines. Topography is adapted from Schick and Lekach, (1993). Lithology is from Shimron (1974).

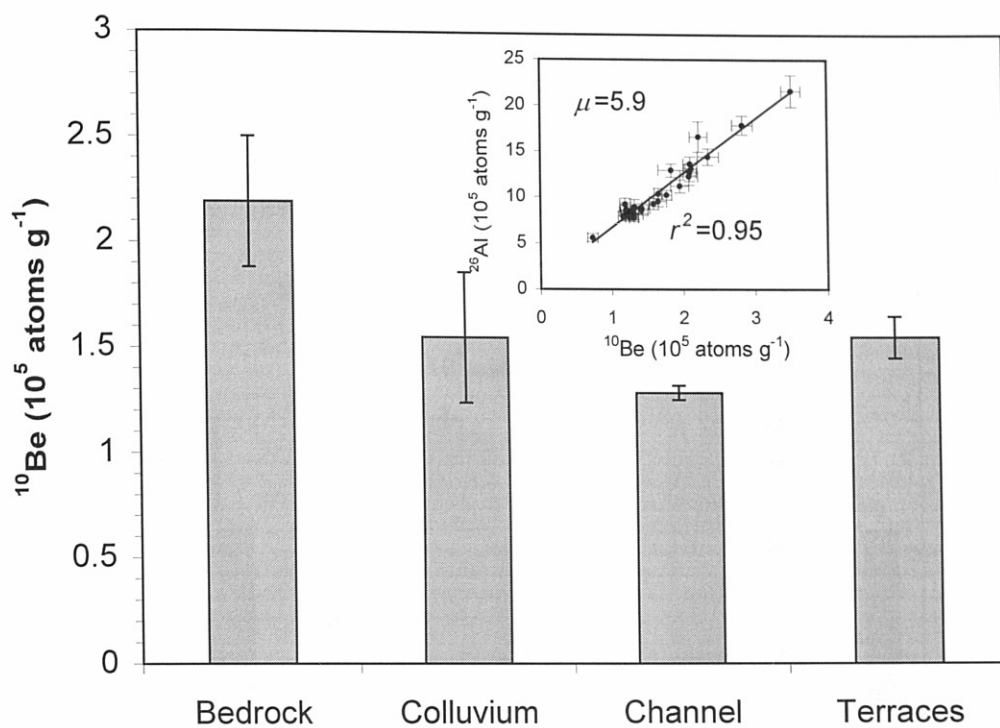


Figure 3-3. Average ^{10}Be concentrations measured in samples from geomorphic features (bedrock outcrops, colluvium, channel sediment, and terraces) of Nahal Yael. Error bars represent 1 standard error of means. Average bedrock nuclide activity is significantly greater (90% confidence) than averages of other features. Inset shows ^{10}Be vs. ^{26}Al for samples collected in Nahal Yael.

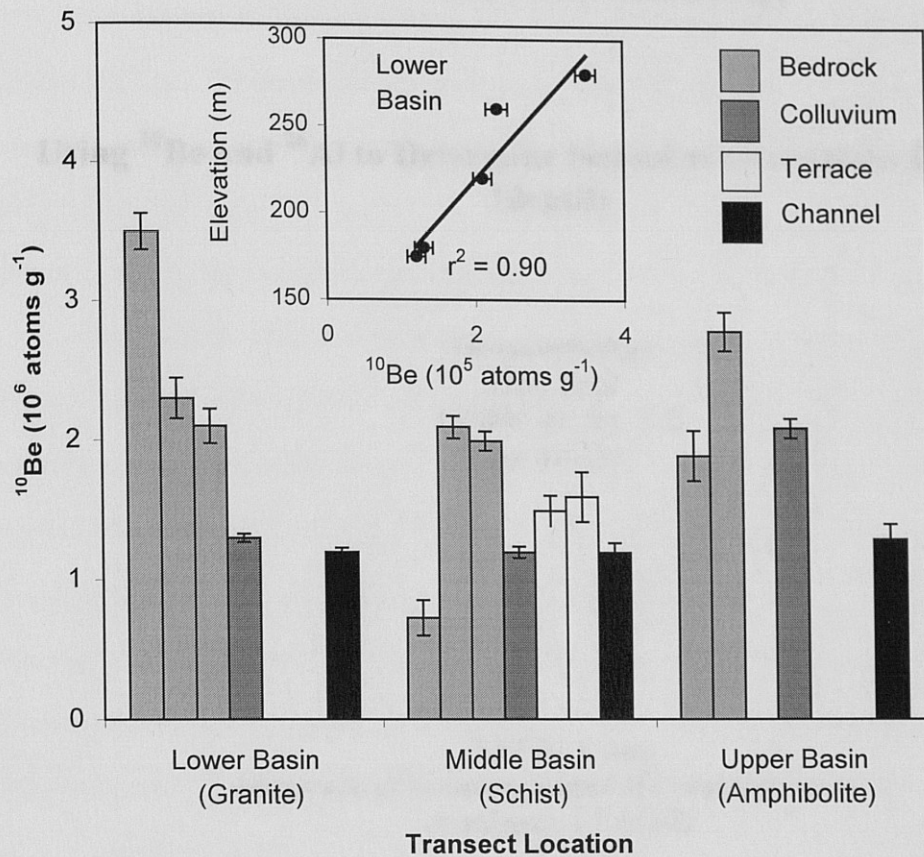


Figure 3-4. ^{10}Be concentrations measured at three transects in Nahal Yael. Nuclide concentrations for bedrock (light gray), hillslope colluvium (dark gray), terrace alluvium (white), and channel alluvium (black). Error bars represent one standard error of means. Inset shows positive linear relationship between ^{10}Be and elevation in granite transect. Points represent nuclide concentrations and elevations of three bedrock, one colluvium, and one stream channel sample.

4.0 Yuma Wash Manuscript

Using ^{10}Be and ^{26}Al to Determine Sediment Generation Rates and Identify

Geomorphology

June 2002

Volume 45, No. 1-2

pp. 89-104

*Erik M. Clapp

*University of Vermont, School of Natural Resources
Burlington VT 05405*

Paul R. Bierman

*University of Vermont, School of Natural Resources and Department of Geology
Burlington VT 05405*

Marc Caffee

*Center for Accelerator Mass Spectrometry
Lawrence Livermore National Laboratory, Livermore CA 94550*

*Current Address: C/O SME, 4 Blanchard Road Box 85A, Cumberland Center, Maine, 04021, email: emc@smemaine.com, voice: (207) 829-5016, fax: (207) 829-5692.

4.1 Abstract

We measured ^{10}Be and ^{26}Al in 64 sediment and bedrock samples collected throughout the arid, 187 km² Yuma Wash drainage basin, southwestern Arizona. From the measurements, we determine long-term, time-integrated rates of upland sediment generation ($81 \pm 5 \text{ g m}^{-2} \text{ yr}^{-1}$) and bedrock equivalent lowering ($30 \pm 2 \text{ m My}^{-1}$) consistent with other estimates for regions of similar climate, lithology, and topography.

In a small ($\sim 8 \text{ km}^2$), upland sub-basin, differences in nuclide concentrations between bedrock outcrops and hillslope colluvium suggest weathering of bedrock beneath a colluvial cover is a more significant source of sediment ($40 \times 10^4 \text{ kg yr}^{-1}$) than weathering of exposed bedrock surfaces ($10 \times 10^4 \text{ kg yr}^{-1}$). Mixing models constructed from nuclide concentrations of sediment reservoirs identify important sediment source areas. Hillslope colluvium is the dominant sediment source to the upper reaches of the sub-basin channel; channel cutting of alluvial terraces is the dominant source in the lower reaches. Similarities in nuclide concentrations of various sediment reservoirs indicate short sediment storage times ($< 10^3 \text{ y}$).

Nuclide concentrations, measured in channel sediment from tributaries of Yuma Wash and in samples collected along the length of the Wash were used to construct mixing models and determine sediment sources to the main stem channel. We find an exponential decrease in the channel nuclide concentrations with distance downstream, suggesting that as much as 40% of sediment discharged from Yuma Wash has been recycled from storage within basin fill alluvium.

Sediment generation and denudation rates determined from the main stem are greater (25%) than rates determined from upland sub-basins suggesting that currently, sediment may be exported from the basin more quickly than it is being generated in the uplands.

Independence of nuclide concentration and sediment grain size indicates that channels transport sediment in discrete pulses before rapidly depositing poorly-sorted material, suggesting differences in transport times for different size materials are minimal.

4.2 Introduction

Estimating rates of erosion, sediment generation, and landscape change is important for understanding the effects of humans, climate, and tectonics on landscapes over both historic and geologic time scales. Concentrations of in situ-produced cosmogenic ^{10}Be and ^{26}Al , measured in sediment, have been used to estimate basin-wide rates of erosion and sediment generation within drainage basins (Small et al., 1999; Bierman and Steig, 1996; Granger et al., 1996; Brown et al., 1995a; Clapp et al., in press). These studies generally focus on small (several km^2 or less), lithologically homogenous, geomorphically uncomplicated basins. Three of these studies included an independent means of confirming the nuclide-based erosion rate calculation. Although the rates of sediment generation determined in these basins appear valid locally, regional estimates of erosion and denudation require the investigation of larger ($>100 \text{ km}^2$), generally more geologically and geomorphically complex basins. The techniques and interpretation methods developed in these small, controlled studies have yet to be tested in larger, more complex basins, where the processes operating to generate, transport, and store sediment are probably different than those in small, simple, upland basins.

We measured ^{10}Be and ^{26}Al in sediment and bedrock from the 187 km^2 Yuma Wash drainage basin in southwestern Arizona (Figure 1), to determine long-term, time-integrated rates of sediment generation and bedrock-equivalent lowering (denudation), identify sediment source areas and mechanisms of sediment delivery, and evaluate the effects of basin scale on the interpretation of cosmogenic nuclide concentrations measured in sediment. Long-term sediment generation and denudation rate estimates for large-scale basins are usually based on extrapolation, assuming steady-state, of measured short-term sediment loads (Ahnert, 1970; Judson, 1968; Judson and Ritter, 1964; Pinet and Souriau, 1988; Saunders and Young, 1983). However, when these extrapolations are

used to infer sediment generation rates over thousands of years, significant errors in estimates of long-term rates are inevitable (Meade, 1988, 1969; Trimble, 1977).

^{10}Be and ^{26}Al are produced in quartz from the interaction of secondary cosmic rays (primarily high-energy neutrons) with Si and O (Lal, 1988). These cosmogenic radionuclides accumulate most rapidly in sediment and bedrock residing at or near Earth's surface (< 3 m depth); accumulation or "production" rates decrease exponentially with depth (Lal, 1988). An inverse relationship exists between the rate at which sediment is being generated and transported from a drainage basin (erosion) and the concentration of in situ-produced cosmogenic nuclides in that sediment (Lal, 1991; Brown et al., 1995a; Bierman and Steig, 1996; Granger et al., 1996). Cosmogenic nuclides present in sediment inherently integrate erosion rates over long periods of time ($\geq 10^3$ years) and over large spatial scales. Thus, they are promising monitoring tools for the estimation of long-term rates of sediment generation (Small et al., 1999; Bierman and Steig, 1996; Granger et al., 1996; Brown et al., 1995a; Clapp et al., in press).

In this work, we apply the techniques developed for determining basin-wide sediment generation rates in small basins (Small et al., 1999; Bierman and Steig, 1996; Granger et al., 1996; Brown et al., 1995a; Clapp et al., in press), to both the entire Yuma Wash drainage and to smaller sub-basins of the Wash. Inconsistencies in rates determined at the two scales reflect scale-related differences in the relative importance of sediment generation, transport, and storage processes. Tracing nuclide concentrations in sediment along the length of Yuma Wash, we identify significant sediment source areas. In small-scale, upland channels, alluvium is supplied primarily from hillslope colluvium and erosion of bedrock outcrops. Along the main stem, incised channels derive much of their sediment load from erosion of basin alluvium stored in terraces, the beveled toes of long-inactive alluvial fans. Nuclide concentrations in upland basins represent the production rate of sediment from the weathering of bedrock (sediment generation). Nuclide

concentrations in main stem samples reflect both upland sediment generation and the long-term effects of sediment storage and reworking.

4.3 Geomorphic Setting

Yuma Wash, an ephemeral tributary to the Colorado River, is located in the Sonoran Desert of southwestern Arizona (Figure 1). The wash drains a 187 km² basin that ranges in elevation from 823 meters above mean sea level (m-msl) at Mojave Peak in the north, to 56 m-msl at the confluence with the Colorado River in the south. The braided channel of Yuma Wash extends approximately 26 km and reaches a maximum width of nearly 600 meters.

Precipitation in the basin (91 mm yr⁻¹ on average) is characterized by short but intense, localized, convective storms, during which most of the sediment transport within the basin occurs (Ayers-Associates, 1996). Stream flow and sediment transport within the wash occur as rapidly moving flood waves. For most runoff events, stream waters quickly infiltrate the alluvium upon which Yuma Wash flows, rather than flowing continuously to the Colorado River.

Yuma Wash drainage basin is underlain by Tertiary volcanic bedrock (primarily rhyolite) in the north and east, and intrusive Jurassic granites in the south and west (Reynolds, 1988). The rhyolitic rocks are highly competent and erosion resistant. Quartz content of the rhyolite is generally low (<5%) yet quartz veins provide sufficient material for separation of quartz and chemical isolation of in situ-produced cosmogenic ¹⁰Be and ²⁶Al. In contrast, the granitic rocks to the south are highly weathered and generally contain > 10% quartz.

The Yuma Wash drainage basin is bordered by the Chocolate Mountains to the east and north, and by the Trigo Mountains to the west (Figure 1). Between the Chocolate and Trigo Mountains, large, coalescing and highly dissected alluvial fans occupy the

valley floor (Figure 2). The fan deposits (maximum thickness > 10 m; Ayers-Associates, 1996) consist of inter-bedded debris flows, mudflows, and fluvial gravels, which are incised by Yuma Wash and its tributaries. These alluvial deposits cover between 60 and 70% of the drainage basin. Well-developed desert pavements and darkly varnished pebbles and cobbles cover parts of the fans, indicating that some surfaces are stable over time periods in excess of several thousand years. Fan deposits in Yuma Wash are believed to correlate with middle to late Pleistocene surfaces found elsewhere in the region (Dohrenwend et al., 1991), although no numerical chronology has been established, and no ^{14}C datable material was found during this study. Some of the fan deposits appear to have been tilted and beveled, suggesting that they might be much older.

The southwest sub-basin (Figures 1 & 3) is characterized by the steep (10° to 30°), weathered, granitic slopes of the Trigo Mountains. Elevations in the sub-basin range from 354 m-msl to 122 m-msl. Much of the sub-basin (~70%) are slopes mantled with very thin colluvium (generally < 20 cm). The upper 40% (by area) of the basin has little sediment storage with the exception of 2 to 3-meter thick colluvial deposits at the base of some steep slopes; channel sediments of the upper wash are likely derived directly from down-slope transport of hillslope colluvium. Lower in the sub-basin, sediment storage becomes more significant where a transition from the steep upper basin terrain to the coalescing fan terrain of the main wash occurs. The poorly consolidated material through which the lower reaches of the southwest fork cuts are 2 to 10-m thick interbedded deposits of fluvial gravels from the channel and colluvial deposits from the hillslopes above.

4.4 Methods

Sample Collection

Samples were collected to quantify cosmogenic nuclide concentrations throughout Yuma Wash and the southwest fork sub-basin (Table 1). Samples of channel sediment were collected from immediately above the junction of 8 tributaries to Yuma Wash and at 5 locations along the main stem of the wash (Figure 1). This sampling strategy allows for an interpretation of relative sediment contributions from each of the tributaries through the use of mixing models. Each of the channel samples is an integration of smaller samples taken at ~ 1 m intervals across the wash. We collected our samples from the top 10 cm of the channel sediment.

In the southwest sub-basin, we collected 3 samples from upland granitic outcrops, 3 composite samples of hillslope colluvium, two depth profiles of the basin alluvium, and 5 homogenized samples of the active channel sediments (Figure 1). The granite samples were collected from ridges surrounding the sub-basin. The hillslope colluvium samples were collected on three different hillslopes; each was an integration of evenly spaced (~ 1 m) samples taken along ~100 m downslope transects YPG-23, 24, and 25 (Figure 1). Each of the hillslope transect samples was also an integration of the total depth (10 to 20 cm) of hillslope colluvium. We assumed complete mixing of sediment would occur for such shallow cover.

Two depth profiles were sampled where the southwest fork cuts through the interbedded alluvial and colluvial deposits (Figure 1). Four sediment samples were collected (each integrated over a 10-cm depth range) from an 8-meter-deep profile at sample location YPG-10. The profile samples were taken 2 m, 4 m, 6 m, and 8 m below the ground surface. A similar profile (YPG-26) was sampled 1400 m down stream. Sediment samples here were taken 1.5 m, 2.5 m, and 3.5 m below the surface of the 3.5-meter-deep channel cut.

Sample Preparation

Sediment samples were dry sieved into seven size fractions (<250 μm , <500 μm , <1000 μm , <2000 μm , <4000 μm , <12,700 μm , and > 12,700 μm) and weighed. Particles smaller than 250 μm were not used for isotopic analysis in order to minimize the effect of potential aeolian contributions from outside the basin. Samples YPG-2 and YPG-19 were used for a detailed nuclide versus grain size evaluation. For sample YPG-2, all six grainsize fractions greater than 250 μm were analyzed separately. For YPG-19, the 1000 to 2000 μm and 2000 to 4000 μm fractions had to be combined to make one sample and the 4000 to 12,700 μm and >12,700 μm fractions were combined to make another sample, due to small sample sizes. The size fractions for twelve of the sediment samples from the southwest sub-basin were recombined according to their weight percentages to yield three composite size fractions (250 to 1000 μm , 1000 to 4000 μm , and >4000 μm) to test nuclide concentration dependence on grainsize. Bedrock samples and the previously sieved sediment samples greater than 1000 μm were crushed and sieved to yield optimal particle sizes for sample processing of 250 to 1000 μm . The remaining 13 sediment samples were sieved to yield only the 250 to 1000 μm size fraction that was used for analysis (sediment grain size data is included in Appendix A).

All samples were heated and ultrasonically etched, once in 6N HCl and then repeatedly in 1% HF and 1% HNO₃ in order to isolate 20 to 30 g of pure quartz and remove any atmospheric ¹⁰Be (Kohl and Nishiizumi, 1992). The samples were then dissolved using HF and the Be and Al were isolated using ion chromatographic techniques. For all samples, 250 μg of Be carrier was added prior to digestion. ¹⁰Be/⁹Be and ²⁶Al/²⁷Al ratios were determined by accelerator mass spectrometry at Lawrence Livermore National Laboratory. ¹⁰Be and ²⁶Al concentrations were then calculated from known amounts of ⁹Be (measured amount added as carrier) and ²⁷Al (native to the quartz

and measured in duplicate aliquots by Inductively Coupled Argon Plasma Spectrometry – Optical Emission).

Data Interpretation

Measurements of both ^{10}Be and ^{26}Al provide a verification of laboratory methods and constrain the exposure history of the samples we analyzed. Measured ratios ($\mu=5.98 \pm 0.32$) of ^{26}Al to ^{10}Be (Figure 4) are consistent with the currently accepted production ratio of $\sim 6:1$ (Nishiizumi et al., 1989), indicating that our laboratory methods are robust, and that the sediment and bedrock we sampled do not have long-term (>100 ky), complex histories of burial and exhumation. Because the two isotopes are well correlated, we present primarily the ^{10}Be measurements in the results and discussion sections. However, the ^{26}Al measurements included in Table 1 have been used in all erosion rate calculations we present.

Production rates of 6.03 and 36.8 (atoms $\text{g}^{-1} \text{yr}^{-1}$) for ^{10}Be and ^{26}Al , respectively (Nishiizumi et al., 1989), scaled for latitude and elevation according to Lal (1991) and assuming no muon production (Brown et al., 1995b) and 20% uncertainty (Clark et al., 1995), were used in calculation of erosion rates. No corrections have been made for quartz enrichment (Small et al., 1999). All statistical comparisons were made using a confidence interval of 90% and independent, t-tests assuming unequal variance (Ott, 1993).

4.5 Results and Discussion

Analyses of ^{10}Be and ^{26}Al from both the small, southwest sub-basin and the larger, Yuma Wash drainage basin, provide considerable information about drainage basin dynamics. Southwest sub-basin data allow us to determine important sources of sediment and understand better, the processes of upland sediment generation (regolith production) by comparing nuclide concentrations measured in specific geomorphic features. Main stem Yuma Wash data allow us to determine areas of significant sediment yield, including entire sub-basins and sediment stored in fans and terraces. Integration of the data collected at both scales identifies scale-related differences in basin dynamics.

Grainsize

Samples collected in both the southwest sub-basin and along the main stem of Yuma Wash demonstrate that nuclide concentrations are independent of sediment grainsize. Within the southwest sub-basin, three grainsize fractions combined from 12 samples, give nearly identical mean concentrations (Figure 5). Standard deviations increase with grainsize as the number of particles analyzed per unit weight of sample decreases. Two samples (YPG-2 and YPG-19) from along the main stem of Yuma Wash, divided into six and four grainsize fractions, respectively, also show no grainsize related trends in nuclide concentrations (Figure 6). In addition, we analyzed separately a single quartz clast (~55 mm diameter) from sample YPG-2. Measurement of the single clast (YPG-2Q) illustrates the idiosyncratic history of clasts and utility of averaging many particles as opposed to measuring a single particle. We find that YPG-2Q has ^{10}Be and ^{26}Al concentrations (0.50 ± 0.10 and $2.77 \pm 0.24 \times 10^5$ atoms g^{-1}) that are less than half the average for all other YPG-2 samples (1.10 ± 0.06 and $7.0 \pm 0.27 \times 10^5$ atoms g^{-1}).

Independence of nuclide concentration and grainsize implies that both large and small particles are produced by similar processes and transported at similar rates. This finding contrasts with that of Brown et al. (1995a) who found distinct isotopic dependence on grainsize in a humid region where deep-seated landslides and rockslides bring large-grained, lightly-dosed material to the channel while fine- to medium-grained material with higher isotopic concentrations is delivered to the stream by gradual, surface-dominated processes of weathering, soil creep, and sheet wash. In Yuma Wash, sediment is generally delivered to the channel by surficial rather than deep-seated processes.

Consistent with arid-region sediment transport theory, we observed no dependence of sediment nuclide concentrations on grainsize. Sediment transport in ephemeral streams of arid regions often occurs in pulses during infrequent, large, storm events. The intense nature of these transport events is characterized by turbulent flows which transport material of many different sizes at similar rates (Laronne and Reid, 1993; Laronne et al., 1994; Reid and Laronne, 1995). These flows often infiltrate the channel after short distances; flow duration is insufficient to armor the bed or selectively transport finer grainsizes.

Southwest Sub-basin

Detailed sampling of the southwest sub-basin provides insight into the generation and transport of sediment in a small, upland, arid drainage basin. The ^{10}Be concentrations measured in bedrock outcrops ($2.73 \pm 0.28 \times 10^5$ atoms g^{-1} , $n=3$) were high (Table 2) compared to those measured in hillslope colluvium ($1.38 \pm 0.15 \times 10^5$ atoms g^{-1} , $n=3$). This result indicates that weathering of bedrock beneath a cover of colluvium is more rapid (less nuclide accumulation) than weathering of exposed bedrock. This observation

is consistent with that of Small et al. (1999) who found that in an alpine region of Wyoming, rates of regolith production beneath a cover of colluvium were nearly twice as fast as on exposed bedrock surfaces.

Lower nuclide concentrations in the sampled colluvium could be the result of cosmic-ray shielding by material now eroded, as nuclide production rates are lower at depth than at the surface. However, to account for the nearly two-fold difference between nuclide concentrations of the bedrock and the colluvium, would require a colluvium depth of ~70 cm, which is unlikely on the steep slopes of this sub-basin and far thicker than we observed. More likely, moisture from infrequent precipitation is stored and held in contact with bedrock for a longer period of time beneath a cover of colluvium than on exposed bedrock surfaces. This longer period of contact facilitates the chemical and mechanical weathering of the sub-colluvial rock (Small et al., 1999; Bull, 1991; Twidale, 1983; Wahrhaftig, 1965; Gilbert, 1877). More rapid weathering of sub-colluvial bedrock compounded with the high percentage of sub-basin area covered with a thin mantle of colluvium (~70%), suggest that sub-colluvial bedrock weathering is the dominant source of sediment to the southwest fork of Yuma Wash. For all surfaces covered with colluvium, a nuclide-based sediment generation rate estimate ($73 \pm 8 \text{ g m}^{-2} \text{ yr}^{-1}$) multiplied by the basin area with colluvial cover (~5.5 km²) yields a yearly sediment generation rate of $40 \times 10^4 \text{ kg yr}^{-1}$ compared to $9.6 \times 10^4 \text{ kg yr}^{-1}$ calculated for bedrock outcrop areas ($40 \pm 9 \text{ g m}^{-2} \text{ yr}^{-1}$ over 2.4 km²).

Comparison of the average ¹⁰Be concentration in southwest sub-basin channel sediment to concentrations in source areas is consistent with sub-colluvial weathering and downslope movement of hillslope colluvium as the dominant source of channel sediment. The average ¹⁰Be concentration in sediment of the southwest sub-basin channel ($1.44 \pm 0.09 \times 10^5 \text{ atoms g}^{-1}$, n=5), is indistinguishable (Table 2) from that measured in the

hillslope colluvium ($1.38 \pm 0.15 \times 10^5$ atoms g^{-1} , $n=3$), but is significantly lower than that measured in the bedrock outcrops ($2.73 \pm 0.28 \times 10^5$ atoms g^{-1} , $n=3$).

In its lower reaches, the southwest sub-basin channel cuts through basin fill stored in terraces of interbedded alluvium and colluvium. Two profiles of this channel-cut basin fill (YPG-10 and YPG-26) show no significant nuclide concentration trends with depth (Figure 7). Field observations of collapsed channel walls indicate that these deposits are an important source of sediment to the lower reaches of the channel. However, the average ^{10}Be concentration of the basin fill ($1.16 \pm 0.07 \times 10^5$ atoms g^{-1}) is statistically less than (Table 2) the average concentration of ^{10}Be measured in the channel sediment ($1.44 \pm 0.09 \times 10^5$ atoms g^{-1}).

Analysis of the spatial distribution of the channel sediment data reveals more detail about the dynamics of sub-basin sediment generation, storage, and transport. In the upper reaches of the southwest sub-basin channel (YPG-11, 12, and 13), average concentrations of nuclides in the channel sediment ($1.56 \pm 0.10 \times 10^5$ atoms g^{-1}) are significantly higher than the average concentration in the lower reaches (YPG-14 & 15 average $1.26 \pm 0.02 \times 10^5$ atoms g^{-1}) indicating different sediment sources. Field observations suggest that in the upper reaches, sediment is derived from either weathering of bedrock beneath a cover of colluvium or by weathering of exposed bedrock outcrops (in and near channel sediment storage is negligible above YPG-14). In lower reaches, there are few direct pathways for hillslope sediment to be delivered to the channel, thus the channel sediments are derived primarily from either channel cutting of basin fill material in the fluvial terraces or from channel alluvium delivered from upstream. These observed sediment sources are consistent with our nuclide measurements.

In upper channel sediment, the average ^{10}Be concentration ($1.56 \pm 0.10 \times 10^5$ atoms g^{-1}) is between that of the bedrock ($2.73 \pm 0.28 \times 10^5$ atoms g^{-1}) and colluvium

($1.38 \pm 0.15 \times 10^5$ atoms g^{-1}) sources. From these concentrations we estimate relative contributions of roughly 13% bedrock and 87% colluvium to the upper channel alluvium, further supporting our conclusion that weathering of bedrock beneath colluvial cover is the dominant source of sediment to the channel. In the lower reaches, the average ^{10}Be concentration ($1.26 \pm 0.02 \times 10^5$ atoms g^{-1}) is between that of the upstream channel alluvium ($1.56 \pm 0.10 \times 10^5$ atoms g^{-1}) and the channel basin fill ($1.16 \pm 0.07 \times 10^5$ atoms g^{-1}) sources. We estimate relative contributions of roughly 25% upstream alluvium and 75% basin fill to the downstream channel alluvium.

Although there are statistical differences between nuclide concentrations of the geomorphic features throughout the basin, the nuclide concentration of the lower channel alluvium is within one standard deviation of all other features excluding the bedrock outcrops. Additionally, the southwest sub-basin data illustrates that as sediment is transported through the basin it is mixed with sediment from different source areas. This mixing of the southwest fork sediment reservoirs implies that ^{10}Be and ^{26}Al concentrations of sediment leaving the sub-basin are representative of nuclide concentrations from throughout the sub-basin drainage. From nuclide concentrations measured near the sub-basin outlet (YPG-15), we calculate average rates of sediment generation and denudation for the southwest sub-basin (Table 3). Results from this sub-basin justify our assumption that channel sediments leaving small, upland sub-basins throughout the Yuma Wash Drainage represent average nuclide concentrations throughout each sub-basin.

Main Drainage Basin

By measuring nuclide concentrations from tributaries and along the main stem of Yuma Wash (Figure 1), we identify sediment source areas and find evidence for long-term trends in sediment transport. In the upper reaches of Yuma Wash (above YPG-19), a simple mixing model, which scales sediment contribution by sub-basin drainage area and nuclide-determined sediment generation rates (Table 4), predicts ^{10}Be and ^{26}Al concentrations in the main stem of Yuma Wash (1.9 and 12.0×10^5 atoms g^{-1} , respectively) consistent with the concentrations measured at YPG-19 (1.8 ± 0.09 and $11.4 \pm 1.3 \times 10^5$ atoms g^{-1} , respectively). In the upper reaches of Yuma Wash, where sediment storage is minimal, our data demonstrate the utility of ^{10}Be and ^{26}Al as sediment-source tracers.

In downstream reaches, as sediment storage increases, our simple mixing model is inconsistent with measurements in Yuma Wash. Along the 26-km of the Wash, we find a regular, downstream decrease in nuclide concentrations, well modeled by an exponential equation (Figure 8). Additionally, at several locations we find that the nuclide concentrations measured in the main stem of the Yuma Wash appear to be slightly lower (although not significant at 2σ) than those of all tributaries upstream (Figure 1). Down basin decreases in elevation (average elevation above sample site) and associated increases in atmospheric shielding (Lal, 1991), could account for only $\sim 14\%$ of the $\sim 50\%$ down-basin decrease in nuclide concentrations. These observations together, suggest an additional and unaccounted for source of low-nuclide concentration sediment to the channel.

Field observations of the Yuma Wash channel cutting into basin fill sediments stored in terraces suggest the source of low-nuclide concentration sediment. To determine

the nuclide concentration of this basin fill, we sampled sediment from a sub-basin that is wholly contained within the basin-fill alluvium (YPG-16). This sample provides an integrated measurement of the nuclide concentrations through a stream-cut cross-section of basin alluvium. The average ^{10}Be concentration we determine for the basin fill ($0.84 \pm 0.05 \times 10^5$ atoms g^{-1}) is substantially lower than sediment supplied directly from the upland sub-basins (1.28 ± 0.05 to $2.19 \pm 0.08 \times 10^5$ atoms g^{-1}). There are several possible explanations for the low-nuclide abundance in the basin fill. First, if the deposits are old (>3 to 4 My), inherited nuclide abundances would have decayed to near zero (deposits as great as 10-m thick would shield much of the material from incoming cosmic rays), and the nuclide concentrations we measure have accumulated since deposition as the basin fill eroded. Alternatively, the alluvium may have been generated at a period of time when the basin was eroding more quickly and average, basin-wide nuclide concentrations were lower. The latter scenario would require sediment generation rates as high as 160 ± 36 $\text{g m}^2 \text{ yr}^{-1}$ at the time of basin-fill deposition.

We use the basin-fill concentrations measured at YPG-16 to calculate mixing ratios between highly-dosed sediment coming from resistant highlands and less-dosed material coming from poorly consolidated and highly-dissected basin fill (Figure 8). As the valley fill thickens downstream and sediment storage becomes more prevalent, our data suggests a downstream increase in sediment contribution from channel incision of the basin fill. Where Yuma Wash discharges to the Colorado River, we estimate over 40% of the sediment it transports has been recycled through the basin fill.

In addition to low-nuclide concentration sediment derived from basin fill, it is likely that lower concentration sediment from more rapidly eroding, quartz-rich, granitic sub-basins contributes to lower nuclide concentrations of the main-stem alluvium. However, only the southern third of the Yuma Wash drainage is influenced by granitic sub-basins and only the lowest of the our main stem sampling locations (YPG-2) could be

influenced. Upstream from YPG-2, YPG-5 receives sediment from only a few low-order tributaries emanating from granitic terrains while receiving most of its sediment from the main stem as it leaves the rhyolitic areas. All other main stem samples are wholly contained within the rhyolitic terrain.

Rates of Sediment Generation and Denudation

From the Yuma Wash data, we calculate rates of sediment generation and denudation (Table 3). Nuclide concentrations measured in the southwest sub-basin support our assumption that sediment exported from small, upland drainage basins is well mixed and representative of sediment generated throughout those basins. We therefore use an average of nuclide-determined sediment generation rates from all sampled basins to estimate the basin-wide sediment generation and denudation rates ($81 \pm 5 \text{ g m}^{-2} \text{ yr}^{-1}$ and $30 \pm 2 \text{ m My}^{-1}$ respectively) for the entire Yuma Wash drainage basin (Table 3). Our rates should be considered minimum estimates as dissolution of non-quartz minerals in regolith can cause concentration of quartz and under-estimation of sediment generation rates (Small et al., 1999). However, quartz enrichment should be minimal in the arid climate and resistant bedrock of Yuma Wash. We also determine basin-wide rates using only nuclide concentrations measured in sediment from near the mouth of Yuma Wash (YPG-2) and find the main stem estimates ($101 \pm 10 \text{ g m}^{-2} \text{ yr}^{-1}$ or $38 \pm 4 \text{ m My}^{-1}$) are slightly higher (~25%) than the estimates from averaging all sub-basins. This dissimilarity between rates suggests that at the larger scale, where sediment storage is significant, nuclide concentrations in alluvium exported from the basin appear to slightly overestimate basin-wide rates of sediment generation and denudation. The higher rate of

denudation we calculate from the main channel sediment analysis suggests that sediment is currently being exported from the basin more quickly than it is being generated in the uplands, an assertion supported by field observations of active stream bank cutting and highly dissected alluvial fan surfaces throughout the basin.

Although the rates calculated from sub-basins and the main stem are statistically separable (at 90% confidence), they are within two standard deviations and well within an order of magnitude. The similarity between the two results suggests that at the larger scale, nuclide concentrations in channel alluvium exported from the basin may be used as a rough approximation of basin-wide rates of sediment generation and denudation.

4.6 Implications

Cosmogenic nuclide concentrations, measured in samples collected from individual geomorphic features in the southwest sub-basin, indicate that sub-colluvial weathering of bedrock generates sediment more quickly ($73 \pm 8 \text{ g m}^{-2} \text{ yr}^{-1}$) than the weathering of exposed bedrock outcrops ($40 \pm 9 \text{ g m}^{-2} \text{ yr}^{-1}$). This difference indicates that the processes of chemical and mechanical weathering by water, held in contact with bedrock, speed the conversion of bedrock to soil in arid environments (Small et al., 1999; Bull, 1991; Twidale, 1983; Gilbert, 1887).

The basin-wide rates of sediment generation ($81 \pm 5 \text{ g m}^{-2} \text{ yr}^{-1}$) and denudation ($30 \pm 2 \text{ m My}^{-1}$) (Table 3) calculated for the uplands supplying sediment to Yuma Wash, are consistent with rates determined by other researchers. Judson and Ritter (1964) calculated denudation rates for 28 major drainages throughout the United States, generally ranging from 10 to 150 m My^{-1} . We expect that our rates should fall on the

lower end of this scale because of the arid climate and erosion-resistant bedrock underlying Yuma Wash. Rates of sediment generation and denudation at Yuma Wash are similar to estimates from a basin of similar climate, elevation and lithology in the Negev Desert of southern Israel (Clapp et al., in press) and are slightly lower than those calculated for a basin at Arroyo Chavez, New Mexico (Clapp et al., 1997) and basins in the Fort Sage Mountains of California (Granger et al., 1996) where the climates are wetter and the elevations higher (Table 3). Our rate estimates are approximately twice those calculated by Small et al. (1999) in the Wind River Range, Wyoming, where samples were collected primarily from summit flats ($<10^\circ$ slopes) as opposed to the steep slopes (10° to 30°) of the Yuma Wash uplands.

Independence of nuclide concentration and sediment grain size is indicative of sediment transport and production processes within arid regions. Arid-region channels transport sediment in discrete pulses before rapidly depositing poorly sorted material. Thus, such channels are likely to leave behind isotopically homogenous sediment as differences in transport times for different size materials are minimal.

Nearly homogenous nuclide concentrations in the southwest sub-basin sediments imply that average sediment storage is so short-lived that stored sediment cannot accumulate detectable amounts of ^{10}Be or ^{26}Al following deposition. This isotopic homogeneity we observe in sediment of small, upland basins, suggests that channel sediment nuclide concentrations are representative of nuclide concentrations throughout such basins.

Cosmogenic nuclide concentrations along the length of the main stem and from individual tributaries of Yuma Wash can be used to determine significant sources of sediment to the channel. Mixing models suggest that in the upper reaches of the wash, sediment supply is predominantly from low-order tributaries transporting material generated by erosion of the uplands. Lower in the basin, where the channel cuts through

poorly consolidated valley alluvium, sediment incorporated from long-term storage becomes an increasingly significant component of the channel load. We use nuclide concentrations to estimate that as much as 40% of sediment exported from Yuma Wash is recycled from the stored basin alluvium.

Basin-wide rates of sediment generation and denudation calculated by averaging rates from all sub-basins are different from rates calculated from nuclides measured in alluvium near the mouth of Yuma Wash. The difference between the rates again suggests that stored sediment is currently being eroded from the basin. Our data clearly show that the effects of sediment storage can be detected and may become even more significant in larger basins with greater storage than Yuma Wash.

4.7 Acknowledgements

Supported by the US Department of Defense, Army Research Office - Terrestrial Sciences (Grants DAAG559710180 & DAAH049610036), NSF Grant EAR-9628559, and Department of Energy contract # W-7405-ENG-48. We thank V. Morrill, K. Nichols, M. Abbott, and C. Massey for assistance in the field, and S. Nies, J. Southan, and B. Copans for assistance in the laboratory, and J. Sevee and P. Maher for additional support.

4.8 References Cited

Ahnert, F., 1970, Functional relationships between denudation, relief, and uplift in large mid-latitude drainage basins: *American Journal of Science*, v. 268, p. 243-263.

Ayers-Associates, 1996, *Geomorphic, Hydrologic, and Vegetation Characterization and Base-Line Conditions of Yuma Wash*. 92-0904.01, U.S. Army Corps of Engineers Waterways Experimental Station, Vicksburg, Mississippi & Conservation

- Program U.S. Army Yuma Proving Grounds, Yuma, Arizona, Yuma Proving Grounds, Arizona: 398 pp.
- Bierman, P. and Steig, E., 1996, Estimating rates of denudation and sediment transport using cosmogenic isotope concentrations in sediment: *Earth Surface Processes and Landforms*, v. 21, p. 125-139.
- Brown, T.B., Stallard, R.F., Larsen, M.C., Raisbeck, G.M. and Francoise, Y., 1995a, Denudation rates determined from accumulation of in situ-produced ^{10}Be in the Luquillo Experimental Forest, Puerto Rico: *Earth and Planetary Science Letters*, v. 129, p. 193-202.
- Brown, E.T. et al., 1995b, Evidence for muon-induced production of ^{10}Be in near surface rocks from the Congo: *Geophysical Research Letters*, v. 22(6), p. 703-706.
- Bull, W.B., 1991, *Geomorphic Responses to Climate Change*: Oxford University Press, New York, 326 pp.
- Clapp, E.M., Bierman, P.B., Pavich, M., and Caffee, M., 1997, Rates of erosion determined using in situ-produced cosmogenic isotopes in a small arroyo basin, northwestern New Mexico: *Geological Society of America Abstracts with Programs*, v. 29, p. 281.
- Clapp, E. M., Bierman, P. R., Schick, A. P., Lekach, J., Enzel, Y., and Caffee, M., 2000, Sediment yield exceeds sediment production in arid region drainage basins: *Geology*, v. 28, p. 995-998.
- Clark, D.H., Bierman, P.R. and Larsen, P., 1995, Improving in situ cosmogenic chronometers: *Quaternary Research*, v. 44, p. 366-376.
- Dohrenwend, J.C., Bull, W.B., McFadden, L.D., Smith, G.I., Smith, R.S.U., and Wells, S.G., 1991, Quaternary Geology of the Basin and Range Province in California: In: R.B. Morrison (Editor), *Quaternary Nonglacial Geology, Conterminous U.S.* Geological Society of America, *The Geology of North America*, p. 353-371.
- Gilbert, G.K., 1877, *Geology of the Henry Mountains (Utah)*: US Geographical and Geological Survey of the Rocky Mountains Region: 170 pp.
- Granger, D.E., Kirchner, J.W. and Finkel, R., 1996, Spatially averaged long-term erosion rates measured from in-situ produced cosmogenic nuclides in alluvial sediment: *Journal of Geology*, v. 104, p. 249-257.
- Judson, S., 1968, Erosion of the land, or what's happening to our continents?: *American Scientist*, v. 56(4), p. 356-374.

- Judson, S. and Ritter, D.F., 1964, Rates of Regional Denudation in the United States: *Journal of Geophysical Research*, v. 69(16), p. 3395-3401.
- Kohl, C.P. and Nishiizumi, K., 1992. Chemical isolation of quartz for measurement of in-situ-produced cosmogenic nuclides: *Geochemica et Cosmochemica Acta*, v. 56, p. 3583-3587.
- Lal, D., 1988, In situ-produced cosmogenic isotopes in terrestrial rocks: *Annual Reviews of Earth and Planetary Science*, v. 16, p. 355-388.
- Lal, D., 1991, Cosmic ray labeling of erosion surfaces: In situ production rates and erosion models: *Earth and Planetary Science Letters*, v. 104, p. 424-439.
- Laronne, J. and Reid, I., 1993, Very high rates of bedload sediment transport by ephemeral desert rivers: *Nature*, v. 366, p. 148-150.
- Laronne, J., Reid, I., Yitshak, Y. and Frostick, L., 1994, The non-layering of gravel streambeds under ephemeral flood regimes: *Journal of Hydrology*, v. 159, p. 353-363.
- Meade, R.H., 1969, Errors in using modern stream-load data to estimate natural rates of denudation: *Geological Society of America Bulletin*, v. 80, p. 1265-1274.
- Meade, R.H., 1988, Movement and storage of sediment in river systems: In: A. Lerman and M. Meybeck (Editors), *Physical and chemical weathering in geochemical cycles*. Kluwer Academic Publishers, p. 165-179.
- Nishiizumi, K., Winterer, E.L., Kohl, C.P., Klein, J., Middleton, R., Lal, D., Arnold, J.R., 1989, Cosmic ray production rates of ^{10}Be and ^{26}Al in quartz from glacially polished rocks: *Journal of Geophysical Research*, v. 94(B12), p. 17907-17915.
- Ott, R.L., 1993, *An Introduction to Statistical Methods and Data Analysis*. Wadsworth Publishing Co., Belmont, CA: 1051 pp.
- Pinet, P. and Souriau, M., 1988. Continental erosion and large-scale relief: *Tectonics*, v. 7(3), p. 563-582.
- Reid, I. and Laronne, J., 1995, Bedload sediment transport in an ephemeral stream and a comparison with seasonal and perennial counterparts: *Water Resources Research*, v. 31, p. 733-781.
- Reynolds, S.J., 1988, *Geologic Map of Arizona*: Arizona Geological Survey.
- Saunders, I. and Young, A., 1983, Rates of surface processes on slopes, slope retreat, and denudation: *Earth Surface Processes and Landforms*, v. 8, p. 473-501.

Small, E.E., Anderson, R.S. and Hancock, G.S., 1999, Estimates of the rate of regolith production using ^{10}Be and ^{26}Al from an alpine slope: *Geomorphology*, v. 27, p. 131-150.

Trimble, S.W., 1977, The fallacy of stream equilibrium in contemporary denudation studies: *American Journal of Science*, v. 277, p. 876-887.

Twidale, C.R., 1983, The research frontier and beyond: granitic terrains: *Geomorphology*, v. 7, p. 187-223.

Wahrhaftig, C., 1965, Stepped topography of the southern Sierra Nevada, California: *Geological Society of America Bulletin*, v. 76, p. 1165-1190.

Year	Area (km ²)	Denudation Rate (mm/yr)	Regolith Production Rate (t/yr)	Regolith Production Rate (t/yr)	Regolith Production Rate (t/yr)	Regolith Production Rate (t/yr)	Regolith Production Rate (t/yr)
1991-1992	1.15	0.15	1.5	1.5	1.5	1.5	1.5
1993-1994	1.15	0.15	1.5	1.5	1.5	1.5	1.5
1995-1996	1.15	0.15	1.5	1.5	1.5	1.5	1.5
1997-1998	1.15	0.15	1.5	1.5	1.5	1.5	1.5
1999-2000	1.15	0.15	1.5	1.5	1.5	1.5	1.5
2001-2002	1.15	0.15	1.5	1.5	1.5	1.5	1.5
2003-2004	1.15	0.15	1.5	1.5	1.5	1.5	1.5
2005-2006	1.15	0.15	1.5	1.5	1.5	1.5	1.5
2007-2008	1.15	0.15	1.5	1.5	1.5	1.5	1.5
2009-2010	1.15	0.15	1.5	1.5	1.5	1.5	1.5
2011-2012	1.15	0.15	1.5	1.5	1.5	1.5	1.5
2013-2014	1.15	0.15	1.5	1.5	1.5	1.5	1.5
2015-2016	1.15	0.15	1.5	1.5	1.5	1.5	1.5
2017-2018	1.15	0.15	1.5	1.5	1.5	1.5	1.5
2019-2020	1.15	0.15	1.5	1.5	1.5	1.5	1.5
2021-2022	1.15	0.15	1.5	1.5	1.5	1.5	1.5
2023-2024	1.15	0.15	1.5	1.5	1.5	1.5	1.5
2025-2026	1.15	0.15	1.5	1.5	1.5	1.5	1.5
2027-2028	1.15	0.15	1.5	1.5	1.5	1.5	1.5
2029-2030	1.15	0.15	1.5	1.5	1.5	1.5	1.5
2031-2032	1.15	0.15	1.5	1.5	1.5	1.5	1.5
2033-2034	1.15	0.15	1.5	1.5	1.5	1.5	1.5
2035-2036	1.15	0.15	1.5	1.5	1.5	1.5	1.5
2037-2038	1.15	0.15	1.5	1.5	1.5	1.5	1.5
2039-2040	1.15	0.15	1.5	1.5	1.5	1.5	1.5
2041-2042	1.15	0.15	1.5	1.5	1.5	1.5	1.5
2043-2044	1.15	0.15	1.5	1.5	1.5	1.5	1.5
2045-2046	1.15	0.15	1.5	1.5	1.5	1.5	1.5
2047-2048	1.15	0.15	1.5	1.5	1.5	1.5	1.5
2049-2050	1.15	0.15	1.5	1.5	1.5	1.5	1.5
2051-2052	1.15	0.15	1.5	1.5	1.5	1.5	1.5
2053-2054	1.15	0.15	1.5	1.5	1.5	1.5	1.5
2055-2056	1.15	0.15	1.5	1.5	1.5	1.5	1.5
2057-2058	1.15	0.15	1.5	1.5	1.5	1.5	1.5
2059-2060	1.15	0.15	1.5	1.5	1.5	1.5	1.5
2061-2062	1.15	0.15	1.5	1.5	1.5	1.5	1.5
2063-2064	1.15	0.15	1.5	1.5	1.5	1.5	1.5
2065-2066	1.15	0.15	1.5	1.5	1.5	1.5	1.5
2067-2068	1.15	0.15	1.5	1.5	1.5	1.5	1.5
2069-2070	1.15	0.15	1.5	1.5	1.5	1.5	1.5
2071-2072	1.15	0.15	1.5	1.5	1.5	1.5	1.5
2073-2074	1.15	0.15	1.5	1.5	1.5	1.5	1.5
2075-2076	1.15	0.15	1.5	1.5	1.5	1.5	1.5
2077-2078	1.15	0.15	1.5	1.5	1.5	1.5	1.5
2079-2080	1.15	0.15	1.5	1.5	1.5	1.5	1.5
2081-2082	1.15	0.15	1.5	1.5	1.5	1.5	1.5
2083-2084	1.15	0.15	1.5	1.5	1.5	1.5	1.5
2085-2086	1.15	0.15	1.5	1.5	1.5	1.5	1.5
2087-2088	1.15	0.15	1.5	1.5	1.5	1.5	1.5
2089-2090	1.15	0.15	1.5	1.5	1.5	1.5	1.5
2091-2092	1.15	0.15	1.5	1.5	1.5	1.5	1.5
2093-2094	1.15	0.15	1.5	1.5	1.5	1.5	1.5
2095-2096	1.15	0.15	1.5	1.5	1.5	1.5	1.5
2097-2098	1.15	0.15	1.5	1.5	1.5	1.5	1.5
2099-2100	1.15	0.15	1.5	1.5	1.5	1.5	1.5

Table 4-1A. Locations and descriptions of samples from Yuma Wash, Arizona for samples with multiple grain-sizes.

Sample	Average Elevation ^a of Basin (km)	Sample Description	Grain Size (microns)	% Sample Mass	¹⁰ Be (10 ⁵ atoms g ⁻¹)	¹⁰ Be Average ^b ± Standard Error (10 ⁵ atoms g ⁻¹)	²⁶ Al (10 ⁵ atoms g ⁻¹)	²⁶ Al Average ^b ± Standard Error (10 ⁵ atoms g ⁻¹)
YPG 2A	0.366	main stem channel sediment	250-500	16%	1.11 ± 0.09		6.54 ± 0.35	
YPG 2B			500-1000	8%	1.39 ± 0.10		7.98 ± 0.46	
YPG 2C			1000-2000	16%	1.08 ± 0.08		7.69 ± 0.44	
YPG 2D			2000-4000	18%	1.18 ± 0.10		6.62 ± 0.42	
YPG 2E			4000-12,700	30%	0.99 ± 0.13		7.11 ± 0.52	
YPG 2F			>12,700	12%	1.09 ± 0.12		1.10 ± 0.06	6.32 ± 0.39
YPG 4A	0.366	main stem channel sediment	250-1000	34%	1.15 ± 0.11		6.46 ± 0.38	
YPG 4B			1000-4000	66%	1.34 ± 0.11		1.28 ± 0.10	6.46 ± 0.38
YPG 10.3A	0.178	sub-basin fill	250-1000	8%	1.25 ± 0.10		7.96 ± 0.48	
YPG 10.3B			1000-4000	32%	1.21 ± 0.07		7.85 ± 0.47	
YPG 10.3C			>4000	60%	1.15 ± 0.08		1.18 ± 0.03	7.65 ± 0.53
YPG 10.5A	0.178	sub-basin fill	250-1000	11%	1.15 ± 0.11		7.68 ± 0.53	
YPG 10.5B			1000-4000	36%	1.47 ± 0.11		6.74 ± 0.71	
YPG 10.5C			>4000	53%	1.36 ± 0.11		1.38 ± 0.09	8.47 ± 1.31
YPG 10.7A	0.178	sub-basin fill	250-1000	10%	0.26 ± 0.20		8.61 ± 0.72	
YPG 10.7B			1000-4000	34%	1.03 ± 0.11		6.92 ± 0.86	
YPG 10.7C			>4000	56%	1.07 ± 0.10		0.98 ± 0.26	7.08 ± 0.54
YPG 10.9A	0.178	sub-basin fill	250-1000	4%	1.19 ± 0.15		10.33 ± 0.76	
YPG 10.9B			1000-4000	14%	1.15 ± 0.11		7.82 ± 0.56	
YPG 10.9C			>4000	82%	1.02 ± 0.09		1.04 ± 0.05	7.85 ± 0.53
YPG 11B	0.241	sub-basin channel sediment	1000-4000	25%	1.51 ± 0.07		na	na
YPG 11C			>4000	75%	1.70 ± 0.09		1.65 ± 0.09	na
YPG 12A	0.241	sub-basin channel sediment	250-1000	7%	1.39 ± 0.10		9.12 ± 0.70	
YPG 12B			1000-4000	37%	1.38 ± 0.07		9.30 ± 0.60	
YPG 12C			>4000	56%	1.32 ± 0.09		1.35 ± 0.02	8.69 ± 1.04
YPG 13A	0.241	sub-basin channel sediment	250-1000	8%	1.36 ± 0.11		9.43 ± 0.66	
YPG 13B			1000-4000	37%	1.58 ± 0.08		8.96 ± 0.49	
YPG 13C			>4000	55%	1.78 ± 0.10		1.67 ± 0.12	15.77 ± 4.45
YPG 14A	0.178	sub-basin channel sediment	250-1000	10%	1.20 ± 0.08		8.50 ± 0.62	
YPG 14B			1000-4000	31%	1.30 ± 0.05		7.43 ± 0.71	
YPG 14C			>4000	59%	1.22 ± 0.06		1.24 ± 0.03	8.11 ± 0.50
YPG 15A	0.178	sub-basin channel sediment	250-1000	15%	1.20 ± 0.07		na	na
YPG 15B			1000-4000	37%	1.22 ± 0.11		na	na
YPG 15C			>4000	48%	1.35 ± 0.06		1.28 ± 0.05	na
YPG 19A	0.545	main stem channel sediment	250-500	7%	1.77 ± 0.10		11.19 ± 0.90	
YPG 19B			500-1000	9%	1.93 ± 0.09		11.37 ± 0.58	
YPG 19C			1000-4000	33%	2.06 ± 0.09		12.33 ± 0.76	
YPG 19F			4000->12,700	51%	1.63 ± 0.08		1.81 ± 0.09	10.90 ± 1.21
YPG 26.1A	0.178	sub-basin fill	250-1000	5%	1.27 ± 0.08		7.63 ± 0.41	
YPG 26.1B			1000-4000	24%	1.22 ± 0.06		7.66 ± 0.41	
YPG 26.1C			>4000	71%	1.28 ± 0.07		1.26 ± 0.02	7.22 ± 0.92
YPG 26.2A	0.178	sub-basin fill	250-1000	4%	1.23 ± 0.11		7.96 ± 0.55	
YPG 26.2B			1000-4000	36%	1.23 ± 0.08		7.40 ± 0.44	
YPG 26.2C			>4000	60%	1.08 ± 0.06		1.14 ± 0.05	7.18 ± 0.42
YPG 26.3A	0.178	sub-basin fill	250-1000	7%	1.17 ± 0.08		6.83 ± 0.63	
YPG 26.3B			1000-4000	25%	1.19 ± 0.07		6.71 ± 0.40	
YPG 26.3C			>4000	68%	1.15 ± 0.06		1.16 ± 0.01	7.65 ± 0.45

Letters indicate multiple grain sizes analyzed at a sampling location.

Numbers following decimals indicate sample order in depth profiles (i.e. YPG 26.3 was the third sample from top of profile).

Table 4-1B. Locations and descriptions of samples from Yuma Wash, Arizona for samples with single grain-size.

Sample	Elevation ^a (km)	Average Elevation ^b of Basin (km)	Sample Description	Grain Size (microns)	¹⁰ Be (10 ⁵ atoms g ⁻¹)	²⁶ Al (10 ⁵ atoms g ⁻¹)
YPG 2Q	0.067	0.366	main stem channel quartz clast	>12,700	0.50 ± 0.10	2.77 ± 0.24
YPG 3A	0.140	0.366	main stem channel sediment	250-1000	1.16 ± 0.07	6.97 ± 0.58
YPG 5A	0.129	0.366	main stem channel sediment	250-1000	1.36 ± 0.07	6.83 ± 0.41
YPG 7	0.323	na	bedrock	na	3.21 ± 0.14	20.77 ± 1.14
YPG 8	0.344	na	bedrock	na	2.25 ± 0.11	12.60 ± 0.70
YPG 9	0.283	na	bedrock	na	2.73 ± 0.15	14.46 ± 0.58
YPG 16A	0.143	0.496	main stem channel sediment	250-1000	0.84 ± 0.05	4.69 ± 0.39
YPG 17A	0.177	0.513	main stem channel sediment	250-1000	1.54 ± 0.06	8.93 ± 0.55
YPG 18A	0.223	0.536	main stem channel sediment	250-1000	1.56 ± 0.06	9.42 ± 0.54
YPG 20A	0.259	0.554	main stem channel sediment	250-1000	1.92 ± 0.11	11.55 ± 0.79
YPG 21A	0.256	0.554	main stem channel sediment	250-1000	2.19 ± 0.08	14.34 ± 0.84
YPG 22A	0.262	0.554	main stem channel sediment	250-1000	1.53 ± 0.14	9.10 ± 1.17
YPG 23	0.207	0.187	hillslope colluvium	250-1000	1.16 ± 0.06	7.56 ± 0.56
YPG 24	0.207	0.187	hillslope colluvium	250-1000	1.32 ± 0.05	8.01 ± 0.47
YPG 25	0.075	0.187	hillslope colluvium	250-1000	1.66 ± 0.05	11.00 ± 0.65
YPG 27	0.238	0.543	main stem channel sediment	250-1000	1.66 ± 0.09	10.39 ± 0.53
YPG 28	0.293	0.547	main stem channel sediment	250-1000	2.16 ± 0.10	14.22 ± 0.73

na-not applicable

all sample location latitudes ~ N33°05'

^a measured using Garmin 75 handheld GPS, verified with USGS topographic map

^b weighted average elevation of drainage basin above the sample location (represents possible elevations of sediment source)

^c YPG-2Q is a single quartz clast from sample YPG-2

Table 4-3. Sediment provenance and geochemical ratios for Yuma Wash Drainage.

Table 4-2. Concentrations of ^{10}Be and test of statistical differences between concentrations in geomorphic features of southwest sub-basin, Yuma Wash.

Geomorphic Feature	Mean \pm Standard Error		Statistical Difference @ 90% Confidence					
	^{10}Be Measured (10^5 atoms g^{-1})	n	Bedrock Outcrop	Hillslope Colluvium	Basin Fill	All Channel	Upper Channel	Lower Channel
Bedrock Outcrops	2.73 \pm 0.28	3	-	Yes	Yes	Yes	Yes	Yes
Hillslope Colluvium	1.38 \pm 0.15	3	Yes	-	No	No	No	Yes
Basin Fill	1.16 \pm 0.07	4	Yes	No	-	Yes	Yes	Yes
Channel Seds (All)	1.44 \pm 0.09	5	Yes	No	Yes	-	-	-
Upper Channel (YPG-11, 12, & 13)	1.56 \pm 0.10	3	Yes	No	Yes	-	-	Yes
Lower Channel (YPG-14 & 15)	1.26 \pm 0.02	2	Yes	Yes	Yes	-	Yes	-

Average ^{10}Be concentrations calculated by first averaging grain-size fractions of each sample then averaging together the samples representing each feature. Statistical differences were determined at 90% confidence using independent t-tests and assuming unequal variances.

Table 4-3. Sediment generation and denudation rates for Yuma Wash Drainage, Arizona.

		This Study			Sediment-Cosmogenic based estimates from other regions				
		Main Stem ^a Channel Sediment	SW Sub-basin ^a Channel Sediment	Average ^b All Sub-basins	Nahal Yae ^c Israel	Arroyo ^c Chavez New Mexico	Fort Sage ^d Mts (A) California	Fort Sage ^d Mts (B) California	Wind River ^e Range Wyoming
Sediment Generation Rate (g m ⁻² yr ⁻¹)	¹⁰ Be	101 ± 10	73 ± 8	81 ± 5	78 ± 16	273 ± 62	162 ± 38	97 ± 24	39 ± 11
	²⁶ Al	100 ± 11	68 ± 8	81 ± 8	70 ± 16	281 ± 73	-	-	35 ± 11
Denudation Rate (m My ⁻¹)	¹⁰ Be	38 ± 4	27 ± 3	30 ± 2	29 ± 6	101 ± 23	60 ± 14	36 ± 9	14 ± 4
	²⁶ Al	37 ± 4	25 ± 3	30 ± 3	26 ± 6	104 ± 27	-	-	13 ± 4

^aDenudation rates calculated using formulation of Bierman & Steig, 1996 and production rates of Nishizumi et al., 1989, scaled for latitude and elevation according to Lal, 1991, and not scaled for slope due to small average slopes (<20%). Conversion between denudation and sediment generation based on densities of 2.7 (g cm⁻³) for bedrock. Rates for main stem calculated using nuclide concentrations from samples collected at location YPG-2 weighted by size fraction relative percent by weight. Rates for SW sub-basin calculated using nuclide concentrations from samples collected at locations YPG-14 and YPG-15 weighted by size fraction relative percent by weight. Average of all sub-basins calculated from samples collected at YPG-4, -15, -18, -20, -21, -22, and -27 weighted by sub-basin drainage area.

^bClapp et al. (in press) -site with similar climate, elevation, and lithologies

^cClapp et al. (1997) -site with higher elevation (~2000 m), wetter climate (377 mm), less resistant bedrock

^dGranger (1996) used both ¹⁰Be and ²⁶Al to calculate erosion rates in two catchments (A & B) - site ~1300 m

^eSmall et al., (1999) -site with higher elevation (~3600 m) and thicker colluvial cover (~90 cm)

Table 4-4. Mixing model results for area upstream from YPG-19 at Yuma Wash, Arizona.

Sample Location (sub-basin)	Sub-basin Drainage Area (km ²)	Sediment Generation Rate (g m ⁻² yr ⁻¹)	Sediment Mass (10 ⁶ kg yr ⁻¹)	% Total Mass	¹⁰ Be	²⁶ Al	¹⁰ Be	²⁶ Al
					Measured Concentration (10 ⁵ atoms g ⁻¹)	Measured Concentration (10 ⁵ atoms g ⁻¹)	Erosion-Weighted Average (10 ⁵ atoms g ⁻¹)	Erosion-Weighted Average (10 ⁵ atoms g ⁻¹)
YPG-21	29.3	59	1.7	42%	2.19	14.3	0.92	5.99
YPG-27	18.6	80	1.5	36%	1.66	10.4	0.60	3.74
YPG-22	5.8	88	0.5	12%	1.53	9.1	0.19	1.13
YPG-20	5.8	70	0.4	10%	1.92	11.6	0.19	1.14
Erosion-weighted average nuclide concentration upstream from YPG-19							1.9	12.0
Measured nuclide concentration at YPG-19 confluence							1.8 ± 0.1	11.4 ± 1.3

Erosion-weighted averages calculated by:

- 1) multiplying sub-basin area by nuclide-determined sediment generation rate to get annual mass of sediment per basin
- 2) calculating the % of the total from all four sub-basins
- 3) multiply % total mass per basin by nuclide concentration and summing the results

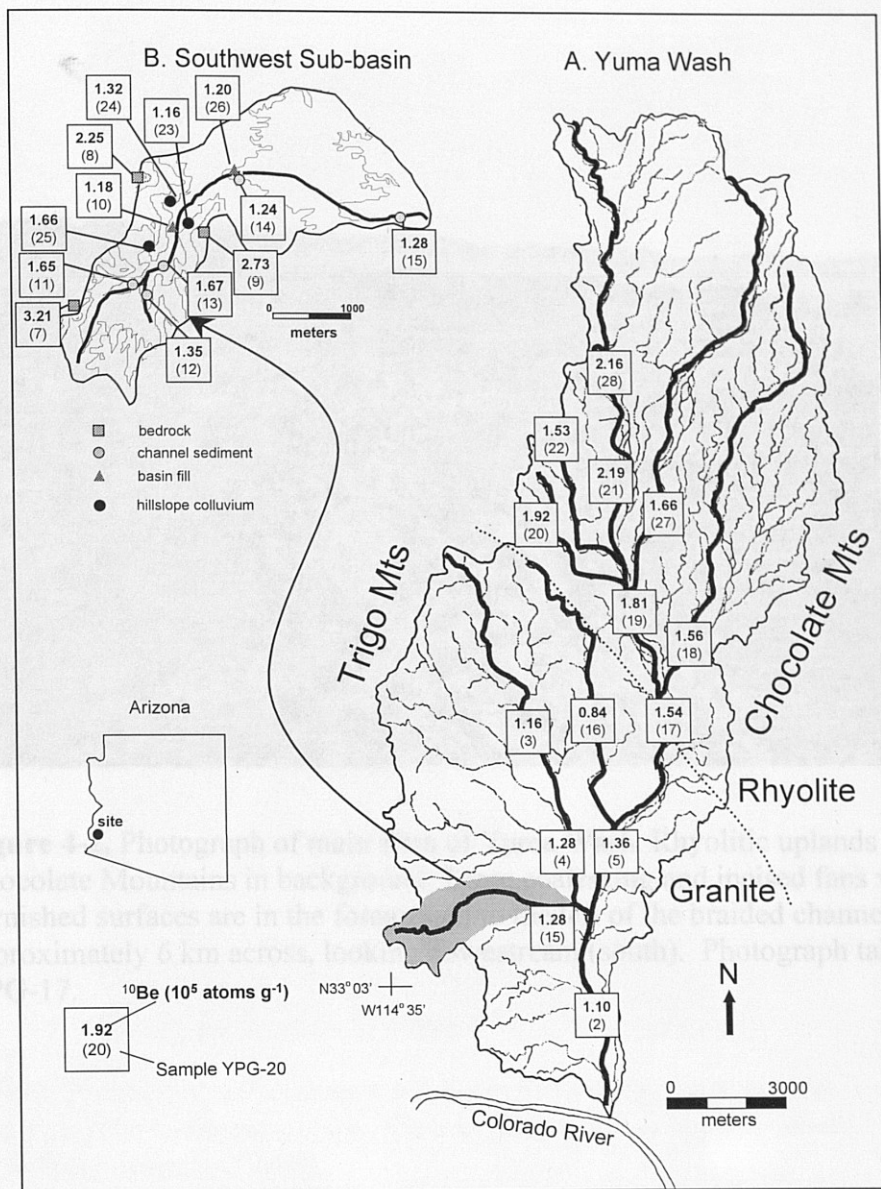


Figure 4-1. Yuma Wash drainage basin located along the Colorado River in southwestern Arizona. A) Sample locations and ^{10}Be concentrations measured in channel alluvium (enclosed in squares). Average ^{10}Be concentrations (**bold**) are plotted with sample identification numbers below in parentheses. Along the main stem, nuclide concentrations decrease closer to the confluence with the Colorado River. Geology adapted from Reynolds, 1988. B) Map of southwest sub-basin with locations of bedrock, hillslope colluvium, basin fill, and channel alluvium samples. Contour interval is 100 ft, ranging from 400 to 1200 ft. Base maps adapted from Ayers-Associates, 1996.



Figure 4-2. Photograph of main stem of Yuma Wash. Rhyolitic uplands of the Chocolate Mountains in background. Large coalescing and incised fans with varnished surfaces are in the foreground to the left of the braided channel. View is approximately 6 km across, looking downstream (south). Photograph taken near YPG-17.



Figure 4-3. Photograph of southwest sub-basin illustrating steep, granitic, upland sections with little sediment storage. View in photograph is approximately 1 km across, looking upstream (west).

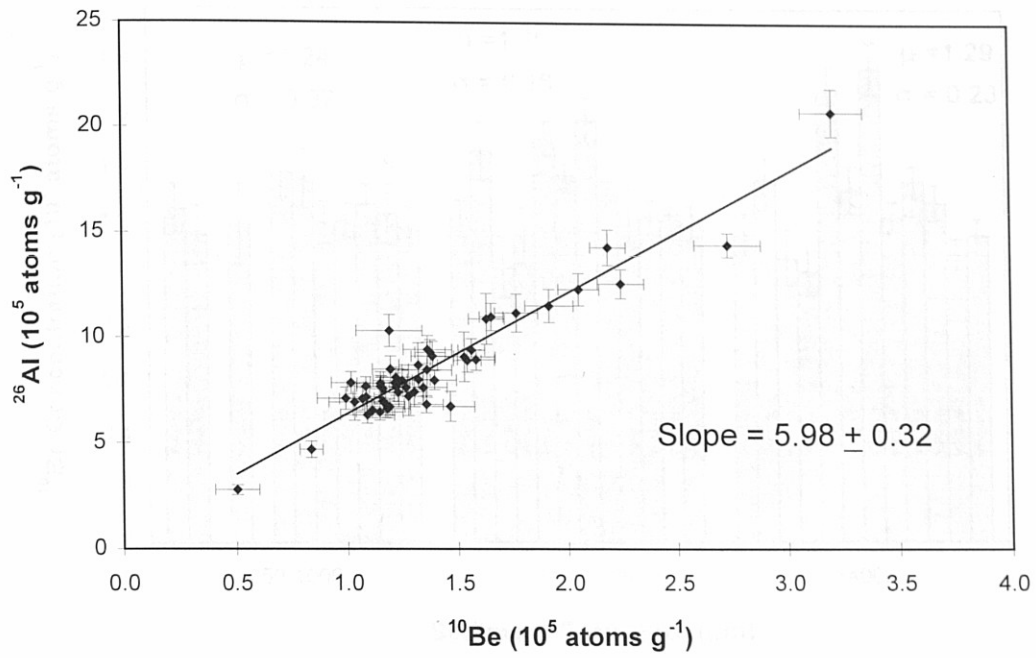


Figure 4-4. ^{10}Be and ^{26}Al concentrations for all Yuma Wash samples. Least squares best fit line has a slope of 5.98 ± 0.32 , and y-intercept near zero (0.40 ± 0.24) consistent with the currently accepted production ratio of ~6:1 (Nishiizumi et al., 1989).

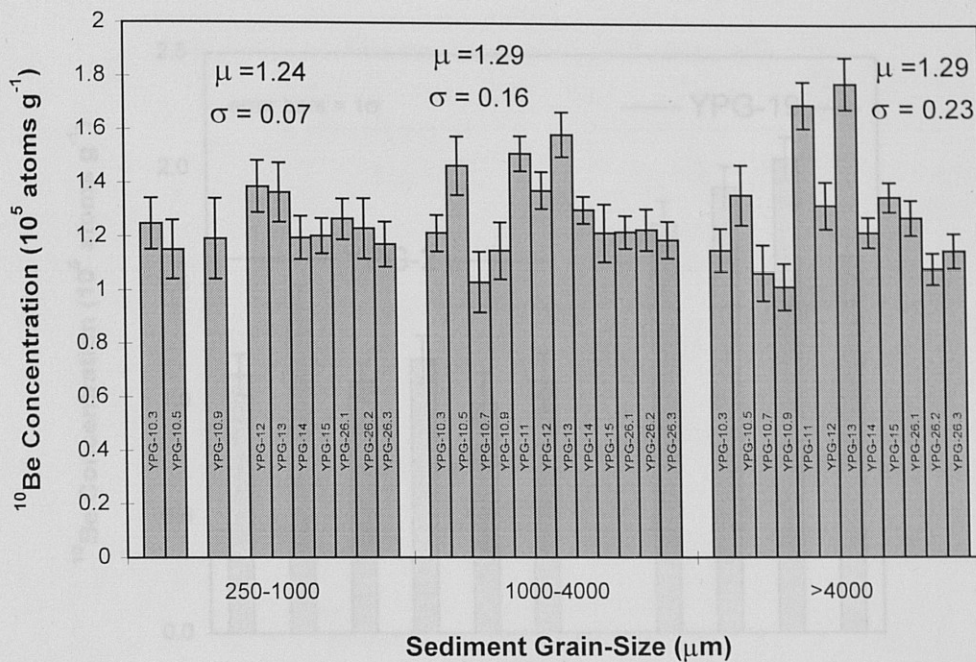


Figure 4-5. Sediment grainsize versus ^{10}Be concentration for all sediment samples analyzed. Mean nuclide concentration is similar for the three grainsize fractions. Variability increases with increasing grainsize because the number of particles analyzed for coarser-grained material is less than the number analyzed for finer-grained material.

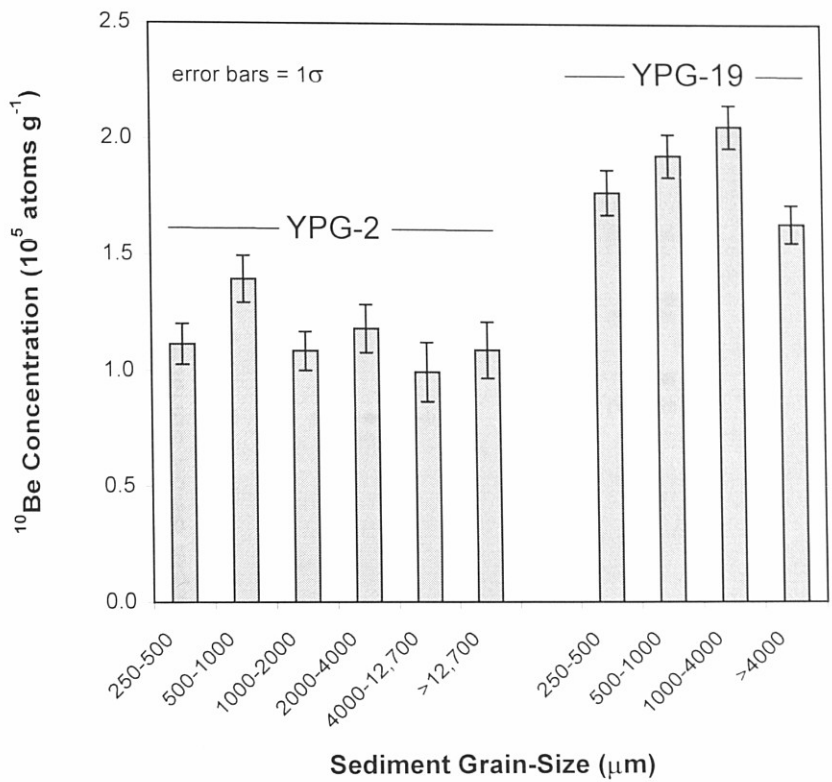


Figure 4-6. Sediment grainsize versus ^{10}Be concentration for YPG-2 (6 size fractions) and YPG-19 (4 size fractions). There are no grainsize related trends in nuclide concentrations.

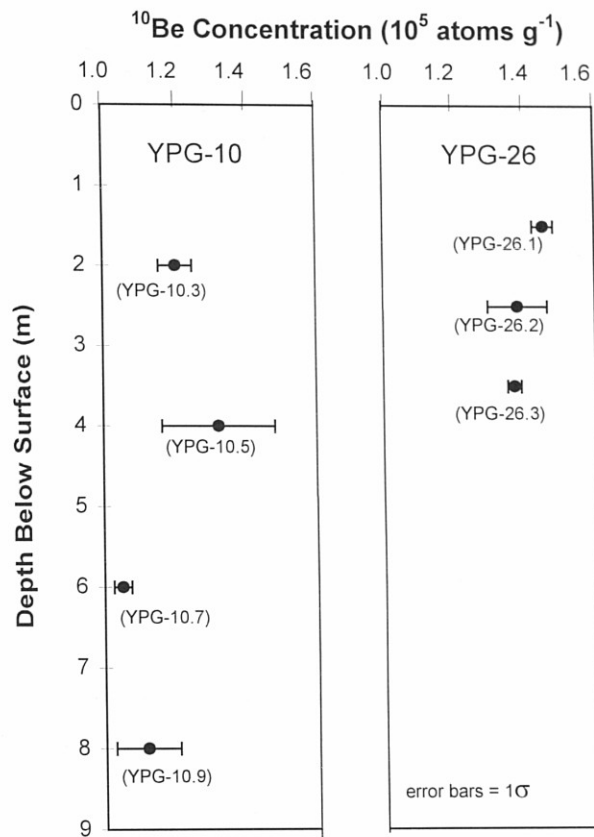


Figure 4-7. ¹⁰Be concentrations plotted against depth for profiles measured in two basin fill deposits (YPG-10 and YPG-26) along the channel of the southwest sub-basin. No significant depth-related trends are evident.

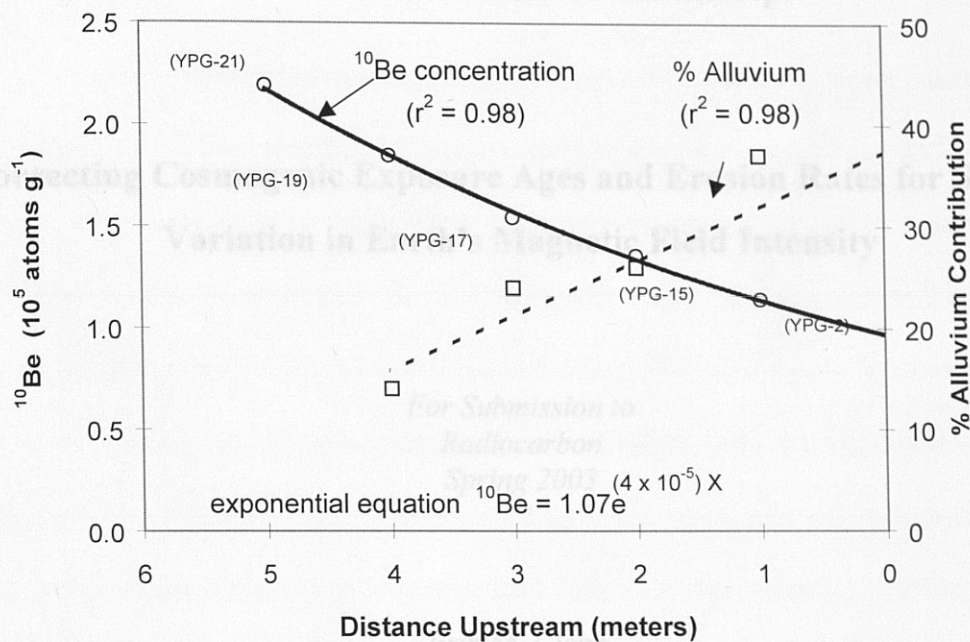


Figure 4-8. Trend of sample distance downstream versus ^{10}Be concentrations along with results of mixing model for the main stem of Yuma Wash. Open circles represent ^{10}Be concentrations at locations designated in parenthesis (see Figure 1 for sample locations). The downstream trend is well modeled by an exponential equation. The mixing model described in Table 4 was also used to predict nuclide concentrations at specific confluences along the main stem of Yuma Wash. Model concentrations higher than measured concentrations indicate the addition of low-nuclide alluvium ($0.84 \times 10^5 \text{ atoms g}^{-1}$, YPG-16) to the channel. Open squares above, represent the % of low-nuclide alluvium necessary to equilibrate model and measured concentrations. The percentage of low-nuclide alluvium added at each point along the main stem increases downstream as nuclide concentrations of main stem channel sediment decrease.

*Present address: Seves & Maher Engineers, Inc., 4 Blanchard Road, Box 85A, Cumberland Center, Maine, 04021. E-mail: ensc@smmaine.com.

Keywords: ^{10}Be , ^{26}Al , cosmogenic, magnetic field, correction, calibration, exposure age, erosion rates

5.0 Cosmo-Calibrate Manuscript

Correcting Cosmogenic Exposure Ages and Erosion Rates for Secular Variation in Earth's Magnetic Field Intensity

*For Submission to
Radiocarbon
Spring 2003*

Erik M. Clapp*
Paul R. Bierman

*School of Natural Resources & Department of Geology,
University of Vermont, Burlington, Vermont, 05401, USA*

**Present address: Sevee & Maher Engineers, Inc., 4 Blanchard Road, Box 85A,
Cumberland Center Maine, 04021. E-mail: emc@smemaine.com.*

*Keywords: ^{10}Be , ^{26}Al , cosmogenic, magnetic field, correction, calibration, exposure age,
erosion rates*

5.1 Abstract

To account for geomagnetically-induced changes in cosmogenic nuclide production rates in situ, and thereby increase the potential accuracy of age dating and erosion rate calculations, we use a Monte Carlo type simulation, forced by a compilation of 33 geomagnetic paleointensity records, to correct model exposure ages and erosion rates for temporal variations in Earth's magnetic field strength. Applying our corrections to several existing data sets generally decreases calculated exposure ages, increases calculated rates of erosion, and suggests systematic age errors associated with time-averaged production rates may be greater than 45% for older samples (> 100 ka) at high elevations (3 to 6 km asl) and low latitudes (0 to 10°). Errors may be on the order of 20% to 30% for samples exposed > 40 ka at lower elevations (sea level to 1 km asl). Our results are generally consistent with other, recent correction methods suggesting our methods are robust; however, our results also suggest that systematic age errors associated with variations in Earth's magnetic field may be greater than previously thought. The corrections we present account for errors associated with the measurement of magnetic field strength over time, the non-dipole component of the field, and other errors associated with modeling exposure ages and erosion rates, including nuclide half-lives, neutron attenuation coefficients, sample latitude, sample latitude, sample thickness, sample density, and exposure geometry.

5.2 Introduction

Cosmogenic nuclides have become a widely used tool for dating bedrock exposures and Quaternary geomorphic features (e.g., Philips et al., 1990, Nishiizumi et

5.1 Abstract

To account for geomagnetically-induced changes in cosmogenic nuclide production rates in situ, and thereby increase the potential accuracy of age dating and erosion rate calculations, we use a Monte Carlo type simulation, forced by a compilation of 33 geomagnetic paleointensity records, to correct model exposure ages and erosion rates for temporal variations in Earth's magnetic field strength. Applying our corrections to several existing data sets generally decreases calculated exposure ages, increases calculated rates of erosion, and suggests systematic age errors associated with time-averaged production rates may be greater than 45% for older samples (> 100 ka) at high elevations (3 to 6 km asl) and low latitudes (0 to 10°). Errors may be on the order of 20% to 30% for samples exposed > 40 ka at lower elevations (sea level to 1 km asl). Our results are generally consistent with other, recent correction methods suggesting our methods are robust; however, our results also suggest that systematic age errors associated with variations in Earth's magnetic field may be greater than previously thought. The corrections we present account for errors associated with the measurement of magnetic field strength over time, the non-dipole component of the field, and other errors associated with modeling exposure ages and erosion rates, including nuclide half-lives, neutron attenuation coefficients, sample latitude, sample latitude, sample thickness, sample density, and exposure geometry.

5.2 Introduction

Cosmogenic nuclides have become a widely used tool for dating bedrock exposures and Quaternary geomorphic features (e.g., Philips et al., 1990, Nishiizumi et

al., 1993, Bierman et al., 1995b, 1999; Brown et al., 1998; Gosse and Phillips, 2001; Zehfuss et al., 2001), and for determining rates of erosion or sediment generation (e.g., Clapp et al., 2000, 2001, 2002; Nichols et al., 2002; Small et al., 1999; Granger et al., 1996; Bierman and Caffee, 2001, 2002). Systematic uncertainties, inherent to the interpretation of cosmogenic nuclide measurements, make correlations with other dating systems uncertain (Clark et al., 1995; Dunai, 2001; Gosse and Phillips, 2001; Masarik et al., 2001; Shanahan and Zreda, 2000). The greatest uncertainties in determining cosmogenic exposure ages or erosion rates of samples for which exposure history is well constrained, are nuclide production rates as a function of time, altitude, and latitude. Recent work has begun to address altitude and latitude scaling for production by neutron spallation (Dunai, 2000, Desilets and Zreda, 2001) and by slow muon capture (Stone, 2000). This paper presents a model building on the earlier works of Clark et al. (1995), Clapp and Bierman (1996), Nishiizumi et al. (1996), and Shanahan and Zreda (2000), which consider the effect of changing dipole field strength on nuclide production rates. The results of our corrections are compared to those of several other groups who have recently made similar corrections using different methodologies. Other models have not accounted for temporal variations in changing field strength coupled with changing production rates with depth, necessary to produce corrected erosion rates.

5.3 Nuclide Systematics

Measured cosmogenic nuclide activities (N) are interpreted using generalized analytical models (Lal, 1988, 1991). Exposure ages are determined using a model (Lal, 1988) that can be solved for exposure age (t) while considering radioactive decay (λ), the nuclide abundance (N), and the production rate of at the site from spallation (P_s) and the production rate at the site from muons (P_m).

$$N = \frac{P_s}{\lambda} (1 - e^{-\lambda t}) + \frac{P_m}{\lambda} (1 - e^{-\lambda t}) \quad \text{eq. (1)}$$

Erosion rates are determined using a model (Lal, 1991) that can be solved for erosion (ε) while considering the density of the overlying material (ρ), the attenuation coefficient of fast neutrons (Λ_s), the attenuation coefficient of slow muons (Λ_m), and radioactive decay.

$$N = \frac{P_s}{\varepsilon \rho \Lambda_s^{-1} + \lambda} + \frac{P_m}{\varepsilon \rho \Lambda_m^{-1} + \lambda} \quad \text{eq. (2)}$$

These model ages and erosion rates are beholden to a variety of assumptions (Lal and Peters, 1967; Gosse and Phillips, 2001) including temporally constant production rates (P). Time-integrated production rates are determined empirically by measuring nuclide activities in samples, the age of which have been established by other dating techniques (e.g., Nishiizumi et al., 1989, Bierman et al., 1996, Stone et al., 1998, Kubik et al., 1998). Most production rates have been determined from samples ≤ 20 ka, for which mass loss by erosion is considered to be minimal.

Production varies systematically with altitude and latitude (Lal, 1991; Dunai, 2000, Desilets and Zreda, 2001) and by convention, rates are normalized to sea level (SL) and high latitudes $> 60^\circ$ (HL) for comparison. Production also varies through time as the strength of Earth's magnetic field changes (Lal, 1988; Kurz et al. 1990; Mazaud et al., 1991; Shanahan and Zreda, 2000; Dunai, 2001; Masarik et al., 2001). Because the effects of field strength change on nuclide production rates differ with altitude and latitude, normalized production rates determined at different sites from samples exposed for different periods of time may not be the same (Clark et al., 1995).

Many estimates of ^{10}Be and ^{26}Al production rates have been published (Nishiizumi et al., 1989; Clark et al., 1995; Gosse and Klein, 1996; Nishiizumi et al.,

1996; Stone et al., 1998; Klein et al., 2000, Stone, 2000, Gosse and Stone, 2001).

Production rates integrated over 2 years to 7 My have converged on ~ 5.2 and 30.9 atoms $\text{g}^{-1} \text{yr}^{-1}$ (for ^{10}Be and ^{26}Al , respectively), when rescaled using common assumptions regarding muon production (3% at SL and HL per Stone, 2000), altitude and latitude scaling for spallation (Lal, 1991), altitude scaling for muons ($\Lambda=247 \text{ g cm}^{-2}$), and latitude scaling for muons the same as for spallation. However, these rates still carry an uncertainty of $>10\%$ (Bierman et al., 2002). One of the most substantial factors controlling the flux of cosmic rays and the production of cosmogenic isotopes is intensity of Earth's magnetic field (Lal, 1988; Kurz et al. 1990; Mazaud et al., 1991; Shanahan and Zreda, 2000; Dunai, 2001; Masarik et al., 2001;), thus correcting for changes in magnetic field strength over time has the potential to increase the accuracy of exposure age and erosion rate calculations.

5.4 Correction for Geomagnetic Field Strength

To demonstrate the importance of magnetic field strength changes and to increase the accuracy of interpreted cosmogenic ages and erosion rates from measured nuclide abundances, we have developed a Visual Basic-based computer model (Cosmo Calbrate) that corrects cosmogenic nuclide calculations for the effects of secular changes in Earth's magnetic field strength (Dunai, 2001; Masarik et al., 2001; Shanahan and Zreda, 2000). The model fully propagates uncertainties and allows for correction of a multitude of nuclides and production rates based on user-defined inputs. Model documentation is included within the model and in Appendix C.

Model Structure

To account for changes in magnetic field intensity over time, all production rate scaling and error estimates are forced by a synthetic paleointensity record which is made up of the SINT-800 record (Guyodo and Valet, 1999) for the time period between 10 and 800 ka, and the $\Delta^{14}\text{C}$ -derived paleointensity record of Stuiver et al. (1998), for the time period between 0 and 10 ka. From the synthetic paleointensity record, a user-defined number of model production rate records (generally, 30 to 100) are calculated. For each given point in time, there will be magnetic field strength values generated and instantaneous production rates calculated, each of which will have a random-normal distribution defined by the error associated with the synthetic record. For each of the model production rate records generated, the model then iterates back along the record to determine a starting age in the past (exposure age) that results in a nuclide activity equal to that measured in the sample to be calibrated, when atoms are accumulated and subtracted (radioactive decay) from past to present. The average and standard error of the mean of the results from all of the records gives the exposure age and associated error. For erosion rates, the model production rate record is applied; the model then iterates backward to determine the rate at which a particle must have traveled from depth to the Earth's surface, accumulating atoms so as to contain a nuclide activity equal to that measured in the sample to be calibrated.

Paleointensity Data

During the past decade, numerous geomagnetic paleointensity records have been published as summarized by Guyodo and Valet (1996, 1999) and Masarik et al. (2001). Because there are site specific, non-dipole, field-strength variations (Raisbeck et al., 1994), no single record is representative of global paleointensity; yet, the existing paleointensity records are well correlated and show similar long-term intensity variations suggesting coherence on a global scale (Guyodo and Valet, 1996; 1999). Guyodo and Valet (1996), compiled and overlaid 17 existing, globally dispersed, paleointensity records to produce a worldwide, synthetic paleointensity record during the past 200 ky (SINT-200). Guyodo and Valet (1999) added an additional 16 paleointensity records to the SINT-200 record, to produce a record over the past 800 ky (SINT-800). SINT-800 provides the most comprehensive, long-term comparison of paleointensity data to date and yields a coherent average intensity and intensity variability versus time record (average coefficient of correlation=0.7). The uncertainty in the synthetic record is the result of variations in sedimentation rates, analytical procedures, and localized, non-dipole variations in paleointensity.

It should be noted that during the past 10 ky, SINT-800 has relatively high statistical uncertainties (Frank et al., 1997, Guyodo and Valet, 1996, 1999; Masarik et al., 2001), and does not correlate well with several other recently published records (Dunai, 2001). Therefore, similar to Masarik et al., (2001) we have chosen the dendrochronologically derived $\Delta^{14}\text{C}$ record of Stuiver et al., (1998) to represent the paleomagnetic record between the present and 10 ka. Similar to recent works by Masarik et al. (2001), and Dunai (2001), we have chosen SINT-800 to represent the

paleomagnetic record for the time period of 10 ka to 800 ka. The two records are combined to create a single synthetic record that is used by our model to correct cosmogenic exposure ages and erosion rates for geomagnetic field intensity variations over time (Figure 1). Statistical methods allow us to account for uncertainties in field strength over various time periods.

Interpretation of Instantaneous Production Rates from Paleointensity Data

For each model iteration, we randomly generate a model paleointensity record (Figure 2A) using a normally distributed random number generator constrained by the mean and standard error of the synthetic paleointensity record. The time-step between points along the model record are not constant, but are controlled by the separation of points in the synthetic record. Each point along the model paleointensity record is converted to an apparent paleolatitude (Figure 2B) according to Nishiizumi et al. (1989) and then to an instantaneous production rate (Figure 2C) by using the altitude/latitude scaling of Lal (1991) with muons scaled separately based on Stone (2000), Nishiizumi et al. (1989), and a user-defined percentage of muon contribution at sea level and high latitude. At low latitudes (where the cosine of the paleolatitude is >1) or during periods of high magnetic field intensity ($M/M_0 > 1$), instantaneous production rates are calculated using the formulation of Elsaesser et al. (1956), consistent with the approach of Shannahan and Zreda (2000). Although this formulation does not generally consider the non-dipole component of the magnetic field, the non-dipole component is considered in our statistical methods. Specifically, the random generation of points that comprise our model paleointensity record is controlled by the errors associated with the synthetic

curve; errors which include the non-dipole component as well as other errors associated with the interpretation of paleointensity values from deep sea cores.

Based on the model production rate record, the model accumulates and decays atoms in 1000 year time steps. The model iterates back in time along the instantaneous production rates curve until two starting points are reached, which bracket the user-defined, measured number of atoms. The model then linearly interpolates between two constraining thousand year increments to determine a model exposure age. A model erosion rate is simultaneously calculated using equation 2, a similar iterative method as described for the model exposure age calculations, and assuming steady-state erosion.

For erosion rates, the model accumulates atoms as a particle moves from a depth of 10 meters below Earth's surface, until the particle reaches the surface, using a time-step determined by the time it takes for a particle to move upward 1-cm at a given erosion rate. For different erosion rates, the time for a particle to travel upward 1-cm is different. The model production rate record is used to determine the surface production rate at a specific time in the past, related to the particle's depth. The surface production rate is then scaled (Lal, 1988) for the depth of the particle at a given time. Thus for each 1-cm increment, the particle will accumulate and decay atoms at the specified production rate. The model iteratively determines two erosion rates which result in nuclide abundance that bracket the user-defined nuclide abundance. The model then linearly interpolates between two constraining erosion rate increments to determine a model exposure age. Erosion rate increments are 1 mMy^{-1} (for 0 to 10 mMy^{-1}), 10 mMy^{-1} (for 10 to 100 mMy^{-1}), and 100 mMy^{-1} (for $>100 \text{ mMy}^{-1}$).

Determination of Initial Production Rates (P_0)

In order to determine instantaneous production rates in the past, we need to establish a nominal, contemporary, model production rate (P_0) which can be forced through each model production rate record. Determination of P_0 was carried out iteratively. ^{10}Be and ^{26}Al rates were determined for the Sierra Nevada (Table 1) site using exposure ages of 11 cal ka (Nishiizumi et al. 1989) as well as 12, 13, and 14 cal ka (Clark et al., 1995). P_0 was adjusted for the data set until the model nuclide activity for the appropriate calibration duration equaled the activity measured at the calibration site. The model also allows for the selection of the contemporary ^{10}Be P_0 measured by Nishiizumi et al. (1996) in water target experiments or allows the model user to determine a P_0 from their own data or the data of others.

Uncertainty Analysis

We use a Monte Carlo approach to propagate uncertainties. For each exposure age or erosion rate correction, we randomly generate multiple (generally 30 to 100) model paleointensity records through which all corrections are forced. The corrected ages or rates from each of the records are averaged together to yield a final corrected value along with an associated error calculated as the standard error of the mean of the results.

In addition to uncertainties in the paleointensity record, the model we present propagates uncertainties in initial production rates, laboratory nuclide measurements, nuclide half-life, neutron attenuation coefficient, sample latitude, sample altitude, sample thickness, exposure geometry, and sample density. For each of these parameters, a normally distributed, random number is generated for each model iteration, based on

errors specified by the user. Default settings include 5% uncertainties for all parameters except nuclide production rate (20% uncertainty) and laboratory nuclide measurement (uncertainty determined by the laboratory). Therefore, for each time-step (exposure age) or depth increment (erosion rates), the model uses randomly generated parameter values to calculate the number of atoms accumulated and decayed. These values are summed to determine the exposure age or erosion rate for an individual model production rate record and the results from multiple iterations give an average and standard error as the final result.

The uncertainties in model exposure ages and erosion rates, directly associated with the paleointensity curves, are approximately $\pm 5\%$. Large uncertainties associated with empirically estimated production rates in conjunction with smaller uncertainties associated with muon production, nuclide attenuation length, laboratory procedures, nuclide half-life, sample density, and sample latitude, account for an additional 15% to 20% error. Because the model accounts for uncertainty present, yet not reported in most cosmogenic studies to date, the geomagnetic correction effectively increases the accuracy of the final calculations yet decreases the perceived precision. As more geomagnetic field intensity data, refined production rate estimates, and better correction schemes become available, the precision and accuracy of the reported exposure ages and erosion rates will improve.

Over short periods of time (several ky) there may be significant differences between the geomagnetic latitude and the geographic latitude of a site. However, the long-term average of the geographic latitude becomes similar to that of the geomagnetic latitude after several thousand years (Merrill and McElhinny, 1983). Therefore, the

model uses the geographic latitude to calculate exposure ages and erosion rates. However, small changes in estimating the geomagnetic latitude can result in relatively large errors in production rates (Klein and Gosse, 1996). Production rates can change by as much as 1.6% per degree between 20 and 30 degrees of latitude as illustrated by Gosse and Phillips (2001, figure 8). The model accounts for errors associated with uncertainty in sample location by propagating a 5% error through the Monte Carlo simulation.

5.5 Results and Discussion

To illustrate the utility and validity of our correction scheme, we present a sensitivity analysis of model results, and compare our methods to previously published geomagnetic corrections. We then apply our model to several previously published studies to show how our correction may effect the conclusions of these and other studies involving cosmogenic nuclides.

Model Sensitivity Analysis

Correction of model exposure ages and erosion rates for changes in magnetic field strength over time has the potential to reduce systematic errors. At low latitudes (0 to 10°), where cosmic rays are most affected by Earth's magnetic field, differences between geomagnetically corrected and uncorrected ages (as great as $\pm 50\%$ at extreme high altitudes) are most notable (Figure 3A). At higher latitudes, where Earth's magnetic field has a decreasing effect on incoming cosmic rays, age errors decrease (Figures 3B and 3C), and approach zero as latitude approaches 60°. These differences are sensitive to the age and location of the original production rate calibration as well as the assumptions used in the original calculations.

Differences between corrected and uncorrected ages also increase with increasing elevation (Figures 3A, 3B, and 3C), due to attenuation of incoming fast neutrons which increases with atmospheric depth. At low latitudes (0 to 10°), age differences near sea level range from ~+12% to ~+35; however, at extreme, high elevations (6 km) the differences increase to ~-50% to ~+50% (Figure 3A). At high latitudes, the elevation-related age differences are reduced and approach zero as latitude approaches 60° (Figures 3B and 3C).

Age differences are also related to the duration of sample exposure to cosmic ray bombardment. Age differences generally increase with the duration of sample exposure. Most production rate estimates are based on age estimates of the Sierra Nevada data of Nishiizumi, et al. (1989) or the age estimates of Clark et al. (1995) for the same Sierra Nevada data. These estimates are for a time period over the past 13 to 15 ky. During the past ~20ky, Earth's magnetic field strength has been greater than the long-term average, and thus uncorrected nuclide production rates are generally lower than the long-term average. At low latitudes and high elevations, where the magnetic field has the greatest effect on production rates, uncorrected ages can be more than 50% less than corrected ages (Figure 3A). Near sea level, or at higher latitudes (>20°), and uncorrected ages are generally greater than corrected ages and age differences continue to increase slowly over time (Figures 3B and 3C).

Comparison to Other Corrections

Several other methods, which have been recently published, can be used to correct exposure ages and erosion rates for the effects of temporal changes in Earth's magnetic

field strength (Mazarik et al., 2001; Dunai, 2001, Shanahan and Zreda, 2000). The methods we use are similar to those suggested by Shanahan and Zreda (2000), and proposed by Clark et al. (1995) and Clapp and Bierman (1996), which make use of scaling factors of Lal (1991) and the magnetic field curves of Goyudo and Valet (1996). Shanahan and Zreda (2000) compared their corrected cosmogenic ages of stromatolites to ages determined independently using ^{14}C (Hillaire-Marcel and Casanova, 1986). Their geomagnetic corrected ages were within one standard deviation of the ^{14}C dates suggesting that geomagnetic correction methods chosen for their study and for this study are robust. The ~20% underestimation of their uncorrected ages (Shanahan and Zreda, 2000) is consistent with results from our model for low latitude ($<10^\circ$), high elevation (>3 km asl) sites (Figure 3A).

Dunai (2001) presents a scaling model similar to that of Lal (1991) with recalculated scaling factors based on data from neutron monitors, nuclear emulsions, and cloud chambers (Desilets and Zreda, 2001). Dunai (2001) also uses the SINT-800 curve to correct for ages >10 ka, but has chosen a slightly different magnetic field record (a combined record from Ohno and Hamano, 1993 and McElhinny and Senanayake, 1982) for ages <10 ka. Scaling factors from our model (Figure 4) show similar temporal patterns to that of Dunai (2001), but result in normalized production rates (normalized to current production rates at SL) that reach as high as ~ 1.37 (atoms $\text{g}^{-1} \text{y}^{-1}$) compared to maximum rates of ~ 1.20 (atoms $\text{g}^{-1} \text{y}^{-1}$) from Dunai (2001), a difference of 14%.

Mazarik et al., (2001) use a model that simulates the interaction of cosmic ray particles with matter, based on the GEANT (Brun et al., 1987) and MCNP (Briesmeister, 1993) codes as described in Mazarik and Beer, 1999. Similar to our model, Mazarik et al.

(2001) use the SINT-800 curve (Guyodo and Valet, 1999) and the ^{14}C curve (Stuiver et al., 1998). Again, our model results show a similar temporal pattern (Figure 4) but result in normalized production rates that reach as high as ~ 1.37 (atoms $\text{g}^{-1} \text{y}^{-1}$) compared to maximum rates of ~ 1.12 (atoms $\text{g}^{-1} \text{y}^{-1}$) from Mazarik et al. (2001); a difference of 22%.

The normalized production rates from our model differ from the other models by 14 to 22%. This difference is likely the result of the different scaling models chosen. Our model currently makes use of the Lal (1991) scaling model which to date is the most widely accepted.

Case Studies

Application of our model to published data suggests that uncorrected cosmogenic data may substantially misestimate exposure ages and rates of erosion. To demonstrate the importance and effect of correcting cosmogenic model ages and erosion rates for paleointensity variations, we use our model to reanalyze data from three recent publications, Zehfuss et al. (2000), Bierman and Caffee (2001), and Clapp et al. (2000).

Age corrections associated with interpretation of data with longer exposure histories (>40 ky) are greater than those with shorter exposure histories (<40 ky) because production rate calibration sites are generally young. Zehfuss et al. (2001), used ^{10}Be and ^{26}Al abundances, measured in boulders of debris flow fans, to determine slip rates along the Fish Springs Fault in Owens Valley, California. A long-term slip rate of approximately 0.25 m ky^{-1} , was determined from the cosmogenic measurements of boulders on the West Fan, which yielded average boulder ages of 107.3 ± 10.9 ky (assuming no erosion). Geomagnetic correction of the Zehfuss et al. (2001) data (Figure

5) results in boulder ages of 99.5 ± 10.8 ky (assuming no erosion). This decrease in boulder ages associated with correction for changes in geomagnetic field strength results in a 9% increase in calculated long-term slip rates along the Fish Springs Fault. The decrease in boulder ages and increase in slip rates associated with the corrections is substantial for these older samples (99 to 124 ky). For younger fans (South Fan, Fan B, and Fan C), with exposure ages less than 30 ky, the correction results in age errors of only a few thousand years. For locations with ages less than 15 ky, uncorrected ages actually become less than the corrected ages.

Larger discrepancies for more heavily dosed samples result from recalculating erosion rates of Bierman and Caffee (2001), who measured ^{10}Be and ^{26}Al abundances in bedrock outcrops across west-central Namibia. These measurements were used to describe the Pleistocene erosional history of Namibia and to show that the Namibian landscape is approaching geomorphic steady-state. Uncorrected erosion rates of the bedrock samples ranged from 1.1 to 7.5 mMy^{-1} . When corrected using our methods (Figure 6), erosion rates range from 1.4 to 13.4 mMy^{-1} , and the long-term average erosion rate of $3.5 \pm 0.3 \text{ m my}^{-1}$, increases to $5.1 \pm 0.5 \text{ m my}^{-1}$, an increase of 47%. This increase is likely the result of low latitude exposure over long periods of time.

In Chapter 3 of this dissertation (Clapp et al., 2000) we used ^{10}Be and ^{26}Al abundances measured in bedrock and sediments to determine basin-wide rates of sediment generation ($78 \pm 16 \text{ tons km}^{-2} \text{ y}^{-1}$) in the Nahal Yael drainage basin, southern Israel (30° , 0.245 km). Sediment generation rates were slightly less than sediment export rates ($126 \pm 13 \text{ tons km}^{-2} \text{ y}^{-1}$) determined from a 30-yr sediment budget (Schick and Lekach, 1993), thus suggesting the stream over the long-term was exporting more

sediment from the basin than was being produced by weathering of bedrock. Correcting the cosmogenic data results in the nuclide-based rates of sediment generation that are 13% greater ($88 \pm 3 \text{ tons km}^{-2} \text{ y}^{-1}$), decreasing the difference between long-term sediment production and short-term sediment yield. Thus, although the conclusion that the basin is currently exporting sediment from storage remains valid, the basin appears to be nearer to steady state than previously thought.

Contemporary Production Rates (P_o)

By iteratively calibrating the model to different production rate sites, we have established nominal contemporary production rates (P_o) from the Sierra Nevada data (Nishiizumi et al., 1989; Clark et al., 1995) ranging from 4.9 to 6.3 atoms $\text{g}^{-1} \text{ y}^{-1}$ (Table 5-1). Our results are similar to the empirically measured, water target-based, contemporary rates ($5.2 \pm 0.3 \text{ atoms g}^{-1} \text{ y}^{-1}$) determined by Nishiizumi et al. (1996) and recent production rate measurements ($5.1 \text{ atoms g}^{-1} \text{ y}^{-1}$) of Kubic et al. (1998). Our results are also in agreement with the average the average production rate of $5.1 \text{ atoms g}^{-1} \text{ y}^{-1}$ (average of all production rate studies to date) suggested by Stone (2000), thus suggesting that our approach is valid. The contemporary rate of Nishiizumi et al. (1996) and the average rate suggested by Stone (2000) fall between our 13 ka and 14 ka contemporary rates determined for the Sierra Nevada site, indicating deglaciation of the site between 13 and 14 ka, consistent with ages suggested by Clark et al. (1995).

5.6 Conclusions

The use of our model (Cosmo-Calibrate) accounts for systematic errors known to affect the interpretation of cosmogenic nuclide data. Our results are similar to those from other correction schemes (Mazarik et al., 2001; Dunai, 2001, Shanahan and Zreda, 2000); however, our method also accounts for the uncertainties associated with the geomagnetic field strength record and is the only model to correct erosion rates as well as exposure ages. The model we present thus has the potential to increase the accuracy of cosmogenic dating techniques and erosion rate calculations and to provide quantitative estimates of the errors associated with data interpretation. Use of our model may allow for the robust dating and correlation of brief geomorphic or climatic events. Our model is available at www.geology.uvm.edu/morphwww/cosmolab.

5.7 Acknowledgments

Research supported by Army Research Office STIR Grant DAAH04-95-1-0408 to Bierman and Clapp; additional support from J. Sevee and P. Maher. Thanks to D. Howell and A. Gillespie for technical advice. Earlier versions of this paper benefited from reviews by M. Stuiver, J. Gosse, and D. Elmore.

5.8 References Cited

- Bierman, P., and Caffee, M., 2001, Slow rates of rock surface erosion and sediment production across the Namib Desert and Escarpment, southern Africa: *American Journal of Science*, v. 301, p. 326-358.
- Bierman, P., Clapp, E. M., Nichols, K. K., Gillespie, A. R., and Caffee, M., 2001, Using cosmogenic nuclide measurements in sediments to understand background rates of erosion and sediment transport: in Harmon, R. S., and Doe, W. M., eds., *Landscape Erosion and Evolution Modelling*: New York, Kluwer, p. 89-116.

- Bierman, P., and Steig, E., 1996, Estimating rates of denudation and sediment transport using cosmogenic isotope abundances in sediment: *Earth Surface Processes and Landforms*, v. 21, p. 125-139.
- Bierman, P., Larsen, P., Clapp, E., and Clark, D., 1996, Refining Estimates of ^{10}Be and ^{26}Al production rates: *Radiocarbon*, v. 38, p. 149.
- Briesmeister, J.F., 1998, MCNP-A general Monte Carlo N-particle transport code, Version 4A: Publication LA-12625-M, Los Alamos National Laboratories.
- Brun R., Caillat, M., Maire, M., Patrick, G.N., and Urban, L., 1987, GEANT User's Guide, Europ Report DD/EE/84-1: European Organization. for Nuclear Research (CERN), Geneva, 584 pp.
- Clapp, E. and Bierman, P., 1996, Cosmo-Calibrate: a program for calibrating cosmogenic exposure ages: *Radiocarbon* v. 38, p. 151-152.
- Clapp, E. M., Bierman, P. R., Schick, A. P., Lekach, J., Enzel, Y., and Caffee, M., 2000, Sediment yield exceeds sediment production in arid region drainage basins: *Geology*, v. 28, p. 995-998.
- Clapp, E.M., Bierman, P.R., Pavich, M., and Caffee, M., 2001, Rates of sediment supply to arroyos from uplands determined using in situ produced cosmogenic ^{10}Be and ^{26}Al in , sediments: *Quaternary Research*, v. 55, p. 235-245.
- Clapp, E.M., Bierman, P.R., and Caffee, M., 2002, Using ^{10}Be and ^{26}Al to determine sediment generation rates and identify sediment source areas in an arid region drainage basin, *Geomorphology*, v. 45, p. 67-87.
- Clark, D., Bierman, P. R. and Larsen, P., 1995, Improving in situ cosmogenic chronometers: *Quaternary Research*, v. 44, p. 366-376.
- Desilets, D., and Zreda, M., 2001, On scaling cosmogenic nuclide production rates for altitude and latitude using cosmic-ray measurements: *Earth and Planetary Science Letters*, v. 193, p. 213-225.
- Dunai, T.J., 2000, Scaling factors for production rates of in situ produced cosmogenic nuclides: a critical reevaluation: *Earth and Planetary Science Letters*, v. 176, p. 157-169.
- Dunai, T.J., 2001, Influence of secular variation of the geomagnetic field on production rates of in situ produced cosmogenic nuclides: *Earth and Planetary Science Letters*, v. 193, p. 197-212.
- Elsaesser, W., Ney, E.P., Winckler, J.R., 1956, Cosmic Ray intensity and geomagnetism: *Nature*, v. 178, p. 1226-1227.

- Frank, M., Schwarz, B., Baumann, S., Kubik, P.W., Suter, M., and Mangini, A., 1997, A 200 kyr record of cosmogenic radionuclide production rates and geomagnetic field intensity from ^{10}Be on globally stacked deep sea sediments: Earth and Planetary Science Letters, v. 149, p. 121-129.
- Gosse, J. C., Evenson, E. B., Klein, J., Lawn, B. and Middleton, R., 1995, Precise cosmogenic ^{10}Be measurements in western North America: Support for a global Younger Dryas cooling event: Geology, v. 23, p. 877-880.
- Gosse, J.C., and Klein, J., 1996, Production rate of in situ cosmogenic ^{10}Be in quartz at high altitude and mid-latitude: Radiocarbon, v.38, p.154-155.
- Gosse, J.C., and Stone, J.O., 2001, Terrestrial cosmogenic nuclide methods passing milestones toward paleo-altimetry: EOS Transactions of the American Geophysical Union, v. 82, p. 82-89.
- Gosse, J. C., and Phillips, F. M., 2001, Terrestrial in situ cosmogenic nuclides: theory and application: Quaternary Science Reviews, v. 20, no. 14, p.1475-1560.
- Granger, D. E., Kirchner, J. W., and Finkel, R., 1996, Spatially averaged long-term erosion rates measured from in-situ produced cosmogenic nuclides in alluvial sediment: Journal of Geology, v. 104, p. 249-257.
- Guyodo, Y., and Valet, J.P., 1999, Global changes in intensity of the Earth's magnetic field during the past 800 kyr: Nature, v. 399, p. 249-252.
- Guyodo, Y., and Valet, J.P., 1996, Relative variations in geomagnetic intensity from sedimentary records: the past 200,000 years: Earth and Planetary Science Letters, v. 143, p. 23-26.
- Hillaire-Marcel, C., Carro, O., and Casanova, J., 1986, ^{14}C and Th/U dating of Pleistocene and Holocene stromatolites from east African paleolakes: Quaternary Research, v. 25, p. 312-329.
- Klein, J., and Gosse, J., 1996, Terrestrial factors that influence production rates: Radiocarbon v. 38, p. 161-162.
- Klein, J., Gosse, J., Davis, P.T., Evenson, E.B., and Sorenson, C.J., 2000, Younger Dryas in the Rocky Mountains and the calibration of $^{10}\text{Be}/^{26}\text{Al}$ production rates: Geological Society of America Abstracts with Programs, v. 31, p. A-473.
- Kubik P.W., Ivy-Ochs, S., Masarik, J., Frank, M., Schluchter, C., 1998, ^{10}Be and ^{26}Al production rates deduced from an instantaneous event within the dendro-calibration curve, the landslide of Koefels, Oetz Valley, Austria: Earth and Planetary Science Letters, v. 161, p. 231-241.

- Kurz, M. D., D. Colodner, T. W. Trull, R. Moore, and K. O'Brien, 1990, Cosmic ray exposure dating with in situ produced cosmogenic ^3He : results from young Hawaiian lava flows: *Earth and Planetary Science Letters*, v. 97, p. 177-189.
- Lal, D., 1988, In situ-produced cosmogenic isotopes in terrestrial rocks: *Annual Reviews of Earth and Planetary Science*, v. 16, p. 355-388.
- Lal, D., 1991, Cosmic ray labeling of erosion surfaces: In situ production rates and erosion models: *Earth and Planetary Science Letters*, v. 104, p. 424-439.
- Lal, D., and Peters, B., 1967, Cosmic ray produced radioactivity on Earth: in *Handbook der Physik*, Sitte, K., (ed), Springer-Verlag, New York, p. 551-612.
- Mazarik, J., and Beer, J., 1999, Simulation of particle fluxes and cosmogenic nuclide production in the Earth's atmosphere: *Journal of Geophysical Research*, v. 104, p. 12099-12111.
- Mazarik, J., Frank, M., Schafer, J.M., and Wieler, R., 2001, Correction of in situ cosmogenic nuclide production rates for geomagnetic field intensity variations during the past 800,000 years: *Geochemica et Cosmochemica Acta*, v. 65, p. 2995-3003.
- Mazaud, A., Laj, C., Bard, E., Arnold, M. and Tric, E., 1991, Geomagnetic field control of ^{14}C production over the last 80 ky: implications for the radiocarbon time scale: *Geophysical Research Letters*, v. 18, p. 1885-1888.
- McElhinny, M.W., and Senanayake, W.E., 1982, Variations in the geomagnetic dipole 1: the past 50000 years: *Journal of Geomagn. Geoelectr.*, v. 34, p. 39-51.
- Merrill, R.T., and McElhinny, M.W., 1983, *The Earth's Magnetic Field, Its History, Origin, and Planetary Prospective*: Academic Press, New York, 235 pp.
- Nichols, K.K., Bierman, P.R., Hooke, R.L., Clapp, E.M., and Caffee, M., 2002, Quantifying sediment transport on desert piedmonts using ^{10}Be and ^{26}Al : *Geomorphology*, v. 45, p. 105-125.
- Nishiizumi, K., Lal, D., Klein, J., Middleton, R., and Arnold, J.R., 1986, Production of ^{10}Be and ^{26}Al by cosmic rays in terrestrial quartz in situ and implications for erosion rates: *Nature*, v. 319, p. 134-136.
- Nishiizumi, K., Winterer, E. L., Kohl, C. P., Klein, J., Middleton, R., Lal, D. and Arnold, J. R., 1989, Cosmic ray production rates of ^{10}Be and ^{26}Al in quartz from glacially polished rocks: *Journal of Geophysical Research*, v. 94, p. 17907-17915.
- Nishiizumi, K., Kohl, C.P., Arnold, J.R., Dorn, R. Klein, J., Fink, D., Middleton, R., and Lal, D., 1993, Role of in situ cosmogenic nuclides ^{10}Be and ^{26}Al in the study of diverse geomorphic processes: *Earth Surface Processes and Landforms*, v. 18, p. 407-425.

Table 5-1. Estimated contemporary production rates at time = 0 (Po).

- Nishiizumi, K., Finkel, R.C., Klein, J., Kohl, C. P., 1996, Cosmogenic production of ^7Be and ^{10}Be in water targets: *Journal of Geophysical Research*, v. 101, p. 225-22,232.
- Ohno, M., and Hamano, Y., 1993, Global analysis of the geomagnetic field: Time variation of the dipole moment and the geomagnetic pole in the Holocene: *Journal of Geomagnetism and Geoelectricity*, v. 45, p. 1455-1466.
- Phillips, F.M., Zreda, M.G., Smith, S.S., Elmore, D., Kubik, P.W., and Sharma, P., 1990, Cosmogenic Chlorine-36 chronology for glacial deposits at Bloody Canyon, eastern Sierra Nevada: *Science*, v. 248, p.1529-1532.
- Raisbeck, G., Yiou, Y., and Zhou, S.Z., 1994, Paleointensity puzzle: *Nature*, v. 371, p. 207-208.
- Schick, A.P., and Lekach, J., 1993, An evaluation of two ten-year sediment budgets, Nahal Yael, Israel: *Physical Geography*, v. 14, p. 225-238.
- Shanahan, T.M., and Zreda, M., 2000, Chronology of Quaternary glaciations in East Africa, *Earth and Planetary Science Letters*, v. 177, p. 23-42.
- Small, E. E., Anderson, R. S., and Hancock, G. S., 1999, Estimates of the rate of regolith production using ^{10}Be and ^{26}Al from an alpine slope: *Geomorphology* v. 27, p. 131-150.
- Stone, J. O., Ballantyne, C. K., and Fifield, L. K., 1998, Exposure dating and validation of periglacial weathering limits, Northwest Scotland: *Geology*, v. 26, no. 7, p. 587-590.
- Stone, J., 2000, Air pressure and cosmogenic isotope production: *Journal of Geophysical Research*, v. 105, p. 23753-23759.
- Stuiver, M., Reimer, P.J., Bard, E., Beck, J.W., Burr, G.S., Hughen, K.A., Kromer, B., McCormac, G., van der Plicht, J., and Spurk, M., 1998, INTCAL98 radiocarbon age calibration, 24,000-0 cal BP.: *Radiocarbon*, v. 40, p. 1041-1083.
- Zehfuss, P.H., Bierman, P.R., Gillespie, A.R., Burke, R.M., and Caffee, M.W., 2001, Slip rates on the Fish Springs fault, Owens Valley, California, deduced from cosmogenic ^{10}Be and ^{26}Al and relative weathering of fan surfaces: *Geological Society of America Bulletin*, v. 113, p. 241-255.

Table 5-1. Estimated contemporary production rates at time = 0 (Po).

Study	Calibration Age (cal ky)	Sample Elevation (km)	Sample Geographic Latitude (degrees)	¹⁰ Be *	¹⁰ Be †	²⁶ Al *	²⁶ Al †
				Production Rate Uncorrected (atoms g ⁻¹ yr ⁻¹)	Production Rate at time=0 (Po) (atoms g ⁻¹ yr ⁻¹)	Production Rate Uncorrected (atoms g ⁻¹ yr ⁻¹)	Production Rate at time=0 (Po) (atoms g ⁻¹ yr ⁻¹)
Nishiizumi et al., (1989)	11	3.34	44	6.1	6.3	37.7	37.3
Clark et al., (1995)	12	3.34	44	5.6	5.7	34.5	34.1
	13	3.34	44	5.2	5.3	31.9	31.5
	14	3.34	44	4.9	5.0	29.6	29.2
Clark et al., (1995)	21.5	0.25 to 0.37	41	4.7	5.1	-	-
Kubik et al., (1998)	9.8	1.68	47	5.8	5.32	38.0	34.7
Stone et al., (1998)	11.5	0.52	58	4.6	4.65	27.7	27.9
Stone (2000)	9.8 to 7,000	-	-	5.1	-	-	-
Nishiizumi (1996)	0.002	3.25	40	4.7	5.21	na	na

* Production rate estimates assuming 3% muon production, sea level, and high latitude.

† Initial production rate (Po) determined iteratively.

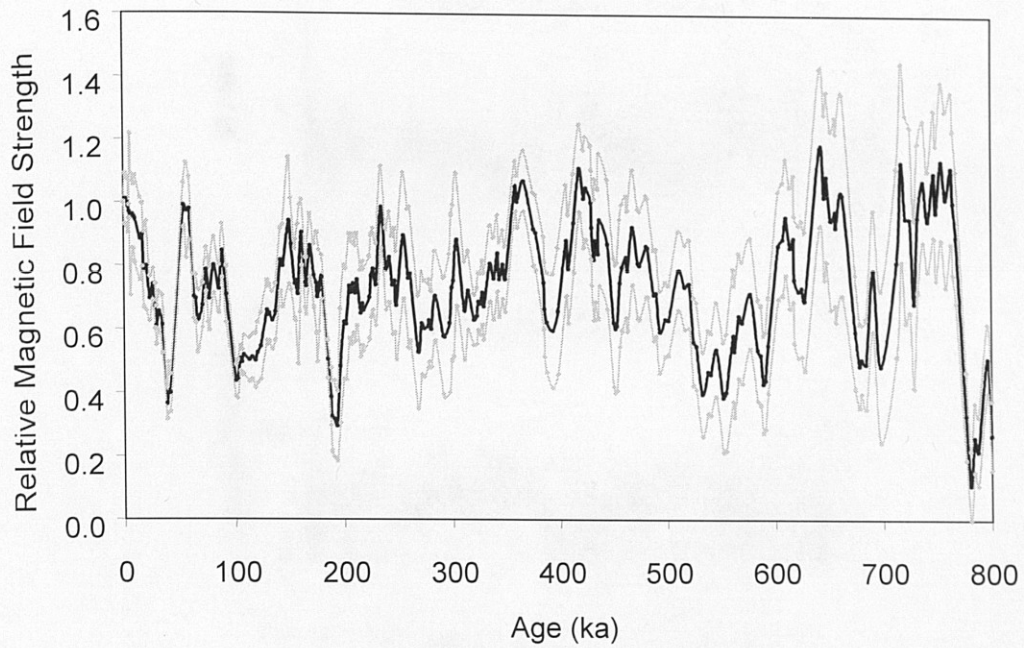


Figure 5-1. Relative magnetic field strength curve used to drive model calculations. Black line is the mean magnetic field strength curve; gray lines are one standard error of the mean. The record is a combination of SINT-800 (Guyodo and Valet, 1999) for the time period between 10 and 800 kyr BP and the dendrochronologically derived $\Delta^{14}\text{C}$ paleointensity estimate of Stuiver et al., (1998) for the time period from 10 ka to present.

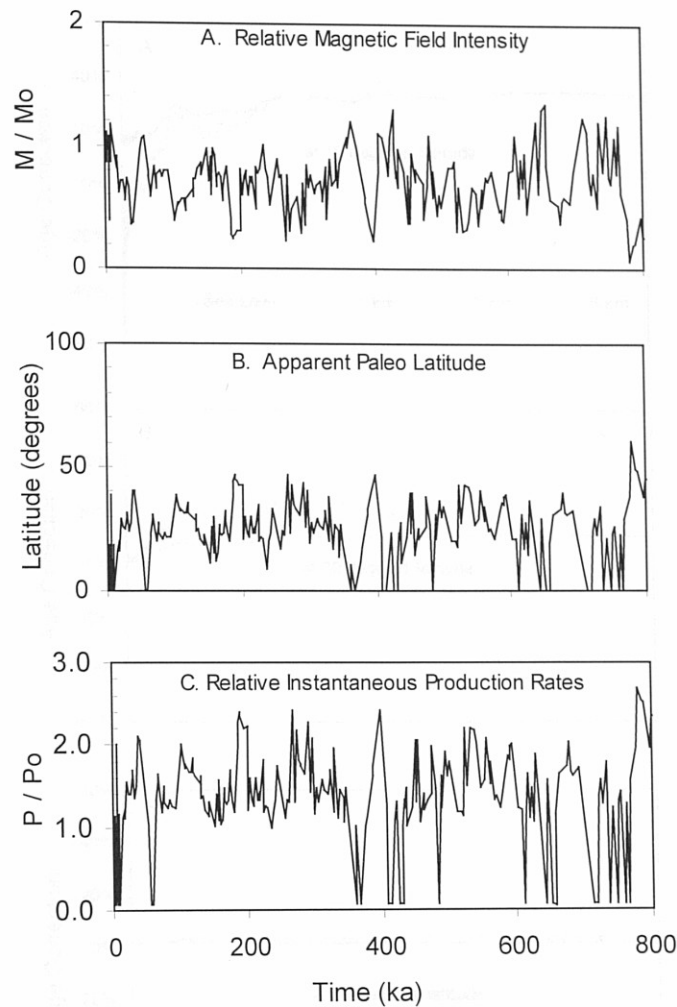


Figure 5-2. Model graphical output. (A) Random-normal model output of relative magnetic field strength (M / M_0), (B) apparent paleolatitude calculated from formulation of Nishiizumi et al. (1989), and (C) relative instantaneous production rates (P / P_0) calculated from Lal (1991) and Elsaesser et al. (1956).

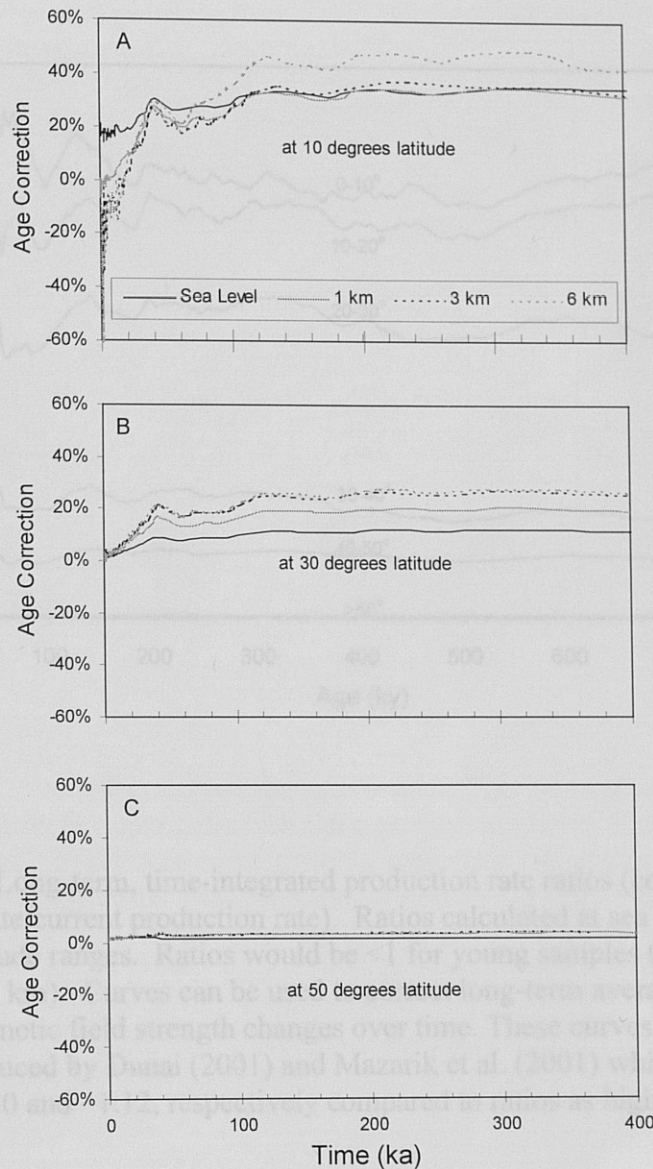


Figure 5-3. Age corrections (difference between corrected and uncorrected ages) calculated for ^{10}Be exposure ages as a function of time and elevation, for geographic latitudes of 10°(A), 30°(B), and 50°(C). Black solid line represents sea level, gray solid line represents 1 km above sea level, black dashed line represents 3 km above sea level, and gray dashed line represents 6 km above sea level. Largest age corrections are noted for high elevation and low latitudes. For older ages (>40 ka), large positive age corrections (uncalibrated > calibrated) may occur. For younger ages, moderate positive age corrections occur at low elevations and large negative age corrections occur at high elevations.

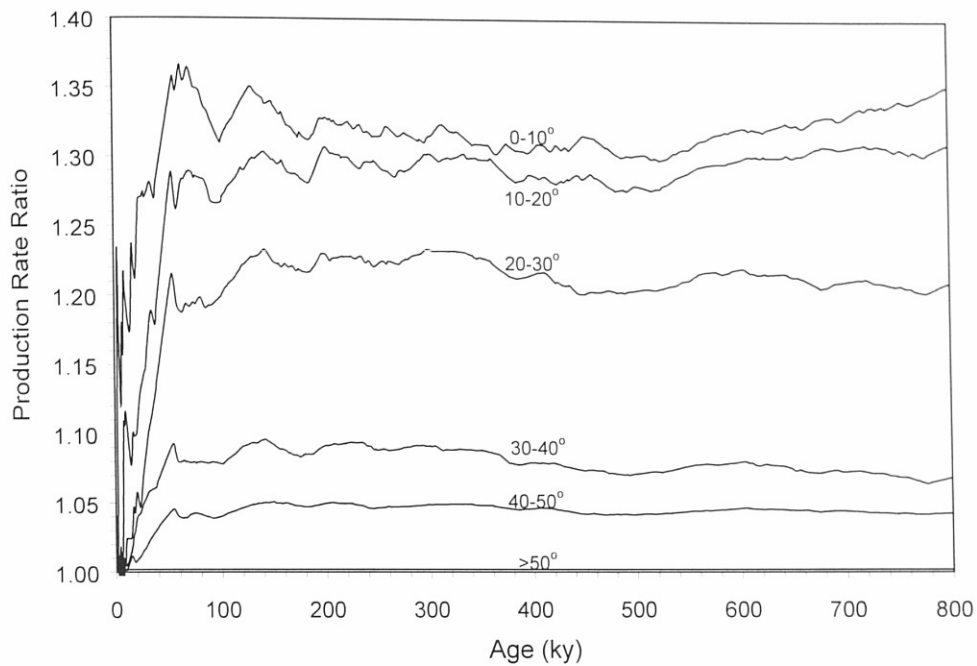


Figure 5-4. Long-term, time-integrated production rate ratios (corrected production rate/current production rate). Ratios calculated at sea level, over a series of latitude ranges. Ratios would be <1 for young samples (< 20 kyr) at high altitudes (> 1 km). Curves can be used to correct long-term average production rates for magnetic field strength changes over time. These curves can be compared to those produced by Dunai (2001) and Mazarik et al. (2001) which give maximum ratios of ~ 1.20 and ~ 1.12 , respectively compared to ratios as high as ~ 1.37 from our model.

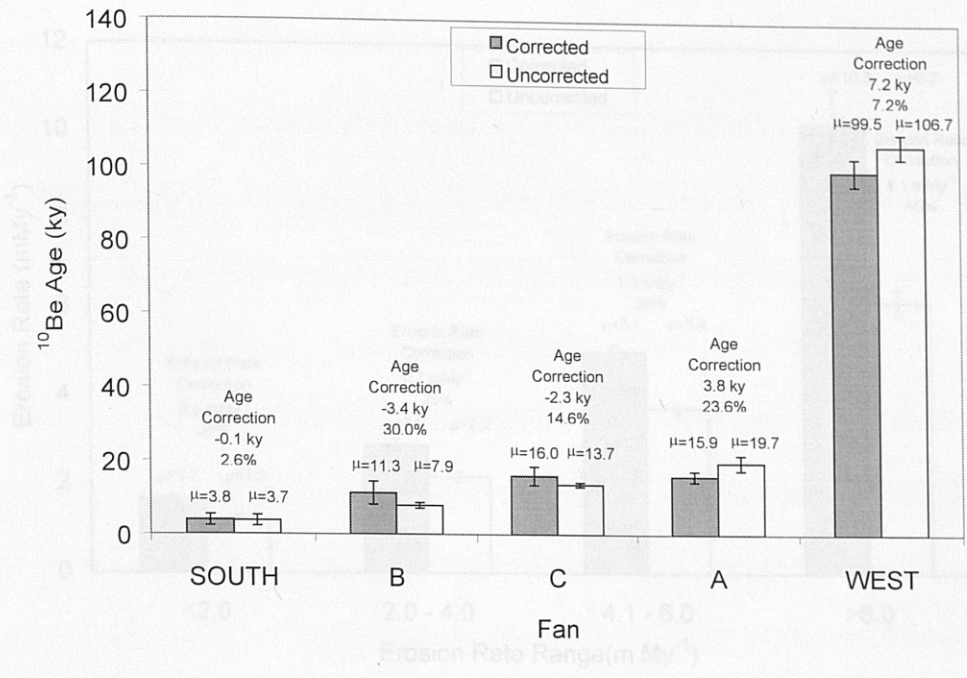


Figure 5-5. Average corrected and uncorrected ^{10}Be exposure ages for boulders of five debris flow fans along the Fish Springs Fault in Owens Valley, California (Zehfuss et al., 2001). Age corrections for older fans (West Fan and Fan A) are positive, while age corrections for younger fans (South Fan, Fan B and Fan C) are negative.

6.0 Conclusions

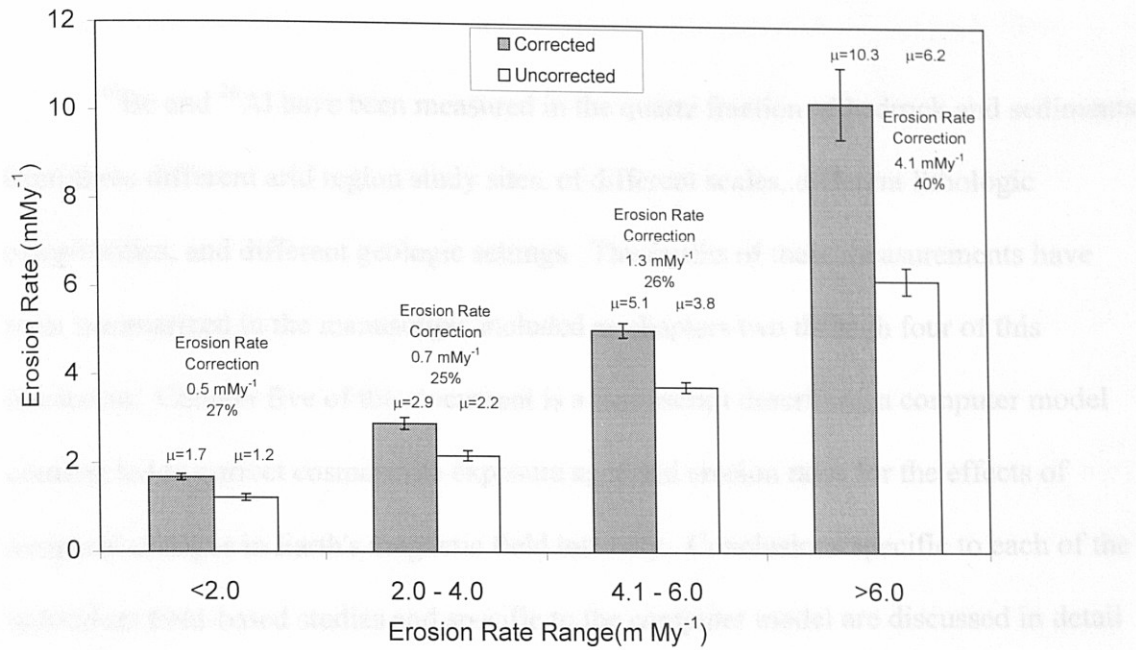


Figure 5-6. Average corrected and uncorrected erosion rates determined from bedrock outcrops across west-central Namibia (Bierman and Caffee, 2001). Large erosion rate corrections of 0.5 to 4.1 mMy⁻¹ (25% to 40%) are suggested for these slowly eroding, highly dosed samples.

6.0 Conclusions

^{10}Be and ^{26}Al have been measured in the quartz fraction of bedrock and sediments from three different arid region study sites, of different scales, different lithologic complexities, and different geologic settings. The results of these measurements have been summarized in the manuscripts included as chapters two through four of this document. Chapter five of this document is a manuscript describing a computer model constructed to correct cosmogenic exposure ages and erosion rates for the effects of temporal changes in Earth's magnetic field intensity. Conclusions specific to each of the individual field-based studies and specific to the computer model are discussed in detail within each of the individual manuscripts contained herein. Based on the combined results of the studies presented in chapters 2 through 5 of this dissertation, the following are my conclusions:

- Cosmogenic nuclide activities measured in sediments throughout a drainage basin can be used to infer baseline, long-term, geomorphic conditions over landscapes of differing scale. The rates of denudation and sediment generation calculated at Arroyo Chavez and Yuma Wash are in general agreement with regional denudation rates calculated using other techniques. Rates calculated at Arroyo Chavez and Nahal Yael are in general agreement with local rates calculated using other techniques.
- Nuclide activities measured in stream channel sediments leaving a drainage basin suggest that the drainage network of a basin sufficiently integrates sediments and

associated cosmogenic nuclides. For small basins, where sediment storage is small or negligible, nuclide activities in stream channel sediments closely resemble the activities measured in bedrock and other geomorphic features throughout a drainage basin. However, as basin scales increase (from \leq a few km^2 to \geq many km^2), the storage of sediment within a basin becomes more significant, and the nuclide activities measured in channel sediments of a high order stream may reflect specific areas where sediment in long or short term storage is currently being evacuated.

Thus, for a large basin, sampling many geomorphic features or many sub-basins may give a better indication of the process rates for the basin as a whole. For smaller basins, collecting a single or several samples from the stream channel may sufficiently characterize the nuclide signature and thus denudation rates of the basin.

- Cosmogenic nuclide activities can be used as a tracer to identify current, specific areas of landscape degradation. For smaller basins, nuclides measured in specific geomorphic features coupled with a simple mixing model, can be used to identify the portion of sediment contributed from individual features, directly to the channel. By collecting samples from the stream channels of a drainage network, from high order streams to low order streams, cosmogenic nuclides can be used to determine the denudation/sediment generation rates for individual sub-basins and using simple mixing models can be used to determine the percent contribution of sediment from each individual sub-basin.

- Cosmogenic nuclide activities can be used to infer specific geomorphic processes that contribute sediment to drainage systems. Specifically, nuclide measurements suggest that in arid regions, weathering of bedrock beneath a cover of colluvium may be more rapid than weathering of exposed bedrock; nuclide measurements indicate where sediment is stored for long or short periods of time and nuclide measurements suggest pathways that sediments may take in route to the outlet of a drainage network.
- Cosmogenic nuclide activities can be used to determine if a basin is in a long-term condition of steady state with respect to denudation, sediment accumulation, sediment generation, and sediment yield. Differences between nuclide signatures in different geomorphic features within a basin should identify catastrophic events, such as landslides or debris flows, that may deliver sediments to a stream rapidly rather than by slow steady processes. Additionally, patterns of nuclide activities measured in sediment depth profiles can identify rapid depositional events related to catastrophic events or accelerated periods of deposition caused by human- or climate-induced landscape changes. Based on the results of the field-based studies, I find no evidence of such catastrophic or rapid depositional events at my field sites. However, the differences between short-term rates of sediment yield and long-term rates of sediment generation as noted at Nahal Yael, indicate that this basin is currently out of long-term steady-state and is currently evacuating more sediment from the basin than is being produced in the uplands.

- The grain size distribution of a sediment sample in an arid region basin does not appear to significantly affect the results of cosmogenic nuclide studies in sediments. This finding is consistent with arid-region sediment transport theory, which suggests that sediment transport often occurs in pulses during infrequent, large, storm events characterized by turbulent flows that transport material of many different sizes at similar rates (Laronne and Reid, 1993; Laronne et al., 1994; Reid and Laronne, 1995). This finding contrasts with that of Brown et al. (1995a) who found distinct isotopic dependence on grain size in a humid region where deep-seated landslides and rockslides bring large-grained, lightly-dosed material to the channel while fine- to medium-grained material with higher isotopic concentrations is delivered to the stream by gradual, surface-dominated processes of weathering, soil creep, and sheet wash.
- The accuracy of cosmogenic exposure ages and erosion rates can be improved by correcting for the effects of changes in the strength of Earth's magnetic field. By not accounting for these effects, erosion rates may be underestimated and exposure ages over estimated by over 40% in certain instances. Additionally, the uncertainties associated with interpretation of cosmogenic nuclide measurements can be more rigorously accounted for in our Monte Carlo approach to data interpretation.

The field-based studies presented in this dissertation illustrate the utility of quantifying long-term basin-wide rates of sediment generation and landscape denudation. Both public and private lands can be better managed and protected if the rates of fundamental

processes controlling landscape evolution are better understood. The methods described in this dissertation provide reasonable estimates of long-term process rates that can be rapidly determined (several months) in contrast to estimating these rates using standard long-term (several years to decades) monitoring programs. Cosmogenic nuclides can be used to identifying areas contributing the most significant amounts of sediment to a drainage, allowing land managers to make critical decisions on where to most efficiently utilize limited resources. Although the current per sample cost is high, when the cost of managing long-term monitoring programs is considered, our methods are likely a more cost effective way to rapidly gain an understanding of sediment generation and landscape denudation over a large region.

This dissertation includes several study sites of different size, geologic setting, and geologic complexity; however, future studies should concentrate on application of our methods to many additional basins, in different climatic zones, and over many different scales. As our methods are tested over many study sites, statistical evaluation of the data will become more significant and will strengthen the conclusions presented above.

Comprehensive Bibliography

- Aby, S. B., 1997, Date of channel trenching (arroyo cutting) in the arid Southwest revisited: Geological Society of America Abstracts with Programs, v. 29, p. 373.
- Ahnert, F., 1970, Functional relationships between denudation, relief, and uplift in large mid-latitude drainage basins: American Journal of Science, v. 268, p. 243-263.
- Anderson, R. S., Repka, J. L., and Dick, G. S., 1996, Explicit treatment of inheritance in dating depositional surfaces using in situ ^{10}Be and ^{26}Al : Geology, v. 24, p. 47-51.
- Ayers-Associates, 1996, Geomorphic, Hydrologic, and Vegetation Characterization and Base-Line Conditions of Yuma Wash. 92-0904.01, U.S. Army Corps of Engineers Waterways Experimental Station, Vicksburg, Mississippi & Conservation Program U.S. Army Yuma Proving Grounds, Yuma, Arizona, Yuma Proving Grounds, Arizona: 398 pp.
- Bierman, P., and Caffee, M., 2001, Slow rates of rock surface erosion and sediment production across the Namib Desert and Escarpment, southern Africa: American Journal of Science, v. 301, p. 326-358.
- Bierman, P., Clapp, E. M., Nichols, K. K., Gillespie, A. R., and Caffee, M., 2001, Using cosmogenic nuclide measurements in sediments to understand background rates of erosion and sediment transport: in Harmon, R. S., and Doe, W. M., eds., Landscape Erosion and Evolution Modelling: New York, Kluwer, p. 89-116.
- Bierman, P. R., Marsella, K. A., Patterson, C., Davis, P. T., and Caffee, M., 1999, Mid-Pleistocene cosmogenic minimum-age limits for pre-Wisconsinan glacial surfaces in southwestern Minnesota and southern Baffin Island; a multiple nuclide approach: Geomorphology, v. 27, p. 25-40.
- Bierman, P., and Steig, E., 1996, Estimating rates of denudation and sediment transport using cosmogenic isotope abundances in sediment: Earth Surface Processes and Landforms, v. 21, p. 125-139.
- Bierman, P., Larsen, P., Clapp, E., and Clark, D., 1996, Refining Estimates of ^{10}Be and ^{26}Al production rates: Radiocarbon, v. 38, p. 149.
- Bierman, P. R., and Turner, J., 1995, ^{10}Be and ^{26}Al evidence for exceptionally low rates of Australian bedrock erosion and the likely existence of pre-Pleistocene landscapes: Quaternary Research, v. 44, p. 378-382.
- Bierman, P.R., 1994, Using in situ cosmogenic isotopes to estimate rates of landscape evolution: A review from the geomorphic perspective: Journal of Geophysical Research, v. 99, p. 13885-13896.
- Briesmeister, J.F., 1998, MCNP-A general Monte Carlo N-particle transport code, Version 4A: Publication LA-12625-M, Los Alamos National Laboratories.
- Brook, E. J., Kurz, M. D., Ackert, R. P., Jr., Denton, G. H., Brown, E. T., Raisbeck, G. M., and Yiou, F., 1993, Chronology of Taylor Glacier advances in Arena Valley,

- Antarctica, using in situ cosmogenic ^3He and ^{10}Be : *Quaternary Research*, v. 39, p. 11-23.
- Brook, E. J., Kurz, M. D., Ackert, R. P., Raisbeck, G. M., and Yiou, F., 1995a, Cosmogenic nuclide exposure ages and glacial history of late Quaternary Ross Sea drift in McMurdo Sound, Antarctica: *Earth and Planetary Science Letters*, v. 131, p. 41-56.
- Brook, E. J., Brown, E. T., Kurz, M. D., Ackert, R. P., Jr., Raisbeck, G. M., and Yiou, F., 1995, Constraints on age, erosion, and uplift of Neogene glacial deposits in the Transantarctic Mountains determined from in situ cosmogenic ^{10}Be and ^{26}Al : *Geology*, v. 23, p. 1063-1066.
- Brook, E. J., Nesje, A., Lehman, S. J., Raisbeck, G. M., and Yiou, F., 1996, Cosmogenic nuclide exposure ages along a vertical transect in western Norway: Implications for the height of the Fennoscandian ice sheet: *Geology*, v. 24, p. 207-210.
- Brown, E. T., Edmond, J. M., Raisbeck, G. M., Yiou, F., Kurz, M. D., and Brook, E. J., 1991, Examination of surface exposure ages of Antarctic moraines using in situ produced ^{10}Be and ^{26}Al : *Geochimica et Cosmochimica Acta*, v. 55, p. 2269-2283.
- Brown, E.T., Stallard, R.F., Larsen, M.C., Raisbeck, G.M. and Francoise, Y., 1995b, Denudation rates determined from accumulation of in situ-produced ^{10}Be in the Luquillo Experimental Forest, Puerto Rico: *Earth and Planetary Science Letters*, v. 129, p. 193-202.
- Brown, E. J., Bourles, D. L., Colin, F., Raisbeck, G. M., Yiou, F., and Desgarceaux, S., 1995a, Evidence for muon-induced production of ^{10}Be in near surface rocks from the Congo: *Geophysical Research Letters*, v. 22, p. 703-706.
- Brown, E. T., Bourles, D. L., Burchfiel, B. C., Deng, Q., Li, J., Molnar, P., Raisbeck, G. M., and Yiou, F., 1998, Estimation of slip rates in the southern Tien Shan using cosmic ray exposure dates of abandoned alluvial fans: *Geological Society of America Bulletin*, v. 110, p. 377-386.
- Brun R., Caillat, M., Maire, M., Patrick, G.N., and Urban, L., 1987, GEANT User's Guide, Europ Report DD/EE/84-1: European Organization. for Nuclear Research (CERN), Geneva, 584 pp.
- Bryan, K., 1925, Date of channel trenching in the arid Southwest: *Science*, v. 62, p. 338-344.
- Bull, W.B., 1991, *Geomorphic Responses to Climate Change*: New York, Oxford University Press, 326 p.
- Bull, W.B., and Schick, A.P., 1979, Impact of climate change on an arid region watershed: Nahal Yael, southern Israel: *Quaternary Research*, v. 11, p. 153-171.
- Burbank, D.W., Leland, J., Fielding, E., Anderson, R.S., Brozovic, N., Reid, M.R., and Duncan, C., 1996, Bedrock incision, rock uplift and threshold hillslopes in the northwestern Himalayas: *Nature*, v.379, p. 505-510.

- Cerling, T. E., and Craig, H., 1994, Geomorphology and in-situ cosmogenic isotopes: Annual Review of Earth and Planetary Science, v. 22, p.273-317.
- Clapp, E.M., 1995, The storage and transport of phosphorus and fecal coliform bacteria in the channel sediments of Englesby Brook: Unpublished Masters Thesis, University of Vermont, Department of Geology, 164 p.
- Clapp, E. M., Bierman, P. R., Schick, A. P., Lekach, J., Enzel, Y., and Caffee, M., 2000, Sediment yield exceeds sediment production in arid region drainage basins: Geology, v. 28, p. 995-998.
- Clapp, E.M., Bierman, P.R., Pavich, M., and Caffee, M., 2001, Rates of sediment supply to arroyos from uplands determined using in situ produced cosmogenic ^{10}Be and ^{26}Al in sediments: Quaternary Research, v. 55, p. 235-245.
- Clapp, E.M., Bierman, P.R., and Caffee, M., 2002, Using ^{10}Be and ^{26}Al to determine sediment generation rates and identify sediment source areas in an arid region drainage basin, Geomorphology, v. 45, p. 67-87.
- Clapp, E. and Bierman, P., 1996, Cosmo-Calibrate: a program for calibrating cosmogenic exposure ages: Radiocarbon v. 38, p. 151-152.
- Clapp, E.M., Bierman, P.B., Pavich, M., and Caffee, M., 1997, Rates of erosion determined using in situ-produced cosmogenic isotopes in a small arroyo basin, northwestern New Mexico: Geological Society of America Abstracts with Programs, v. 29, p.281.
- Clapp, E.M., Bierman, P.B., and Caffee, M.W., 1998, Estimating long-term erosion rates in a hyper-arid region using in situ-produced cosmogenic ^{10}Be and ^{26}Al in sediment and Bedrock: Geological Society of America Abstracts with Programs, v. 30, p. 361.
- Clark, D.H., Bierman, P.R. and Larsen, P., 1995, Improving in situ cosmogenic chronometers: Quaternary Research, v. 44, p. 366-376.
- Cooke, R. U., and Reeves, R. W., 1976, "Arroyos and Environmental Change in the American Southwest." Clarendon Press, Oxford, 295 p.
- Davis, P. T., Bierman, P. R., Marsella, K. A., Caffee, M. W., and Southon, J. R., 1999, Cosmogenic analysis of glacial terrains in the eastern Canadian Arctic; a test for inherited nuclides and the effectiveness of glacial erosion: Annals of Glaciology, v. 28, p. 181-188.
- Desilets, D., and Zreda, M., 2001, On scaling cosmogenic nuclide production rates for altitude and latitude using cosmic-ray measurements: Earth and Planetary Science Letters, v. 193, p. 213-225.
- Dethier, D. P., Harrington, C.D., and Aldrich, M.J. 1988, Late Cenozoic rates of erosion in the western Espanola basin, New Mexico - Evidence from geologic dating of erosion surfaces: Geological Society of America Bulletin, v. 100, p. 928-937.
- Dohrenwend, J.C., Bull, W.B., McFadden, L.D., Smith, G.I., Smith, R.S.U., and Wells, S.G., 1991, Quaternary Geology of the Basin and Range Province in California:

In: R.B. Morrison (Editor), Quaternary Nonglacial Geology, Conterminous U.S. Geological Society of America, The Geology of North America, p. 353-371.

- Drake, J.D., and Heaney, I., 1987. Occurrence of phosphorus and its potential remobilization in the littoral sediments of a productive English lake: *Freshwater Biology*, v.17, p. 513-523.
- Dunai, T.J., 2000, Scaling factors for production rates of in situ produced cosmogenic nuclides: a critical reevaluation: *Earth and Planetary Science Letters*, v. 176, p. 157-169.
- Dunai, T.J., 2001, Influence of secular variation of the geomagnetic field on production rates of in situ produced cosmogenic nuclides: *Earth and Planetary Science Letters*, v. 193, p. 197-212.
- Elliott, J. G., Gellis, A. C., and Aby, S. B., 1999, Evolution of arroyos: Incised channels of the southwestern United States: In "Incised River Channels." (S. E. Dorby, and A. Simon, Eds.), John Wiley and Sons, Chinchester, pp. p. 153-185.
- Elsaesser, W., Ney, E.P., Winckler, J.R., 1956, Cosmic Ray intensity and geomagnetism: *Nature*, v. 178, p. 1226-1227.
- Frank, M., Schwarz, B., Baumann, S., Kubik, P.W., Suter, M., and Mangini, A., 1997, A 200 kyr record of cosmogenic radionuclide production rates and geomagnetic field intensity from ^{10}Be on globally stacked deep sea sediments: *Earth and Planetary Science Letters*, v. 149, p. 121-129.
- Gellis, A.C. Pavich, M.J., Bierman, P.R., Ellwein, A., Aby, S., Clapp, E.M., 2000, Measuring erosion rates using modern geomorphic and isotopic measurements in the Rio Puerco, New Mexico: *Geological Society of America Abstracts with Programs*, v. 32, p. 207.
- Gellis, A. C., and Elliott, J. G., 1998, Arroyo changes in selected watersheds of New Mexico, United States. In "Applying Geomorphology to Environmental Management, a special publication honoring Stanley A. Schumm." (M. Harvey, and D. Anthony, Eds.), Water Resources Publications, LLC, Highlands Ranch, Colorado pp. p. 271-284.
- Gilbert, G. K., 1877, *Geology of the Henry Mountains (Utah): US Geographical and Geological Survey of the Rocky Mountains Region*, 160 pp.
- Gosse, J. C., Evenson, E. B., Klein, J., Lawn, B. and Middleton, R., 1995a, Precise cosmogenic ^{10}Be measurements in western North America: Support for a global Younger Dryas cooling event: *Geology*, v. 23, p. 877-880.
- Gosse, J. C., Klein, J., Evenson, E. B., Lawn, B., and Middleton, R., 1995b, Beryllium-10 dating of the duration and retreat of the last Pinedale glacial sequence: *Science*, v. 268, p. 1329-1333.
- Gosse, J.C., and Klein, J., 1996, Production rate of in situ cosmogenic ^{10}Be in quartz at high altitude and mid-latitude: *Radiocarbon*, v.38, p.154-155.

- Gosse, J.C., and Stone, J.O., 2001, Terrestrial cosmogenic nuclide methods passing milestones toward paleo-altimetry: EOS Transactions of the American Geophysical Union, v. 82, p. 82-89.
- Gosse, J. C., and Phillips, F. M., 2001, Terrestrial in situ cosmogenic nuclides: theory and application: Quaternary Science Reviews, v. 20, no. 14, p.1475-1560.
- Granger, D. E., Kirchner, J. W., and Finkel, R., 1996, Spatially averaged long-term erosion rates measured from in-situ produced cosmogenic nuclides in alluvial sediment: Journal of Geology, v. 104, p. 249-257.
- Granger, D. E., Kirchner, J. W., and Finkel, R. C., 1997, Quaternary downcutting rate of the New River, Virginia, measured from differential decay of cosmogenic ^{26}Al and ^{10}Be in cave-deposited alluvium: Geology, v. 25, p. 107-110.
- Granger, D. E., Fabel, D., and Palmer, A. N., 2001, Pliocene-Pleistocene incision of the Green River, Kentucky, determined from radioactive decay of cosmogenic ^{26}Al and ^{10}Be in Mammoth Cave sediments: Geological Society of America Bulletin, v. 113, p. 825-836.
- Guyodo, Y., and Valet, J.P., 1996, Relative variations in geomagnetic intensity from sedimentary records: the past 200,000 years: Earth and Planetary Science Letters, v. 143, p. 23-26.
- Guyodo, Y., and Valet, J.P., 1999, Global changes in intensity of the Earth's magnetic field during the past 800 kyr: Nature, v. 399, p. 249-252.
- Hancock, G. S., Anderson, R. S., and Whipple, K. X., 1998, Beyond power; bedrock river incision process and form: Geophysical Monograph, v.107, p. 35-60.
- Hancock, G. S., Anderson, R. S., Chadwick, O. A., and Finkel, R. C., 1999, Dating fluvial terraces with ^{10}Be and ^{26}Al profiles; application to the Wind River, Wyoming, in Harbor, J., ed., Cosmogenic isotopes in geomorphology Geomorphology, v. 27, p. 41-60.
- Heimsath, A. M., Dietrich, W. E., Nishiizumi, K., and Finkel, R. C. ,1999, Cosmogenic nuclides, topography, and the spatial variation of soil depth: Geomorphology, v. 27, p. 151-172.
- Heimsath, A. M., Dietrich, W. E., Nishiizumi, K., and Finkel, R. C. ,1997, The soil production function and landscape equilibrium: Nature, v. 388, p. 358-361.
- Hillaire-Marcel, C., Carro, O., and Casanova, J., 1986, ^{14}C and Th/U dating of Pleistocene and Holocene stomatolites from east African paleolakes: Quaternary Research, v. 25, p. 312-329.
- Holeman, J. N. ,1968, The sediment yield of major rivers of the world: Water Resources Research, v. 4, p. 737-747.
- Ivy-Ochs, S., Schluchter, C., Kubik, P. W., Dietrich-Hannen, B., and Beer, J., 1995, Minimum ^{10}Be exposure ages of early Pliocene for the Table Mountain plateau

- and the Sirius Group at Mount Fleming, Dry Valleys, Antarctica: *Geology*, v. 23, p. 1007-1010.
- Judson, S., 1968, Erosion of the land, or what's happening to our continents?: *American Scientist*, v. 56(4), p. 356-374.
- Judson, S., and Ritter, D. F., 1964, Rates of regional denudation in the United States: *Journal of Geophysical Research*, v. 69, p. 3395-3401.
- Keller, E.A., 1992, *Environmental Geology*, Sixth Edition, MacMillan Publishing Company, New York, NY, p. 56-60.
- Klein, J., and Gosse, J., 1996, Terrestrial factors that influence production rates: *Radiocarbon* v. 38, p. 161-162.
- Klein, J., Gosse, J., Davis, P.T., Evenson, E.B., and Sorenson, C.J., 2000, Younger Dryas in the Rocky Mountains and the calibration of $^{10}\text{Be}/^{26}\text{Al}$ production rates: *Geological Society of America Abstracts with Programs*, v. 31, p. A-473.
- Kohl, C. P., and Nishiizumi, K., 1992, Chemical isolation of quartz for measurement of in-situ-produced cosmogenic nuclides: *Geochemica et Cosmochemica Acta*, v. 56, p. 3583-3587.
- Kubik P.W., Ivy-Ochs, S., Masarik, J., Frank, M., Schluchter, C., 1998, ^{10}Be and ^{26}Al production rates deduced from an instantaneous event within the dendro-calibration curve, the landslide of Koefels, Oetz Valley, Austria: *Earth and Planetary Science Letters*, v. 161, p. 231-241.
- Kurz, M. D., D. Colodner, T. W. Trull, R. Moore, and K. O'Brien, 1990, Cosmic ray exposure dating with in situ produced cosmogenic ^3He : results from young Hawaiian lava flows: *Earth and Planetary Science Letters*, v. 97, p. 177-189.
- Lal, D., 1988, In situ-produced cosmogenic isotopes in terrestrial rocks: *Annual Reviews of Earth and Planetary Science*, v. 16, p. 355-388.
- Lal, D., 1991, Cosmic ray labeling of erosion surfaces: In situ production rates and erosion models: *Earth and Planetary Science Letters*, v. 104, p. 424-439.
- Lal, D., and Arnold, J. R., 1985, Tracing quartz through the environment: *Proceedings of the Indian Academy of Science (Earth and Planetary Science)*, v. 94, 1-5.
- Lal, D., and Peters, B., 1967, Cosmic ray produced radioactivity on Earth: in *Handbook der Physik*, Sitte, K., (ed), Springer-Verlag, New York, p. 551-612.
- Laronne, J. and Reid, I., 1993, Very high rates of bedload sediment transport by ephemeral desert rivers: *Nature*, v. 366, p. 148-150.
- Laronne, J., Reid, I., Yitshak, Y. and Frostick, L., 1994, The non-layering of gravel streambeds under ephemeral flood regimes: *Journal of Hydrology*, v. 159, p. 353-363.
- Lekach, J., Amit, R., Ayalon, A., Porat, N., and Schick, A., 1999, Fluvio-pedogenic processes in an active desert stream, in Lekach, J., and Hassan, M.A., eds.,

- Drainage basin dynamics and morphology, Negev Desert, conference excursion: Jerusalem, Hebrew University of Jerusalem, p. 114-122.
- Leland, J., Reid, M. R., Burbank, D. W., Finkel, R., and Caffee, M., 1998, Incision and differential bedrock uplift along the Indus River near Nanga Parbat, Pakistan Himalaya, from ^{10}Be and ^{26}Al exposure age dating of bedrock straths: *Earth and Planetary Science Letters*, v. 154, p. 93-107.
- Leopold, L. B., Emmett, W.W., and Myrick, R.M., 1966, Channel and hillslope processes in a semiarid area, New Mexico: U.S. Geological Survey Professional Paper, 352-G, p. 193-253.
- Love, D. W., 1986, A geological perspective of sediment storage and delivery along the Rio Puerco: In "Drainage Basin Sediment Delivery." (R. F. Hadley, Ed.), IAHS Publication 159, Wallingford, UK, p. 305-322.
- Love, D. W., and Young, J. D., 1983, Progress report on the late Cenozoic geologic evolution of the lower Rio Puerco: In "New Mexico Geological Society Guidebook 33, Socorro Region II." (S.G. Wells, J.A. Grambling, and J.F. Calender, Eds.), p. 277-284.
- Marsella, K. A., Bierman, P. R., Davis, P. T., and Caffee, M. W., 2000, Cosmogenic ^{10}Be and ^{26}Al ages for the last glacial maximum, eastern Baffin Island, Arctic Canada: *Geological Society of America Bulletin*, v. 112, p. 1296-1312.
- Mazarik, J., and Beer, J., 1999, Simulation of particle fluxes and cosmogenic nuclide production in the Earth's atmosphere: *Journal of Geophysical Research*, v. 104, p. 12099-12111.
- Mazarik, J., Frank, M., Schafer, J.M., and Wieler, R., 2001, Correction of in situ cosmogenic nuclide production rates for geomagnetic field intensity variations during the past 800,000 years: *Geochemica et Cosmochemica Acta*, v. 65, p. 2995-3003.
- Mazaud, A., Laj, C., Bard, E., Arnold, M. and Tric, E., 1991, Geomagnetic field control of ^{14}C production over the last 80 ky: implications for the radiocarbon time scale: *Geophysical Research Letters*, v. 18, p. 1885-1888.
- McElhinny, M.W., and Senanayake, W.E., 1982, Variations in the geomagnetic dipole 1: the past 50000 years: *Journal of Geomagn. Geoelectr.*, v. 34, p. 39-51.
- Meade, R.H., 1969, Errors in using modern stream-load data to estimate natural rates of denudation: *Geological Society of America Bulletin*, v. 80, p. 1265-1274.
- Meade, R.H., 1988, Movement and storage of sediment in river systems: In: A. Lerman and M. Meybeck (Editors), *Physical and chemical weathering in geochemical cycles*. Kluwer Academic Publishers, p. 165-179.
- Merrill, R.T., and McElhinny, M.W., 1983, *The Earth's Magnetic Field, Its History, Origin, and Planetary Prospective*: Academic Press, New York.

- Nichols, K. K., Bierman, P. R., and Caffee, M. W., 2000, The Blackhawk keeps its secrets: landslide dating using in situ 10-Be: Geological Society of America Abstracts with Programs, v. 32, p. A-400.
- Nichols, K. K., and Bierman, P. R., 2001, Fifty four years of ephemeral channel response to intense military activity at Camp Iron Mountain, Mojave Desert, California, Environmental and Engineering Impacts of Military Operations: Geological Society of America Reviews of Engineering Geology, v.14, p. 123-136.
- Nishiizumi, K., Lal, D., Klein, J., Middleton, R., and Arnold, J.R., 1986, Production of ^{10}Be and ^{26}Al by cosmic rays in terrestrial quartz in situ and implications for erosion rates: Nature, v. 319, p. 134-136.
- Nishiizumi, K., Winterer, E. L., Kohl, C. P., Klein, J., Middleton, R., Lal, D., and Arnold, J. R., 1989, Cosmic ray production rates of ^{10}Be and ^{26}Al in quartz from glacially polished rocks: Journal of Geophysical Research, v. 94, p. 17907-17915.
- Nishiizumi, K., Kohl, C. P., Arnold, J. R., Klein, J., Fink, D., and Middleton, R., 1991, Cosmic ray produced ^{10}Be and ^{26}Al in Antarctic rocks: exposure and erosion history: Earth and Planetary Science Letters, v. 104, p. 440-454.
- Nishiizumi, K., Kohl, C.P., Arnold, J.R., Dorn, R. Klein, J., Fink, D., Middleton, R., and Lal, D., 1993, Role of in situ cosmogenic nuclides ^{10}Be and ^{26}Al in the study of diverse geomorphic processes: Earth Surface Processes and Landforms, v. 18, p. 407-425.
- Nishiizumi, K., Finkel, R.C., Klein, J., Kohl, C. P., 1996, Cosmogenic production of ^7Be and ^{10}Be in water targets: Journal of Geophysical Research, v. 101, p. 225-22,232.
- Ohno, M., and Hamano, Y., 1993, Global analysis of the geomagnetic field: Time variation of the dipole moment and the geomagnetic pole in the Holocene: Journal of Geomagnetism and Geoelectricity, v. 45, p. 1455-1466.
- Ott, R. L., 1993, "An Introduction to Statistical Methods and Data Analysis." Wadsworth Publishing Co., Belmont, California, 1049 p.
- Perg, L. A., Anderson, R. S., and Finkel, R. C., 2001, Use of a new ^{10}Be and ^{26}Al inventory method to date marine terraces, Santa Cruz, California, USA: Geology, v. 29 p. 879-882.
- Phillips, F. M., Zreda, M. G., Gosse, J. C., Klein, J., Evenson, E. B., Hall, R. D., Chadwick, O. A., and Sharma, P., 1997, Cosmogenic ^{36}Cl and ^{10}Be ages of Quaternary glacial and fluvial deposits of the Wind River Range, Wyoming: Geological Society of America Bulletin, v. 109, p.1453-1463.
- Pilleboue, E., and Dorioz, J.M., 1986, Mass-balance and transfer of phosphorus in a rural watershed of Lac Lemans, France: in Sediment and Water Interactions, Proceedings of the 3rd Sediment/Freshwater Symposium, Springer, New York, P.G. Sly (ed.), p. 91-101.

- Phillips, F.M., Zreda, M.G., Smith, S.S., Elmore, D., Kubik, P.W., and Sharma, P., 1990, Cosmogenic Chlorine-36 chronology for glacial deposits at Bloody Canyon, eastern Sierra Nevada: *Science*, v. 248, p.1529-1532.
- Pinet, P. and Souriau, M., 1988. Continental erosion and large-scale relief: *Tectonics*, v. 7(3), p. 563-582.
- Raisbeck, G., Yiou, Y., and Zhou, S.Z., 1994, Paleointensity puzzle: *Nature*, v. 371, p. 207-208.
- Reheis, M. C., and Kihl, R., 1995, Dust deposition in southern Nevada and California, 1984-1989: relations to climate, source area and source lithology: *Journal of Geophysical Research*, v. 100, p. 8893-8918.
- Reid, I. and Laronne, J., 1995, Bedload sediment transport in an ephemeral stream and a comparison with seasonal and perennial counterparts: *Water Resources Research*, v. 31, p. 733-781.
- Repka, J. L., Anderson, R. S., and Finkel, R. C., 1997, Cosmogenic dating of fluvial terraces, Fremont River, Utah: *Earth and Planetary Science Letters*, v.152, p. 59-73.
- Reynolds, S.J., 1988, *Geologic Map of Arizona*: Arizona Geological Survey.
- Ritz, J. F., Brown, E. T., Bourles, D. L., Philip, H., Schlupp, A., Raisbeck, G. M., Yiou, F., and Enkhtuvshin, B., 1995, Slip rates along active faults estimated with cosmic-ray exposure dates: Application to the Bogd fault, Gobi-Altai, Mongolia: *Geology*, v. 23, p. 1019-1022.
- Rosensteel, B.A., and Strom, P.S., 1991, River phosphorus dynamics and reservoir eutrophication potential: *Water Resources Bulletin*, v. 27, p. 957-965.
- Saunders, I., and Young, A., 1983, Rates of surface processes on slopes, slope retreat, and denudation: *Earth Surface Processes and Landforms*, v. 8, p. 473-501.
- Schick, A.P., and Lekach, J., 1993, An evaluation of two ten-year sediment budgets, Nahal Yael, Israel: *Physical Geography*, v. 14, p. 225-238.
- Schumm, S.A., 1963, Disparity between present rates of denudation and orogeny, U.S. Geological Survey Professional Paper 454-H, 13 p.
- Shanahan, T.M., and Zreda, M., 2000, Chronology of Quaternary glaciations in East Africa, *Earth and Planetary Science Letters*, v. 177, p. 23-42.
- Sharma, P., and Middleton, R., 1989, Radiogenic production of ^{10}Be and ^{26}Al in uranium and thorium ores: Implications for studying terrestrial samples containing low levels of ^{10}Be and ^{26}Al : *Geochimica et Cosmochimica Acta*, v. 53, p. 709-716.
- Shepard, M. K., Arvidson, R. E., Caffee, M., Finkel, R., and Harris, L., 1995, Cosmogenic exposure ages of basalt flows; Lunar Crater volcanic field, Nevada: *Geology*, v. 23, p. 21-24.

- Shimron, A., 1974, Geology of the Nahal Yael watershed, in Schick, A.P., and Sharon, D., eds., *Geomorphology and climatology of arid watersheds: Project Report DAJA-72C-3874*, U.S. Army European Research Office, Department of Geography, Hebrew University of Jerusalem, p. 12-23.
- Small, E. E., Anderson, R. S., and Hancock, G. S., 1999, Estimates of the rate of regolith production using ^{10}Be and ^{26}Al from an alpine slope: *Geomorphology*, v. 27, p. 131-150.
- Stone, J. O., Ballantyne, C. K., and Fifield, L. K., 1998, Exposure dating and validation of periglacial weathering limits, Northwest Scotland: *Geology*, v. 26, no. 7, p. 587-590.
- Stone, J., 2000, Air pressure and cosmogenic isotope production: *Journal of Geophysical Research*, v. 105, p. 23753-23759.
- Stuiver, M., Reimer, P.J., Bard, E., Beck, J.W., Burr, G.S., Hughen, K.A., Kromer, B., McCormac, G., van der Plicht, J., and Spurk, M., 1998, INTCAL98 radiocarbon age calibration, 24,000-0 cal BP.: *Radiocarbon*, v. 40, p. 1041-1083.
- Summerfield, M.A., 1991, *Global Geomorphology*: Longman Scientific and Technical, New York, NY, p. 191-203.
- Thoman, R.V., and Mueller, J.A., 1987, *Principles of Surface Water Quality Monitoring and Control*: Harper and Row Publishers, New York, NY, p. 219-258.
- Trimble, S.W., 1977, The fallacy of stream equilibrium in contemporary denudation studies: *American Journal of Science*, v. 277, p. 876-887.
- Trimble, S.W., 1999, Decreased rates of alluvial sediment in the Coon Creek Basin: *Science*, v. 285, p. 1244-1246.
- Twidale, C.R., 1983, The research frontier and beyond: granitic terrains: *Geomorphology*, v. 7, p. 187-223.
- U.S. Geological Survey, 1961, San Luis, New Mexico Quadrangle: USGS, Reston, Virginia.
- Wahrhaftig, C., 1965, Stepped topography of the southern Sierra Nevada, California: *Geological Society of America Bulletin*, v. 76, p. 1165-1190.
- Walling, D.E., 1983, The sediment delivery problem: *Journal of Hydrology*, v. 65, p. 209-237.
- Weissel, J. K., and Seidl, M. A., 1998, Inland propagation of erosional escarpments and river profile evolution across the southeast Australian passive continental margin: *Geophysical Monograph*, v. 107, p. 189-206.
- York, D., 1969, Least squares fitting of a straight line with correlated errors: *Earth and Planetary Science Letters*, v. 5, p. 320-324.
- Zehfuss, P.H., Bierman, P.R., Gillespie, A.R., Burke, R.M., and Caffee, M.W., 2001, Slip rates on the Fish Springs fault, Owens Valley, California, deduced from

cosmogenic ^{10}Be and ^{26}Al and relative weathering of fan surfaces: Geological Society of America Bulletin, v. 113, p. 241-255.

Zreda M., and Phillips, F., 1998, Quaternary dating by cosmogenic buildup in surficial materials: in Sowers, J.M., Noller, J.S., and Lettis, W.R. (eds), Dating and earthquakes: review of Quaternary geochronology and its application to paleoseismology, U.S. Nuclear Regulatory Commission, p. 2.101-2.127.

Appendix A

Sediment Grainsize Data

ARROYO CHAVEZ
GRAIN SIZE DATA

SAMPLE	WEIGHT (GRAMS) BY GRAIN SIZE FRACTION						TOTAL
	150 to 250 (µm)	250 to 500 (µm)	500 to 1000 (µm)	1000 to 2000 (µm)	2000 to 4000 (µm)	>4000 (µm)	
ECAC-8	58	282	172	148	250	457	1375
ECAC-11	464	572	179	182	175	67	1627
ECAC-14	116	230	131	51	108	560	1026
ECAC-19A	106	87	6	4	3	<1	205
ECAC-19B	61	180	33	64	65	75	478
ECAC-19G	120	247	17	23	21	3	428

Samples ECAC-8, 11, 14, 19A, 19B, and 19G were sieved into 6 grain size fractions.

For samples ECAC-11, 14, 19A, and 19D, samples were combined according to weight percentage to create three size fractions which were analyzed separately to test nucleide dependence on grain size.

For all other ECAC samples, the 250 to 1000µm size fraction was isolated and used for analysis.

ARROYO CHAVEZ
GRAIN SIZE DATA

SAMPLE	WEIGHT (GRAMS) BY GRAIN SIZE FRACTION						TOTAL
	125 to 250 (µm)	250 to 500 (µm)	500 to 1000 (µm)	1000 to 2000 (µm)	2000 to 4000 (µm)	>4000 (µm)	
ECAC-8	38	292	172	166	250	457	1375
ECAC-11	454	572	179	182	173	67	1627
ECAC-14	116	230	131	91	108	350	1026
ECAC-19A	106	87	6	3	3	<1	205
ECAC-19D	61	150	38	54	85	75	463
ECAC-19G	120	247	17	23	21	9	437

Samples ECAC-8, 11, 14, 19A, 19D, and 19G were sieved into 6 grain size fractions.

For samples ECAC-11, 14, 19A, and 19D, samples were combined according to weight percentage to create three size fractions which were analyzed separately to test nuclide dependence on grain size

For all other ECAC samples, the 250 to 1000µm size fraction was isolated and used for analyses

YUMA WASH
GRAIN SIZE DATA

SAMPLE	WEIGHT (GRAMS) BY GRAIN SIZE FRACTION							TOTAL
	<250 (µm)	250 to 500 (µm)	500 to 1000 (µm)	1000 to 2000 (µm)	2000 to 4000 (µm)	4000 to 12700 (µm)	>12700 (µm)	
YPG-2	0	2902	1271	2844	3281	5281	2178	17757
YPG-3	652	1722	2817	3094	3335	3716	1036	16372
YPG-4	0	1472	2334	3253	3944	0	0	11003
YPG-5	2485	2267	2695	2866	2983	5454	2535	21285
YPG-10.3	329	194	335	607	814	1349	1301	4929
YPG-10.5	271	262	479	791	708	855	1395	4761
YPG-10.7	320	173	385	560	759	1196	1015	4408
YPG-10.9	531	207	220	245	437	2248	1740	5628
YPG-11	173	85	259	800	1662	3245	4129	10353
YPG-12	166	345	701	1243	2125	3917	1237	9734
YPG-13	303	633	813	1555	2128	3003	2538	10973
YPG-14	770	714	1013	1346	1739	3165	2724	11471
YPG-15	1452	1243	1306	1533	1571	2111	1963	11179
YPG-16	1401	724	725	1057	1507	2470	2070	9954
YPG-17	1108	766	1024	1472	1770	2859	1420	10419
YPG-18	1204	722	890	1329	1699	2766	1552	10162
YPG-19	0	599	795	1289	1703	2977	1633	8996
YPG-20	859	849	1071	1365	1576	3114	1792	10626
YPG-21	260	465	1071	1646	1980	3247	1999	10668
YPG-22	162	315	596	1079	1571	3374	2871	9968
YPG-26.1	306	145	177	306	627	1312	1417	4290
YPG-26.2	289	128	170	468	1044	1492	996	4587
YPG-26.3	458	161	198	303	484	916	1197	3717

Samples above were sieved into 7 grainsize fractions.

For sample YPG-2, all fractions >250µm were analyzed separately to test nuclide dependence on grainsize.

For sample YPG-19, 4 size fractions were analyzed separately to test nuclide dependence on grainsize.

All other samples above were combined according to weight percentage to create three size fractions which were analyzed separately to test nuclide dependence on grainsize.

For all other YPG samples, the 250 to 1000µm size fraction was isolated and used for analyses.

NAHAL YAEEL
GRAIN SIZE DATA

SAMPLE	WEIGHT (GRAMS) BY GRAIN SIZE FRACTION							TOTAL
	<250 (µm)	250 to 500 (µm)	500 to 1000 (µm)	1000 to 2000 (µm)	2000 to 4000 (µm)	4000 to 12700 (µm)	>12700 (µm)	
MY-8	471	157	261	389	553	1102	1370	4303
NY-12	567	223	282	368	455	1447	2019	5361
NY-15	444	381	530	586	542	854	1411	4748
NY-16	1574	795	671	699	797	2136	4499	11171
NY-17	1551	540	447	453	509	1825	5882	11207
NY-18	482	560	851	970	962	1889	1590	7304
NY-19	548	643	934	1273	1320	1998	972	7688
NY-20	586	783	1086	1337	1203	1792	2305	9092

Samples above were sieved into 7 grain size fractions.

All samples above were combined according to weight percentage to create three size fractions which were analyzed separately to test nuclide dependence on grain size.

For all other NY samples, the 250 to 1000mm size fraction was isolated and used for analyses.

Appendix B

Appendix B.

Nahal Yael Supporting Information

Sample preparation and analysis

Samples were heated and ultrasonically etched in 6N HCl, then 1% HF and 1% HNO₃ (Kohl and Nishizumi, 1992) in order to purify quartz. Samples were dissolved in HF with 250 µg of Be carrier. Be and Al were isolated using ion chromatography. ¹⁰Be/⁹Be and ²⁶Al/²⁷Al ratios were determined by accelerator mass spectrometry at Lawrence Livermore National Laboratory. Measured ratios (0.032 ± 0.48) of ²⁶Al to ¹⁰Be (Fig. 1, inset) are consistent with the currently accepted production ratio of ~0.1 (Nishizumi et al., 1989), indicating that our laboratory methods are robust, and that the sediment and bedrock we sampled do not have long-term (>10⁶ ky), complex histories of burial and exhumation. Because the two isotopes are well correlated ($r^2 = 0.97$), we present primarily the ¹⁰Be measurements; however, the ²⁶Al measurements are used in all calculations (Table 1 and data repository Table A).

Additional References

- Kohl, C.P., and Nishizumi, K., 1992. Chemical isolation of quartz for measurement of in-situ-produced cosmogenic nuclides: *Geochimica et Cosmochimica Acta*, v. 56, p. 3583-3587.
- Larouze, J., and Reid, I., 1993. Very high rates of bedload sediment transport by ephemeral-desert rivers: *Nature*, v. 366, p. 148-150.
- Lehock, J., Schick, A.P., and Schleninger, A., 1992. Bedload yield and in-channel provenance in a flash flood fluvial system, in Billi, P., ed., *Dynamics of gravel-bed rivers*: Chichester, John Wiley and Sons, p. 537-551.
- Reid, I., and Larouze, J., 1995. Bedload sediment transport in an ephemeral stream and a comparison with seasonal and perennial counterparts: *Water Resources Research*, v. 31, p. 733-781.

Appendix B.

Sample preparation and analysis

Samples were heated and ultrasonically etched in 6N HCl, then 1% HF and 1% HNO₃ (Kohl and Nishiizumi, 1992) in order to purify quartz. Samples were dissolved in HF with 250 µg of Be carrier; Be and Al were isolated using ion chromatography. ¹⁰Be/⁹Be and ²⁶Al/²⁷Al ratios were determined by accelerator mass spectrometry at Lawrence Livermore National Laboratory. Measured ratios ($\mu=5.9 \pm 0.48$) of ²⁶Al to ¹⁰Be (Fig. 3, inset) are consistent with the currently accepted production ratio of ~ 6:1 (Nishiizumi et al., 1989), indicating that our laboratory methods are robust, and that the sediment and bedrock we sampled do not have long-term (>100 ky), complex histories of burial and exhumation. Because the two isotopes are well correlated ($r^2 = 0.95$), we present primarily the ¹⁰Be measurements; however, the ²⁶Al measurements are used in all calculations (Table 1 and data repository Table A).

Additional References

- Kohl, C.P., and Nishiizumi, K., 1992, Chemical isolation of quartz for measurement of in-situ-produced cosmogenic nuclides: *Geochemica et Cosmochemica Acta*, v. 56, p. 3583-3587.
- Laronne, J., and Reid, I., 1993, Very high rates of bedload sediment transport by ephemeral desert rivers: *Nature*, v. 366, p. 148-150.
- Lekach, J., Schick, A.P., and Schlesinger, A., 1992, Bedload yield and in-channel provenance in a flash flood fluvial system, *in* Billi, P., ed., *Dynamics of gravel-bed rivers*: Chichester, John Wiley and Sons, p. 537-551.
- Reid, I., and Laronne, J., 1995, Bedload sediment transport in an ephemeral stream and a comparison with seasonal and perennial counterparts: *Water Resources Research*, v. 31, p. 733-781.



Figure A. Geomorphic features sampled at Nahal Yael. View to south, toward samples NY9 - NY12, NY17, and NY19 (see Fig. 2), shows braided alluvial channel bordered by alluvial terraces and colluvial deposits. Pelitic schist with crosscutting quartz intrusions is in background. Photo was taken downstream of NY19.

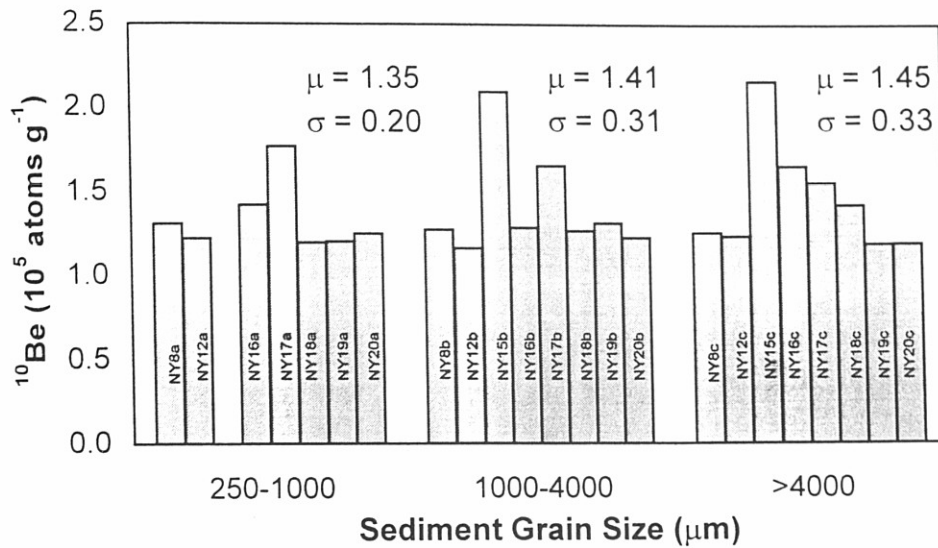


Figure B. Nuclide measurements of grain size fractions from sediment samples indicate that ^{10}Be and ^{26}Al concentrations are independent of sediment grain size implying that large and small particles are produced by similar processes and transported at similar rates. Variance however, increases slightly with grain size due to smaller number of particles analyzed per unit weight of sediment. This finding is consistent with observations that arid region streams transport sediment of many different sizes at similar rates in turbulent flows during infrequent, large, storm events (Lekach et al., 1992; Laronne and Reid, 1993; Reid and Laronne, 1995) and are consistent with cosmogenic measurements elsewhere (Clapp et al., 1997, 1998).

TABLE A. NUCLIDE DATA AND SAMPLE DESCRIPTIONS
NAHAL YAEL, ISRAEL

Sample ^e	Sample [†] elevation (km)	Sample [§] type	¹⁰ Be (10 ⁵ atoms g ⁻¹)	²⁶ Al (10 ⁵ atoms g ⁻¹)
NY4	0.245	CHA	1.32 ± 0.10	8.96 ± 0.78
NY5	0.220	BR	2.08 ± 0.12	12.27 ± 0.92
N 6	0.258	BR	2.35 ± 0.15	14.39 ± 0.88
NY7	0.283	BR	3.51 ± 0.13	21.58 ± 1.75
N 8A	0.230	COL	1.31 ± 0.13	8.14 ± 0.56
NY8B	0.230	COL	1.28 ± 0.09	7.95 ± 0.45
NY8C	0.230	COL	1.25 ± 0.06	7.86 ± 0.46
NY9	0.230	BR	1.96 ± 0.13	11.21 ± 0.69
NY10	0.258	BR	2.12 ± 0.08	13.09 ± 0.67
NY11	0.280	BR	0.73 ± 0.08	5.61 ± 0.43
NY12A	0.250	COL	1.22 ± 0.12	8.53 ± 0.48
NY12B	0.250	COL	1.17 ± 0.07	7.93 ± 0.52
NY12C	0.250	COL	1.23 ± 0.05	8.06 ± 0.44
NY13	0.304	BR	1.83 ± 0.18	12.93 ± 0.73
NY14	0.275	BR	2.83 ± 0.14	17.87 ± 1.03
NY15B	0.280	COL	2.22 ± 0.12	16.60 ± 1.67
NY15C	0.280	COL	2.10 ± 0.09	12.67 ± 0.90
NY16A	0.270	TER	1.42 ± 0.11	8.77 ± 0.54
NY16B	0.270	TER	1.29 ± 0.09	8.20 ± 0.66
NY16C	0.270	TER	1.65 ± 0.12	9.54 ± 0.56
NY17A	0.256	TER	1.77 ± 0.07	10.25 ± 0.53
NY17B	0.256	TER	1.65 ± 0.06	10.41 ± 0.58
NY17C	0.256	TER	1.55 ± 0.10	N.D.
NY18A	0.262	CHA	1.20 ± 0.07	8.61 ± 0.78
NY18B	0.262	CHA	1.27 ± 0.07	8.18 ± 0.48
NY18C	0.262	CHA	1.42 ± 0.09	8.59 ± 0.54
NY18C	0.262	CHA	1.59 ± 0.07	9.27 ± 0.59
NY19A	0.250	CHA	1.20 ± 0.08	8.32 ± 0.84
NY19B	0.250	CHA	1.31 ± 0.06	7.78 ± 0.47
NY19C	0.250	CHA	1.19 ± 0.07	9.23 ± 0.65
NY20A**	0.245	CHA	1.25 ± 0.05	8.26 ± 0.49
NY20B**	0.245	CHA	1.23 ± 0.05	8.16 ± 0.45
NY20C**	0.245	CHA	1.19 ± 0.05	8.02 ± 0.60

Note: All sample latitudes are ~ N30°, elevation differences throughout basin are small (<150 m) and thus comparisons between sample nuclide abundances are made without elevation or latitude corrections. N.D. = No Data.

^e Letters indicate grain-size fraction of sample. A = 250 - 1000 μm, B = 1000 - 4000 μm, and C > 4000 μm.

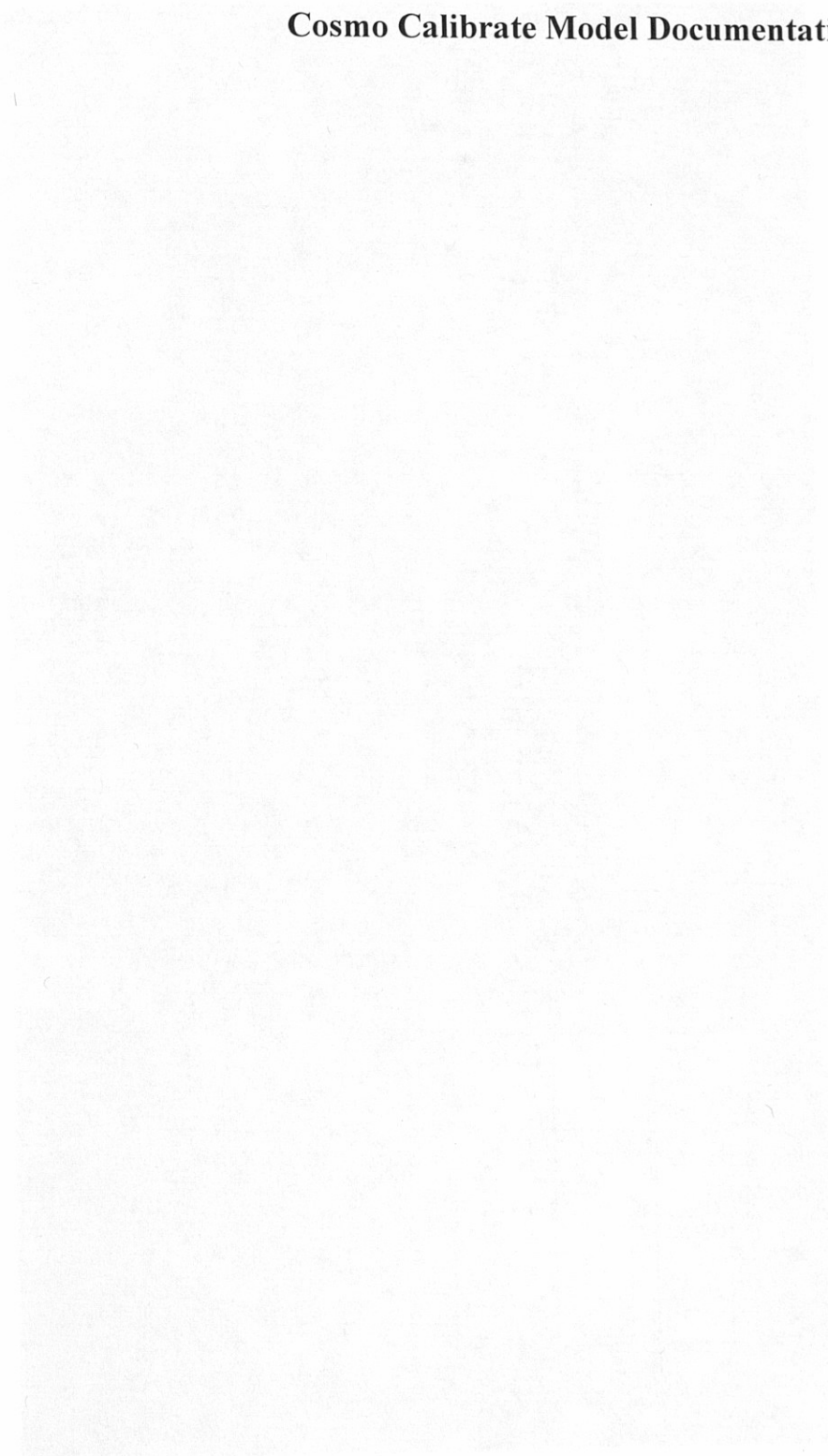
[†] For channel, colluvium, and terrace samples, elevation is a weighted average elevation of drainage basin above the sample location (represents possible elevations of sediment source).

[§] Sample type: CHA = channel alluvium, BR = bedrock outcrop, COL = hillslope colluvium, TER = terrace sediment.

**Sample location closest to the basin outlet (NY20A-C) used to determine basin-wide rates of sediment generation.

Appendix C

Cosmo Calibrate Model Documentation



**WELCOME
TO
COSMO-CALIBRATE**

**2002
Version 1.0
for Windows & Mac**

Erik Clapp
&
Paul Bierman
University of Vermont
School of Natural Resources
& Department of Geology

- BEGIN
- INSTRUCTIONS
- GO DIRECTLY TO BATCH

Control-H will always get you home

INPUT SCREEN

HELP

Instructions

BATCH SCREEN

HOME

INTRODUCTION

Cosmo Calibrate is a Microsoft Excel and Visual Basic - based program for calibrating cosmogenic exposure ages and erosion rates for the effects of secular variations in Earth's geomagnetic field strength. The program forces corrections for magnetic field strength, latitude and altitude based on the formulations of Nishiizumi et al., 1989 and correction factors of Lal, 1991. An individual magnetic field strength curve is generated for each simulation run. The user can choose between 3 or 100 iterations, which are used as a "Monte Carlo" type simulation to determine the error associated with the calculations. Uncertainties for nuclide

GETTING STARTED

To start, simply input: Latitude, Elevation, Measured Concentration, Sample Thickness, Material Density, and Attenuation Length in the designated location of the input section of the screen. You must also choose a Nuclide and Production Rate Calibration from the pull down menus and adjust the Shielding Geomoeetry% and the Production Rate Uncertainty. Then simply choose the button that gives the number of desired iterations. The more iterations, the better statistics. Each iteration takes approximately 1 second, so 100 iterations will take over a minute to complete. 30 to 50 iterations gives the similar results as 100 iterations but with slightly greater errors. Click on the "RUN" button to run the model. The "NO-CALIBRATION" Button can be used to determine uncalibrated ages or rates that are corrected for latitude and elevation.

SINGLE RUN vs BATCH RUN

The model can be run either for a SINGLE sample, or the user can run a BATCH of up to 25 samples. To run a SINGLE sample, use the INPUT screen and enter the sample information in the spaces provided. Then click on the "RUN" button. To run a BATCH of samples, use the BATCH screen and enter the sample information in the spaces provided. Then click on the "RUN-BATCH" button.

For more details on model specifics, click on the "HELP" button above.

HOME

HELP

COSMO-CALIBRATE

INPUT

Latitude: 10 (degrees)
 Elevation: 3 (km)
 Nuclide Concentration: 100 ± 0.10 (10⁶ atoms g⁻¹)
 Sample Thickness: 1 (cm)
 Rock or Soil Density: 2.6 (g cm⁻³)
 Attenuation Length (L): 165 (g cm⁻²)
 Geometry: 100 (% 2p surface)
 Nuclide: 10-Be
 Production Rate: Nishizumi (1.1 KY) & Half-Life (optional)
 Other - P₀: (atoms g⁻¹ y⁻¹)
 Muon %: 10

SIMULATION

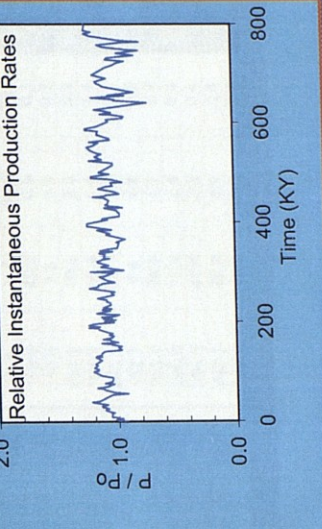
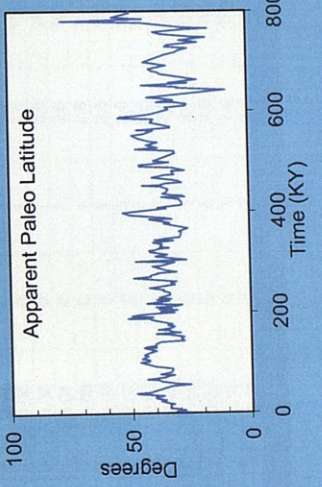
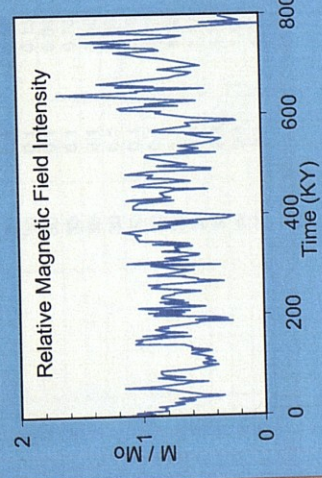
No. of Iterations (100 max): 2
 RUN
 BATCH DATA
 NO CALIBRATION

OUTPUT

Mean ± Std Error: 188.9 ± 45.0 (K yrs)
 Exposure Age: 4.0 ± 0.6 (M my⁻¹)
 Erosion Rate: 4.0 ± 0.6 (M my⁻¹)
 Half-Life (10⁶ yrs): 1.5
 P₀-normalized (atoms g⁻¹ yr⁻¹): 6.13
 P₀-Site (atoms g⁻¹ yr⁻¹): 5.91
 C-factor (unitless): 1.0

UNCERTAINTIES

UPDATE GRAPHS



HELP

VIEW GRAPHS

RETURN TO INPUTS

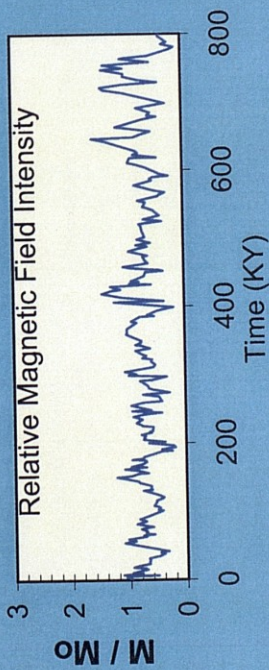
UNCERTAINTIES

RUN - BATCH

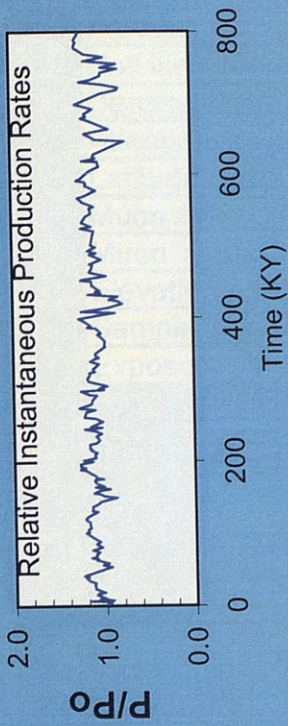
Batch Name: NY200		Date: 4/10/03		Analyst: Erik Clapp		# Iterations per Sample (n): 3					
Nuclide: ¹⁰ Be		Nishizumi (11 KY)		Laboratory: UVM Geology							
Production Rates:		Elevation (km)		Rock/Soil Density (g cm ⁻³)		Attenuation Length (L) (g cm ⁻²)		Exposure Geometry (%)			
Sample ID	P ₀ (atoms g ⁻¹ y ⁻¹) (OPTIONAL)	Latitude (degrees)	Elevation (km)	Nuclide Concentration (10 ⁶ atoms)	Analytical Error (10 ⁶ atoms)	% Moun Production (%)	Sample Thickness (cm)	Age (K yrs)	Std Err (K yrs)	Erosion (m My ⁻¹)	Std Err (m My ⁻¹)
EMC-01		30	0.1	1.10	± 0.02	0	1	197.2	8.8	2.5	0.3
EMC-02		30	0.1	0.13	± 0.00	0	1	22.4	1.4	46.7	13.6
EMC-03		30	0.1	0.90	± 0.02	0	1	162.3	18.8	4.4	0.3
EMC-04		30	0.1	0.70	± 0.01	0	1	131.6	14.8	4.3	0.7
EMC-05		30	0.1	1.30	± 0.03	0	1	276.9	53.0	2.5	0.7
EMC-06		30	0.1	1.00	± 0.02	0	1	163.8	11.0	3.6	0.3
EMC-07		30	0.1	1.10	± 0.02	0	1	232.4	30.3	2.9	0.5
EMC-08		30	0.1	0.78	± 0.02	0	1	152.4	16.8	4.1	0.2
EMC-09		30	0.1	1.10	± 0.02	0	1	168.8	12.9	3.5	0.2
EMC-10		30	0.1	1.12	± 0.02	0	1	204.2	18.8	2.5	0.3
EMC-11		30	0.1	1.30	± 0.03	0	1	234.3	29.8	3.1	0.4
EMC-12		30	0.1	1.50	± 0.03	0	1	295.6	52.2	2.1	0.3
EMC-13		30	0.1	1.00	± 0.02	0	1	160.9	22.4	3.8	0.8
EMC-14		30	0.1	0.13	± 0.00	0	1	28.5	7.7	45.0	15.2
EMC-15		30	0.1	0.90	± 0.02	0	1	199.0	43.2	2.9	0.1
EMC-16		30	0.1	0.70	± 0.01	0	1	110.0	7.5	5.9	0.2
EMC-17		30	0.1	1.30	± 0.03	0	1	230.2	19.4	2.3	0.1
EMC-18		30	0.1	1.00	± 0.02	0	1	167.3	25.4	4.4	1.1
EMC-19		30	0.1	1.10	± 0.02	0	1	255.1	73.1	2.9	0.7
EMC-20		30	0.1	0.78	± 0.02	0	1	132.7	4.4	4.8	0.6
EMC-21		30	0.1	1.10	± 0.02	0	1	203.4	34.5	3.1	0.8
EMC-22		30	0.1	1.12	± 0.02	0	1	198.6	17.9	2.4	0.4
EMC-23		30	0.1	1.30	± 0.03	0	1	298.3	41.6	2.2	0.4
EMC-24		30	0.1	1.50	± 0.03	0	1	242.5	22.6	3.1	0.4
EMC-25		30	0.1	1.00	± 0.02	0	1	188.9	45.0	4.0	0.6

GRAPHS

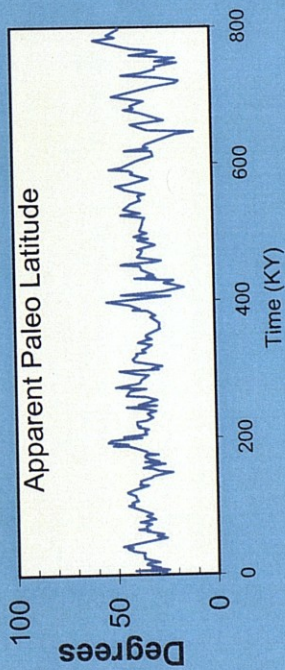
RETURN TO BATCH



RETURN TO INPUTS



UPDATE GRAPHS



UNCERTAINTIES

Production rate uncertainty	20	%
Half life uncertainty	5	%
Density uncertainty	5	%
Attenuation (λ) uncertainty	5	%
Latitude uncertainty	5	%
Muon Atten (λ) uncertainty	5	%
Muon % uncertainty	5	%
Elevation uncertainty	5	%
Sample Thickness uncertainty	5	%
Exposure Geometry uncertainty	5	%

DEFAULTS

RETURN TO INPUTS

RETURN TO BATCH

MODEL DOCUMENTATION

CALCS SHEET	
Column A	time in k-years note: the time step is large for time periods in the distant past and decreases closer to the present. Timestep at >2mya = 0.5my, Timestep at >1mya = 0.1my, Timestep > 200kya = 50y, Timestep at <200kya = 1ky.
Column B	Relative Paleo Intensity (M/Mo) from Sint 800 Curve note: prior to 200 ka, no record exists and thus the time weighted average intensity of Sint 800 is used
Column C	Standard error of mean at each point along the Sint 800 curve
Column D	spacer
Columns E-G	Random Number Generator =ROUND(RAND()*(5000-1)+1,0) =VLOOKUP(E4,5000#;\$A\$1:\$B\$5000,2)
Column F	generates a random number between 0 and 5000 generates a random normal number between 1 and 100. Takes the random number from Column E and looks-up an associated number from a list of 5000 numbers, normally distributed between 1 and 100 (found in sheet titled "5000#s")
Column G	generates a random/normal M/Mo number for each time step. Uses random normal number from column F and scales the number between three standard errors below the Sint 800 curve value in column B, and 3 standard errors above the Sint 800 curve value for a specific time interval.
Column H	=IF((COS(INPUT\$Q\$75*(180*PI)/((G4)*0.25))>1.0,180*PI/(ACOS(COS(INPUT\$Q\$75*(180*PI)/((G4)*0.25)))) Calculates an Apparent Paleo Latitude (APL) based on the sample geographic latitude scaled according to Nishizumi, 1989. if the cosign of the current latitude is > 1, the model assumes a value of zero degrees.
Columns I-K	Determines instantaneous production rates at a specific time interval Selects the Instantaneous Production Rate (IPR) from either column J or column K depending on whether APL is between 0 and 30 degrees or between 31 and 90 degrees. Scales the IPR for exposure geometry, sample depth, and Muon contribution according to Stone (2000) below.
Column J	For APLs less than 31 degrees, determines the IPR from the APL and sample elevation using the scaling factors of Lal, 1991.
Column K	For APLs greater than 30 degrees, determines the IPR from the APL and sample elevation using the scaling factors of Lal, 1991.
Column L	Sums up the number of atoms produced during a given time step by multiplying the scaled IPR (Column I) by the Time step (Column A)-1
Columns M to U	Calculate a running total of the accumulated atoms while subtracting the # of atoms decayed during each timestep. each column begins to accumulate atoms at a different starting time in the past Column M sums from 5mya to present, Column AC sums from 1mya to present, Column EO sums from 100kya to present...etc Column M sums from 5mya to present, Column AC sums from 1mya to present, Column EO sums from 100kya to present...etc The final value in row 238 (columns M to U) are the total number of atoms that would accumulate for a given starting point in the past
Columns IM to IO	Calculates a time-weighted average instantaneous production rate over the exposure history of the sample. Used to calculate erosion rates.
Columns IP to IT	Calculate production from muons according to Stone (2000)
Columns K, L, M (Rows 247 to 346)	Final Exposure Age and Erosion Rate for each iteration placed in these columns
Rows 238 & 239 (columns M to U)	Determines in which two columns, the total number of atoms accumulated (row 238) bracket the target number of atoms (cell L239) as measured in a sample. places a "true" if the value is an upper or lower bracket otherwise places a "false".
Rows 240 & 241 (columns K to U)	Determines the upper and lower bracketing nuclide abundances
Rows 242 & 243 (columns K to U)	Determines the upper and lower bracketing sample exposure age (starting time in past) associated with bracketing nuclide abundances
Cell L245	Determines the exposure age by scaling between upper and lower bracketing age based on the relationship between the upper and lower bracketing nuclide abundances and the target (measured) nuclide abundance.
Cells E238 to L243	Calculates an average rate of erosion. The time-weighted, average instantaneous production rate (columns IM to IO) is calculated over the length of exposure. Erosion is then calculated using equation: $E = (\text{Avg Inst. Production Rate} - \text{Attenuation Coeff}) / (\text{Material Density} * \text{Nuclide Abundance})$
Cells L348 to M351	Calculate the Average, Standard Deviation, Standard Error of the Mean, and total number of iterations of all iterations for Exposure Age and Erosion Rate
Cells E252 to I255	Calculates an unconnected production rate, scaled for altitude and latitude.
Cell IS9	Note: calibrated production rates include a relationship(equation) depending on the %Muons selected Converts elevation to pressure (g cm-2) using the Standard atmosphere equation of Lide, 1999
Cell IS4	Calculates a muon scaling factor considering elevation and latitude using scaling of Stone (2000) equation 3 which is based on inverse, exponential relationship between muon flux and pressure with attenuation length between 240 hPa and 280 hPa (Conversi, 1950; Rossi, 1952). Consistent with Stone (2000) and Lal (1991) a value of 242 hPa or 247 g cm-2 is used.
Macros	A series of Excel Macros, coded in Visual Basic, are used to control the flow of information and to control basic operational functions of the model. No calculations or data transformations are made within the Macros

Lower Input Sheet Cells A45 through W112 are used to transfer data used in calculations throughout the model.
Cells O49 to S50 contain CORRECTED contemporary production rates (SL, >60 degrees) used in the model. The production rates are scaled for Muons according to Stone (2000)
Cells O79 to S80 contain UNCORRECTED contemporary production rates (SL, >60 degrees) used in the model. The production rates are scaled for Muons according to Stone (2000)
The production rate/muon scaling factors for cells O49:S50 and O79:S80 were determined iteratively.

Depth Calc Sheet The Depth Calc sheet is used to calculate the % of production that occurs with sample depth below the Earth's surface for both Spallogenic and Muogenic production.
Calculations are according to the depth scaling of Lal (1988).

5000#s Sheet The 5000#s is the program random number generator. Column B contains 5000 normally distributed numbers between 1 and 100 with a mean of 50.
Column A are reference numbers in numerical order from 1 to 5000, each associated with one of the numbers in column B.
The program generates a random number between 1 and 5000, which it uses as a lookup value to choose a number from column A
and return a random normal number from column B.

INPUT SCREEN

HELP

BATCH SCREEN

search help topics below

[Attenuation Length of Fast N's](#)

[Batch Data](#)

[Elevation](#)

[Error Calculations](#)

[Iterations](#)

[Latitude](#)

[Material Density](#)

[Model Documentation](#)

[Un-Corrected Dates](#)

[Uncertainties](#)

[Model Documentation](#)

[Muon Scaling](#)

[Nuclide Concentration](#)

[Nuclide Choices](#)

[Other Po and Half-life](#)

[Paleointensity Records](#)

[Production Rates](#)

[Sample Thickness](#)

[Site Specific Production Rates](#)

Attenuation Length (Δ) of Fast Neutrons & Muons

BACK

Δ , is the characteristic attenuation length (g cm^{-2}) or absorption mean free path, for fast neutrons. Δ , is generally between 150 and 170 g cm^{-2} (see compiled table in Gosse and Phillips, 2001) and locations has been shown to be similar at different locations on Earth's surface (Kurz, 1986; Lal, 1991; Brown et al., 1992; Sarda et al., 1993). The slow muon attenuation length is generally between 246hPa and 287 g cm^{-2} (Conversi, 1950; Rossi, 1952). Consistent with Stone (2000), we adopt Rossi's (1952) value of 247 g cm^{-2} for the slow muon attenuation length.

Batch Data

BACK

Using the Batch Data Screen up to 25 samples can be entered for unattended correction. The user must choose the appropriate nuclide (10-Be or 26-Al) and the desired production rate calibration. The user can define other nuclides by choosing "other" from the nuclide pull-down menu and then entering the half-life of the desired nuclide. However, an initial production rate Po must also be entered in the batch input sheet. For more information on determining a Po, please refer to [BackPo](#) and [HalfLife](#).

The user must also define the number of iterations per sample correction (30 to 100 iterations is recommended), and must define the sample latitude, elevation, nuclide concentration & analytical error, muon %, sample thickness, sample density, attenuation length, and exposure geometry (-% shielding). Uncertainties can be changed by going to the uncertainty page using the button at the top of the page.

Note: all data must be filled in under the input section of the batch sheet with the exception of the optional Po's (only needed if "other Po" is chosen above). The results section of the batch sheet will automatically clear itself when "Run Batch" is initiated.

Once all data is entered, hit the RUN-BATCH button at the top of the page. The model will take approximately 1 second per iteration, so at 30 to 100 iterations, about 0.5 to 1.5 minutes per sample.

Elevation

BACK

Enter the elevation of your sample site (kilometers). For sediment samples enter the average elevation of the basin above you sample site, which represents the possible source areas for your sample. A default uncertainty of 5% is carried through the calculations unless otherwise specified in the UNCERTAINTIES input sheet

Error Calculations

BACK

Error Calculations are based on a monte-carlo type method. For each model parameter, the associated uncertainty is entered into the UNCERTAINTIES input page. During each model iteration, a random-normal number is generated for each parameter. These random-normal numbers are normally distributed between $+2\sigma$ and -2σ centered around μ . These errors result in a slightly different age estimate for each iteration. The model takes the average and standard error of the ages from all iterations and reports them as an age \pm uncertainty.

[BACK](#)

Iterations

Enter the number of iterations desired. 30 to 100 iterations is recommended. There is marginal gain by running more than 50.

For each iteration, the model randomly generates a new magnetic field curve which is used to correct the sample model age for the effects of changes in magnetic field strength. The curve is based on the mean of the SINT-200 curve (Guyodo and Valet, 1996) and varies according to the standard error of the mean of the curve. Using this curve, each iteration produces a random-normal estimate of the sample age. A single iteration can produce an estimate that is off by as much as three standard errors from the actual age. The model takes the average and standard deviation of the results of all iterations and reports them as the age and age error.

The more iterations, the more stable the average becomes, and the better the estimate of the age.

[BACK](#)

Latitude

Enter the geographic latitude (degrees) of your sample site. Although the model and correction factors are based on the geomagnetic latitude of the samples, over periods of greater than several thousand years it can be assumed that the average geographic and geomagnetic latitudes are similar (Merrill and McElhinny, 1983). The model accounts for errors associated with this difference by propagating a 5% error through the Monte Carlo simulation. By including the latitude error, our methods account for the large errors in production rates that result from small differences between geographic and geomagnetic sample latitude and that are particularly notable at latitudes between 20 and 40 degrees (Klein and Gosse, 1996).

[BACK](#)

Material Density

Enter the density of your sample (pre-processing) in grams cm^{-3} . This value is used to determine the shielding of cosmic rays directly related to the depth of the sample beneath Earth's surface.

[BACK](#)

Model Documentation

technical documentation of the model can be accessed online at www.uvm.edu/ul???

[BACK](#)

Muon Scaling

Slow muon production rates are scaled according to Stone (2000). The slow muon attenuation length is generally between 246hPa and 287 g cm⁻² (Conversi, 1950; Rossi, 1952). Consistent with Stone (2000), we adopt Rossi's (1952) value of 247 g cm⁻² for the slow muon attenuation length and we assume that the muon capture rate varies with latitude (at sea level) in proportion to the spallation rate (Nishiizumi et al., 1989).

Nuclide Concentration

BACK

Enter the nuclide concentration and laboratory uncertainty measured in your sample. The uncertainty is propagated through all calculations

Nuclide Choices

BACK

The user can choose to run the model for ¹⁰Be, ²⁶Al, or can choose to run the model for "OTHER" nuclides. If you choose either ¹⁰Be or ²⁶Al, the nuclide half-life is automatically input into the model, and you have the option of choosing pre-calibrated production rates.

If you choose "OTHER" nuclides, you MUST:

- 1) Enter the nuclide half-life in the adjacent, highlighted box
- 2) Choose "OTHER Po" from the production rate menu
- 3) Enter a nominal contemporary production rate in the Po column SEE: Other Po & Half-Life below

Other Po & Half-Life

BACK

The user can choose to input production rates from other studies or their own data, and for nuclides other than ¹⁰Be and ²⁶Al. However, the user must determine the nominal contemporary production rate that is consistent with the production rate data they are choosing. To do so, you must have the site specific geographical information, the measured nuclide abundances, and an independently determined age estimate.

To determine the contemporary production rate the user should follow the steps listed below:

- 1) Using the BATCH input sheet, choose the nuclide you are working with. If you choose "OTHER", you must enter the nuclide half-life in the adjacent highlighted box.
- 2) Choose OTHER from the production rate menu.
- 3) Input the data from the production rate site you are using. Input the same site data in all rows of the input columns (Latitude, Elevation, Nuclide Abundance & Error, %Muons, Thickness, Density, Attenuation, and Geometry).
- 4) In the "Po" column, enter a range of Po's that you might anticipate for your data. For the first run, you can start with Po's that are moderately spaced.
- 5) Run the model using a small number of iterations (5-10) and determine the range of Po's that bracket the independent age of your site.
- 6) Enter a refined estimate of Po's from the first model run, with Po's that are closely spaced and run the model again.
- 7) Repeat until you are satisfied with the Po estimate. NOTE: as you approach your Po, you will want to increase the number of model iterations to give a more refined estimate of Po.

ONCE YOU HAVE DETERMINED YOUR Po, YOU CAN INPUT IT INTO THE Po COLUMN ANY TIME YOU RUN THE MODEL.

BACK

Production Rates

Chooses a production rate from the production rate menu. The user can choose ^{10}Be and ^{26}Al production rates that are based on the Nishiizumi et al. (1989) data for the Sierra Nevada. The model provides a choice of the Nishiizumi 11ky production rate age or allows for the user to select a 12ky, 13ky, or 14ky production rate age based on Clark et al. (1995).

IMPORTANT: the production rates included in the model are nominal contemporary production rates determined through iterative processes. These rates are based on the nuclide abundances measured by Nishiizumi et al. (1989), and the independently determined ages of the Sierra Nevada Sites. Nominal contemporary production rates were determined by iteratively running the model with different production rates until a production rate was found that yields a geomagnetically corrected age consistent with the desired calibration age (11ky, 12ky, 13ky, or 14ky).

Additionally, the model can be run using the contemporary production rates determined by Nishiizumi et al. (1996) by measuring production of ^{10}Be in water targets. The water target rates yield similar results to the 13 ky calibration age supporting the conclusions by Clark et al. (1995), which suggest the Sierra Nevada Site was likely exposed earlier (13kya to 14 kya) than originally assumed (11kya) by Nishiizumi et al. (1989).

FINALLY the user can choose to input their own production rates or production rates for other nuclides; however, the user **MUST** determine the nominal contemporary production rate for their calibration data. See: [Other Po & Ra Nuclides](#)

BACK

Sample Thickness

Enter the thickness of the sample collected in centimeters.

BACK

Un-Corrected Dates & Erosion Rates

Uncorrected dates and Erosion rates are determined using altitude/latitude scalings of Lal (1991) and the production rates chosen from the production rate menu. The uncorrected results will also be scaled for the selected % muons, sample thickness, and sample geometry.

The uncorrected results assume a long-term average production rate and does not consider the effects of variations in Earth's magnetic field strength over time.

BACK

Uncertainties

In addition to uncertainties in the magnetic field strength curve, the model we present propagates uncertainties in production rates, AMS nuclide measurements, nuclide half-life, neutron attenuation coefficient, sample altitude, muon %, sample thickness, exposure geometry, and sample density. For each of these parameters, a normally distributed, random number is generated for each model iteration and based on errors specified by the user. Default settings include 5% uncertainties for all parameters except nuclide production rate (20% uncertainty) and AMS nuclide measurement (determined by the laboratory).

The nuclide concentration uncertainty is input along with the measured nuclide concentration in the INPUT screen or the BATCH run screen.

The magnetic field strength curve uncertainties are fixed and come directly from the SINT-800 curve (Goyodo and Valet, 1999).

The other uncertainties can be changed by going to the UNCERTAINTIES screen.

Site Specific Production Rates

[BACK](#)

The Site Specific Production Rate is the chosen production rate at sea level and $>60^\circ$ Latitude, scaled to the specified latitude and elevation of your site using the scaling factors of Lal 1991.

Paleointensity Records

[BACK](#)

Guyodo and Valet (1996) compiled and overlaid 17 existing, globally dispersed, paleointensity records to produce a worldwide, synthetic paleointensity curve during the past 200 kyr (SINT-200). Guyodo and Valet (1999) added an additional 16 paleointensity records to the SINT-200 curve, to produce a curve over the past 800 kyr (SINT-800). The SINT-800 curve provides the most comprehensive, long-term comparison of paleointensity curves to date and yields a coherent average intensity and intensity variability versus time record (average coefficient of correlation=0.7). However, it should be noted that during the past 10 kyr, the SINT-800 curve may have relatively high statistical uncertainties (Frank et al., 1997, Guyodo and Valet, 1996, 1999; Masarik et al., 2001), and does not correlate well with several other recent curves (Dunai, 2001). Therefore, similar to Masarik et al., (2001) we have chosen the dendrochronologically derived ^{14}C record of Stuiver et al., (1998) to represent the paleomagnetic record between the present and 10ky. Similar to recent works by Masarik et al. (2001), and Dunai (2001), we have chosen to the SINT-800 synthetic record to represent the paleomagnetic record for the time period of 10 kya to 800 kya. The two records are combined to create a single synthetic curve which is used to geomagnetically correct cosmogenic exposure ages and erosion rates in our model.

